3/10

Final Report

MECHANISM OF THE PHOTOVOLTAIC EFFECT IN II-VI COMPOUNDS

National Aeronautics and Space Administration
Lewis Research Center
Cleveland, Ohio

April 1, 1967 to June 30, 1972

School of Engineering
Department of Materials Science
Stanford University
Stanford, California

Grant NGL-05-020-214 S-1

Principal Investigator
Richard H. Bube, Professor

Ph.D. Thesis of Alan L. Fahrenbruch

HEAT TREATMENT EFFECTS IN Cu_2S-CdS HETEROJUNCTION PHOTOVOLTAIC CELLS

A DISSERTATION

SUBMITTED TO THE DEPARTMENT OF MATERIALS SCIENCE

AND THE COMMITTEE ON GRADUATE STUDIES

OF STANFORD UNIVERSITY

IN PARTIAL FULFILLMENT OF THE REQUIREMENTS

FOR THE DEGREE OF

DOCTOR OF PHILOSOPHY

By

Alan Lee Fahrenbruch

May 1973

ACKNOWLEDGMENTS

I wish to express my sincere appreciation to Professor R. H. Bube for suggesting the topic of this dissertation and especially for his helpful support and counsel throughout the work.

I am also indebted to Dr. Stefan Kanev for introducing me to the TROD effect in CdS crystals and for his help on a portion of the experimental work.

To Dr. P. F. Lindquist I owe a debt of gratitude for many helpful discussions and for not laughing out loud at my first questions. To Mr. Arthur Jonath, I am grateful for understanding moral support during the painful throes of thesis writing.

For many discussions, both helpful and enjoyable, I appreciate the association with my colleagues, especially Mr. Tom Arnoldussen, Mr. Derek Cheung, Dr. Hugh MacMillan, Mr. Herb Maruska, and Dr. Walden Rhines.

My deep appreciation also goes to the people of Gondolyn and especially to Marta Erlich for their patience and moral support.

The work was supported by the National Aeronautics and Space Administration at Lewis Research Center and the Stanford Center for Materials Research.

Finally I owe a real debt to my parents, Mr. and Mrs. John Fahrenbruch for their financial and moral support during my years at Stanford.

TABLE OF CONTENTS

Chapter		Page
1.	INTRODUCTION	1
	1.1 Nature of the Problem	1
	1.2 Historical Survey	3
	1.2.1 The Cu_2S-CdS Photovoltaic Cell	4
	1.2.2 Cu Diffusion in CdS	6
	1.2.3 Properties of Cu_2S	8
	1.2.4 Recent Models of the Cu_2S-CdS Cell	10
2.	THEORY	17
	2.1 The Basic p-n Diode and Photovoltaic Cells	17
	2.2 Heterojunctions	22
	2.3 Junction Capacitance	28
	2.4 Photochemical Reactions	32
3.	EXPERIMENTAL METHODS	37
	3.1 Preparation of Samples	37
	3.2 Apparatus	41
4.	EXPERIMENTAL RESULTS	47
	4.1 Junction Formation	47
	4.1.1 Growth of the Cu_2S Layer	47
	4.1.2 CdS Substrate Etching and Surface Roughness Effects	49
	4.1.3 Cu Diffusion into CdS	54
	4.2 Thermally Restorable Optical Degradation	57
	4.2.1 Time Dependence of Optical Degradation	57
	4.2.2 Temperature Dependence of Optical Degradation	59
	4.2.3 Wavelength Dependence of Optical Degradation	61
	4.2.4 Temperature Dependence of Thermal Restoration	65
	4.3 Junction Properties of the Heat-Treated Cell	68

TABLE OF CONTENTS (Contd)

Chapter			Page
	4.3.1	Relationships of the R, D, E and Q states	68
	4.3.2	Effect of Heat Treatment on Short-Circuit Current	70
	4.3.3	Effect of Heat Treatment on Dark Current-Voltage Curves	72
	4.3.4	Spectral Response of Short-Circuit Current	74
	4.3.5	Effect of Optical Degradation of the Cell	79
	4.3.6	Effect of Degradation on the Rates of Enhancement and Quenching in the Cell	83
	4.3.7	Enhancement and Quenching Effects in the Photoconductor	85
	4.3.8	Junction Capacitance Measurements	92
	4.3.9	Effects of Depletion Layer Width on I_{sc}	103
	4.3.10	Effect of Cell State on the Dark I-V Curves	106
	4.3.11	Variation of Dark Forward Bias Current with Temperature	109
	4.3.12	Thermal Cycles for I_{sc}	120
	4.3.13	Relationship of I_{sc} to I_f	124
	4.3.14	The 82°C Phase Change	125
	4.3.15	The Cooling Enhancement Effect	131
	4.3.16	Variation of Photocurrent with Light Intensity	133
5.	DISCUSSION		135
	5.1	Introduction	135
	5.1.1	Perspective	135
	5.1.2	Preliminary Implications	141
	5.2	Junction Structure from $1/C^2$ Versus V_f Analysis	143
	5.3	Implications of the TROD Effect	152
	5.3.1	Comparison of TROD Effects in the Photoconductor and the Cell	153

TABLE OF CONTENTS (Contd)

Chapter		Page
	5.3.2 Relation of the TROD Effect to Junction Properties	156
	5.3.3 The Mechanism of the TROD Effect	160
	5.4 On the Mechanism for Dark Forward-Bias Current Flow	161
	5.5 Electric Field Control of I_{sc}	174
6.	CONCLUSIONS	183
APPENDIX I -	RELEVANCE TO THIN FILM CELLS	189
APPENDIX II -	EFFECT OF H_2 ANNEALING ON THE CELL	193
REFERENCES	. . . . .	195

LIST OF TABLES

Number		Page
4-1	Dark current activation energies, eV	117
5-1	Properties of a typical cell in the various electronic states before and after heat-treatment	140
5-2	Electron quasi-Fermi levels and lifetimes for various states in the photoconductor	154

LIST OF FIGURES

Number		Page
2-1	Energy band diagram for a forward biased p-n homojunction	18
2-2	Dark and light I-V characteristics for an ideal photovoltaic cell	20
2-3	Equivalent circuit for the photovoltaic cell	20
2-4	Energy band diagram for an abrupt p-n heterojunction . .	23
3-1	Reaction vessel for dip forming Cu_2S layer	39
3-2	Sample environment	42
3-3	Schematic diagram of electrical measurement circuit . .	44
4-1	Cu_2S layer thickness versus dipping time at 75°C	50
4-2	Scanning electron microscope photograph of Cu_2S-CdS cell at 2000x	51
4-3	Depletion layer width w_d versus the square root of HT time for cell #81	55
4-4	(a) Schematic TROD curve. (b) Short-circuit current and photocurrent versus time during optical degradation	58
4-5	Optical degradation versus reciprocal temperature for cell #81 and photoconductor #94 relative to the fully restored state	62
4-6	Effectiveness of optical degradation versus wavelength of the degrading light at 300°K	64
4-7	Thermal restoration versus reciprocal temperature for cell #89 and photoconductor #94 relative to the fully restored state	66
4-8	Symbolic plot of low intensity probe short-circuit current (at 0.70μ) versus degree of optical degradation in the enhanced (E) and quenched (Q) states for cell #81	69
4-9	Properties of cell #81 versus cumulative HT time	71
4-10	Dark current-voltage curves for cell #61 at 300°K in the DQ state	73

LIST OF FIGURES (Contd)

Number		Page
4-11	Typical transient measurements for the enhanced-first and quenched-first cases	75
4-12	Short-circuit current spectral response for cell #81 at 300°K (full lines) and 150°K (dashed lines)	78
4-13	Fast scan spectra for the photoconductor crystal at 300°K and 150°K in the restored and degraded states . .	80
4-14	Cell #81 parameters versus cumulative time of degradation at 300°K: probe light (0.70μ, 9.3 $\mu w/cm^2$) current with cell enhanced $I_{sc}(E)$ and quenched $I_{sc}(Q)$; junction capacitance, enhanced C(E), and quenched C(Q), and their difference ΔC	82
4-15	(a) Typical curves of I_{sc} versus time during enhancement and quenching at 300°K for cell #81. (b) Enhancement rate $1/\tau_E$ and quenching rate $1/\tau_Q$ versus cumulative degradation time at 300°K	84
4-16	(a) Probe photocurrent versus time at 300°K for the pre-enhanced, pre-quenched, and pre-dark-equilibrated conditions. (b) Probe photocurrent with simultaneous bias light versus wavelength of probe light	87
4-17	Probe photocurrent (0.70μ at 9.3 $\mu w/cm^2$) versus time for the restored case at 150°K	89
4-18	Photoconductivity decay curves	90
4-19	Plot of $1/C^2$ versus bias voltage for cell #61 after small HT (∿2 min at 100 to 130°C)	94
4-20	$1/C^2$ versus bias voltage at 300°K for cell #61 after ∿6 min of HT	97
4-21	$1/C^2$ versus bias voltage at 150°K for cell #61 after ∿6 min of HT	98
4-22	Net donor density (N_D-N_A) versus depletion layer width w_d for cell #61	99
4-23	Plot of $1/C^2$ versus bias voltage at 150°K for cell #81 in the restored state after ∿1 hour of HT	100
4-24	Plot of $1/C^2$ versus bias voltage at 150°K for cell #81 in the degraded state after 1 hour of HT	101

LIST OF FIGURES (Contd)

Number		Page
4-25	Net donor density (N_D-N_A) versus depletion layer width w_d for cell #81 at 150°K	102
4-26	Short-circuit current versus reciprocal capacitance for cell #81 (∿1 hour of HT) at 150°K	104
4-27	Short-circuit current versus reciprocal capacitance for cell #61 at 150°K	105
4-28	Dark current versus forward bias voltage at 150°K for cell #81	107
4-29	Dark current versus forward bias voltage at 300°K for cell #81	108
4-30	Dark forward bias current versus $V^{1/2}$ for cell #61 . . .	110
4-31	Dark forward bias current versus reciprocal temperature for cell #81	112
4-32	Dark current versus temperature for Cu_2S hotter than CdS, with zero bias and with various values of forward and reverse bias	115
4-33	White light short-circuit current versus inverse temperature	121
4-34	Photocurrent (white light, 1400 $\mu w/cm^2$) versus reciprocal temperature for the photoconductor	123
4-35	Short-circuit current versus dark forward-bias current	126
4-36	White light short-circuit current versus temperature for cell #36	127
4-37	Dark forward-bias current versus temperature for cell #89	129
4-38	Cell #81 currents versus temperature	130
5-1	$1/C^2$ versus bias voltage for an un-HT cell at 110°K with and without photocapacitance excited	144
5-2	Semiconductor-metal-semiconductor band profile from Fig. 5-1	145

LIST OF FIGURES (Contd)

Number		Page
5-3	Schematic $1/C^2$ versus V plot for perfectly insulating i-layer	147
5-4	Schematic charge density profile (a) and derived band profile (b)	149
5-5	Schematic $1/C^2$ versus V plot for charge density profile of Fig. 5-4	150
5-6	Relationship of I_{sc} and the CdS:Cu layer conductivity, σ, during a transient measurement	158
5-7	Idealized energy band profile for $\Delta E_c < 0$ and $\Delta E_c > 0$	166
5-8	Band profiles without forward bias (a), with 0.2 V forward bias (b), and hypothetical density of tunneling-recombination centers (c)	169
5-8(d)	Band profiles showing effects of enhancement (ΔC = maximum) and quenching ($\Delta C = 0$)	170
5-9	Band profile for I_{sc} control model	175
5-10	Log (J_{sc}/J_o) versus reciprocal electric field	176
5-11	J_{sc} versus distance from the interface	180

ABSTRACT

The optical and electronic properties of single crystal Cu_2S-CdS photovoltaic cells have been investigated. In these cells trapped charge near the interface which is manifested by a persistent increase in junction capacitance (the photocapacitance) plays a significant role in determining the carrier transport properties.

We have found that the severe degradation in short-circuit current observed in heat-treated cells can be separated into two components:

(1) a relatively small thermal component occurring on heat-treatment in the dark and,

(2) a much larger degradation caused by exposure to light at room temperature.

By a short additional heat-treatment above $\sim$100°C the cell can be completely restored to its condition before the optically caused degradation with no effect on the depletion layer width. The optical degradation effect is phenomenologically similar to so-called photochemical changes in electron lifetime seen in CdS single crystal photoconductors.

The subsequent aims of our work have been:

(1) to gain a deeper understanding of heat-treatment effects in single crystal cells

(2) to explore the effects of the thermally-restorable optical degradation effect described above in both cells and photoconductors and determine the relationship of these effects to the photocapacitance phenomena and carrier transport properties

(3) to determine the nature of the mechanism of short-circuit current control in the cell.

In order to accomplish these aims the dependence of short-circuit current on wavelength of illumination, temperature, the state of optical degradation, and of excitation of photocapacitance were measured in cells with various degrees of heat-treatment. Similar measurements of the dependences of dark, forward-bias current and junction capacitance versus bias data were used to gain information on the structure of the junction barrier.

Measurements on a Cu doped CdS crystal photoconductor verified the presence of the same basic phenomena and showed that such a layer was actively controlling carrier transport properties in the cell.

Work on the optical degradation effect itself shows it to be a thermally controlled process with an activation energy of $\sim$0.4 eV occurring at T > $\sim$200°K for the cell and T > $\sim$250°K for the photoconductor. Thermal restoration was shown to occur at T > 350°K with an activation energy of $\sim$1.6 eV.

Other important results of our research are:

(1) While the short-circuit current changes over a range of 10^3 with variation of state of degradation and of enhancement, the shape of the spectral response of current curves are almost constant. This implies that the CdS:Cu layer controls the current while the properties of the Cu_2S remain relatively unchanged.

(2) The similarity of the properties of the cell and the photoconductor including all the optical degradation effects again show that the CdS:Cu layer controls carrier transport in the cell.

(3) Short-circuit current versus junction capacitance data show that for the restored, low temperature and before heat-treatment conditions the current depends exponentially on depletion layer width.

(4) The dark, forward-bias current is directly proportional to the short-circuit current over a wide range of cell states at room temperature suggesting that the same mechanism controls both currents.

Finally, a model is proposed in which both the short-circuit current and the dark, forward bias current are controlled by a tunneling-recombination process through interface states. Our model proposes that changes in the junction profile resulting from optical charging of centers near the interface modifies the electric field at the barrier modulating both currents in a fashion which is consistent with the observed behavior.

B

SYMBOLS

α	exponential factor in diode equation, $I = I_o(\exp\alpha V - 1)$, (volts^{-1})
B	constant
C	junction capacitance (pF)
ΔC	photocapacitance increment (pF)
D	degraded; diffusion constant (cm^2/sec)
δ	rate of degradation (sec^{-1})
E	enhanced
E_b	tunneling barrier (eV)
ΔE_c	conduction band edge discontinuity at heterojunction (eV)
E_f	Fermi energy (eV)
E_g	bandgap (eV)
ε	permittivity (farads/m)
$\mathfrak{E}$	electric field (volts/m)
HT	heat-treated
I_{sc}	short-circuit current in cell (amp)
I_f	dark, forward-bias current in cell (amp)
I_p	current in photoconductor (amp)
J, J_{sc}	current density (amp/cm^2)
k	Boltzmann constant $(0.864 \times 10^{-4}$ eV/°K)
λ	wavelength (μ)
m*	effective mass of electron (kg)
N_A	acceptor density (cm^{-3})
N_D	donor density (cm^{-3})
N(x)	effective positive charge density in depletion region (cm^{-3})

n	electron carrier density (cm^{-3})
η	factor expressing effective quantum efficiency of Cu_2S layer (amp/watt) or (coul/photon)
P_t	tunneling probability
Q	quenched
q	magnitude of electronic charge (1.60×10^{-19} coul)
R	restored
σ	conductivity (1/ohm cm)
T	temperature (°C, °K)
t	time (sec)
TROD	thermally-restorable optical degradation
τ	time constant for photoconductivity decay (sec)
τ_n	electron lifetime (sec)
V, V_f	forward bias voltage (volts)
V_b	barrier voltage (volts)
ψ	factor expressing effectiveness of current control by CdS:Cu layer
w_d	depletion layer width (μ)
w_i	width of i-layer (μ)
x	distance from metallurgical interface (μ)
χ	electron affinity (eV)

Chapter 1

INTRODUCTION

1.1 Nature of the Problem

The photovoltaic properties of p-n homojunctions have long been known and the theory is well established. In the homojunction the effective photoexcitation occurs within a minority carrier diffusion length of the junction and since illumination by photons with energy greater than or equal to the band gap energy must be used, there must be a compromise with ineffective absorption in the bulk of the p- or n-type material. If the p-type material, for example, is made increasingly thin then recombination at surface states begins to play an important role in this compromise as well. In order to extend the range of spectral sensitivity and to increase efficiency, it is desirable to replace one side of the junction with a material of larger band gap, thus forming a heterojunction. This in effect adds a window to the cell permitting all the light with photon energy between the two band gap energies to reach the junction region where effective photoexcitation occurs. The use of heterojunction structures also effectively removes the fast recombination surface states from the region where effective photoexcitation is taking place.

The two most widely used systems for solar energy conversion at present are the p-n Si (single crystal) cell and the Cu_2S-CdS (thin film) cell. The Si p-n junction properties are well known and the cell has the advantages of higher efficiency and better long-term stability. The thin film version of the Cu_2S-CdS cell (the Cu_2S is deposited by an aqueous displacement reaction on an evaporated polycrystalline film of Cds) is

potentially less expensive to produce than its single crystal counterparts such as Si or $Ga_{1-x}Al_xAs$-GaAs cells. In addition it has the advantage of mechanical flexibility and greater high energy radiation resistance.

There are several areas of difficulty in obtaining an understanding of the Cu_2S-CdS system. (1) The basic heterojunction structure is inherently complex because of joining materials with different electron affinities, band gaps, carrier densities, and different crystal structures. (2) The lattice mismatch and interdiffusion of components causes defect states at or near the interface which strongly affect the junction properties. (3) A variety of $Cu_{2-x}S$ phases may exist at room temperature. (4) There are the undetermined effects of grain boundaries, random crystal orientation, and interface roughness in the thin film CdS cells. We have chosen to eliminate the last category by working with single crystal cells.

One of the basic problems with the CdS cell has been the loss of efficiency with time. It has been proposed that a large fraction of this loss is associated with Cu diffusion into the CdS which may occur during heat treatment, over long periods of time during operation, or perhaps by electric field assisted diffusion at high operating voltages. Other sources of loss of efficiency are a change of phase of the $Cu_{2-x}S$ layer due to the Cu diffusion above, or to chemical action of the atmosphere.

A major contribution to the investigation of loss of efficiency associated with Cu diffusion has been the thermally-restorable optical degradation (TROD) effect described in this thesis.* The degradation

*We shall reserve the term "degradation" for this phenomenon.

occurring on heat treatment of a Cu_2S-CdS cell (which is most severe in single crystal cells) can be separated into two components: (1) a relatively small decrease in short-circuit current, I_{sc}, caused by heat treatment in the dark, and (2) a much larger decrease in I_{sc} on subsequent exposure to light. This optical degradation can be removed by an additional, short heat treatment at a lower temperature in the dark, restoring the cell to its preoptically-degraded condition. This optical degradation effect can be used to separate various heat treatment effects. A similar effect has been observed in CdS photoconducting crystals by many workers, but not previously in Cu_2S-CdS cells (because room light quickly degraded the cells after heat treatment). To the best of our knowledge, all previous measurements on these cells have been in the optically degraded condition.

The aims of this research are:

(1) to gain understanding of heat treatment effects in single crystal cells,

(2) to determine the conduction band profile in the junction region and the nature of the current transport mechanisms, and

(3) to investigate the thermally-restorable optical degradation effect and its relationship to the electrical properties of the cell.

1.2 Historical Survey

"... *with a little help from my friends*" - The Beetles

An historical survey of the development of the Cu_2S-CdS cell and of models describing its operation is presented here. Also outlined is

current thought on other aspects of the problem: Cu diffusion in CdS and the properties of Cu_2S.

1.2.1 The Cu_2S-CdS photovoltaic Cell

The first reported observation of a photovoltaic effect in CdS with Cu, Ag, or Au contacts was made by Reynolds, et al.[1] in 1954. These authors explained the cell's sensitivity to extrinsic radiation by a two-step photoexcitation process through impurity levels in the CdS. Nadjakov, et al.[2] appears to have made the first thin film CdS cells in 1954 using Al and Au electrodes. About the same time efficient Si p-n junction solar cells were developed by Chapin, Fuller, and Pearson[3].

The need for power supplies for spacecraft simulated research directed toward finding the mechanism for the photovoltaic effect in the Cu_2S-CdS system. In 1960 Williams and Bube[4] compared electroplated junctions of many metals on CdS and found that Cu gave the largest response. Their junctions were not heat treated and they assumed that very little Cu had diffused into the CdS. Thus they explained the observed extrinsic response in terms of photoemission from the Cu metal into the CdS. In 1962, Fabricus[5], Grimmeiss and Memming[6], and Woods and Champion[7] explained the operation of the Cu-CdS cell by postulating a p-n junction either due to impurity band hole conduction ($\sim$1.2 eV below the conduction band)[5,6] or due to p-type CdS[7]. Grimmeiss and Memming found that the output of their cells could be maximized by careful heat treatment. The duration of the heat treatment was very critical--a maximum in the short-circuit current was reached within $\sim$100 sec at $\sim$600°C surface temperature and then a severe decrease took place for longer heat treatment times. Then they dissolved away the Cu contact completely in a

cyanide solution after heat treatment. Since these cells without metallic Cu had essentially the same spectral response for photon energies below ∿2.4 eV as the Cu-CdS cells of other workers with metallic Cu, they argued that the photoexcitation must take place in the CdS.

Cusano[8] and Keating[9] in 1963 offered a model in which the CdS formed a heterojunction with Cu_2S. Cusano, working with both CdS and CdTe cells, proposed that the p-type Cu_2S layer formed the necessary potential barrier and that the exciting radiation was absorbed in the CdS or CdTe. Cusano felt that previous workers had in reality formed thin layers of Cu_2S even without apparent heat treatment.

Up to this time no great difference in properties had been found between the Cu-CdS and the Cu_2S-CdS cells. In both cases there may be Cu diffusion into the CdS and in both cases there is the possibility of a layer of Cu_2S. As late as 1966 Duc Cuong and Blair[10] thought that the important response was due to excitation from Cu impurity states in the CdS.

Apparently beginning with Selle, et al.[11] (using evaporated Cu_2S) and Potter and Schalla[12] in 1967, workers in the last few years have attributed the significant photoresponse to the Cu_2S itself. Although the spectral response of CdS:Cu is similar to that of Cu_2S, the absorption in CdS:Cu is far too small to account for the observed quantum efficiencies (approaching unity). Ergova[13] and Mytton[14] in 1968 showed that the heat treatment was a necessary step in making an efficient cell and proposed that the photoelectrons were injected from the Cu_2S into the CdS. Potter and Schalla[12] noted enhancement of long wavelength response by shorter wavelength illumination. They suggested that this effect might be due to impurity levels in the CdS.

Several of the more recent models including those of Shiozawa[15], Gill[16], and Lindquist[17] are discussed in Section 1.2.4.

Modern commercial processes for the production of thin film cells include a spray technique outlined by Chamberlain and Skarman[18]. However, the dipping process (in which Cu_2S is formed on CdS by an exchange reaction in an aqueous solution of Cu^+ ions) produces the most reliable and efficient cells (5 to 6% in normal sunlight) at present. This method is described by Shirland and Hietanen[19].

One of the persistent problems connected with the Cu_2S-CdS cell has been the loss of efficiency over long periods of operation. This has been extensively chronicled with reams of data which appear to measure the reliability of the testing apparatus rather than the cell. However, the problem remains largely unsolved. Spakowski[20] and Shiozawa[15] have given outlines of cell stability research.

Proceeding on the assumption that the loss of cell efficiency is connected with Cu diffusion and/or oxidation, Konstantinova and Kanev[21] have recently produced CdS cells by a replacement reaction using a Cu-doped $BiNO_3$ solution rather than the Cu^+ ion solution usually used. Efficiencies of 3 to 5% and good stability have been reported without an attempt to maximize these parameters.

1.2.2 Cu Diffusion in CdS

Throughout the development of Cu_2S-CdS system cells, Cu has remained a necessary constituent and heat treatment a vital step in fabrication. The diffusion and solubility of Cu in CdS is intimately connected with the junction structure of the cell. Various workers measuring the diffusion coefficient of Cu in CdS have obtained results differing

by as much as a factor of 100 at 200°C. Among them are Purohit[22] (using a radioactive tracer method), Clarke[23], Woodbury[24] (who found two diffusion rates--a slow one for high surface concentrations of Cu and a faster one for low surface concentrations), and Heyding[25]. Szeto[26] used an optical absorption method to measure Cu diffusion. A very thorough investigation has been done by Sullivan[27] in the 1946 to 400°C temperature range by a compensation-capacitance technique. He obtained for the diffusion constant parallel to the c axis, $D_{||}$, and the solubility, $[Cu]_{max}$,

$$D_{||} = 2.1 \times 10^{-3} \exp\{-0.96 \text{ eV/kT}\} \text{ cm}^2/\text{sec}$$

and

$$[Cu]_{max} = 6.6 \times 10^{22} \exp\{-0.505 \text{ eV/kT}\} \text{ /cm}^3.$$

Diffusion perpendicular to the c axis of the CdS is 10 to 100 times as fast as that parallel to the c axis. Sullivan's data appear to be the only data taken at common cell heat treatment temperatures (200 to 250°C) and his value of $D_{||}$ is lower than any other value obtained by extrapolation to that temperature range from higher temperature data.

As suggested by Woodbury[24], Cu diffusion in CdS may be complex, involving two separate processes which proceed at different rates. This may in part account for the disparity in the values of D reported in the literature. Another reason for this disparity may be the extremely rapid diffusion along dislocations close to the CdS surface coupled with the higher diffusion rate perpendicular to the c axis, both effects reported by Sullivan[27].

Incorporation of Cu in CdS is thought to be substitutional at Cd sites, most commonly in the form of complexes associated with native

defects in the CdS (Aven and Prener[28]). Other workers have discovered precipitates of Cu_2S in CdS at room temperature: Dreeben[29,30] (for Cu concentrations exceeding 0.02 weight %), Vitrikhovskii[31] (who explained apparent hole conductivity of CdS by precipitates of Cu_2S in a matrix of CdS), and Szeto[32]. A retrograde solubility (solubility increasing, reaching a maximum, and then decreasing with increasing temperature) has been reported by Dreeben[30] with a maximum of 0.2 weight % of Cu at 475 to 650°C. Quenching preserves this solubility metastably and precipitation occurs on aging at room temperature. This precipitation may account for some of the temporal changes reported in the photoconductivity of CdS. Dreeben found no p-type conductivity in the supersaturated condition at room temperature however.

Field assisted diffusion in CdSe has been studied by Matsuda[33] who showed that there was diffusion from a Cu contact positive with respect to the CdSe. No diffusion occurred when the Cu contact was negative.

The corresponding problem of Cd diffusion away from the junction region during Cu_2S layer growth is qualitatively discussed by Hill and Kermidas[34].

1.2.3 Properties of Cu_2S

A number of "copper sulfides" exist at room temperature with compositions close to the stoichiometric value. Little research has been done to identify the particular composition forming the "Cu_2S-CdS" cell (except for teVelde[63]) so most workers have not been specific about the limits of composition. In this paper we refer to the material as Cu_2S unless it is necessary to be more specific, in which case $Cu_{2-x}S$ is used.

Cu_2S is a degenerate p-type semiconductor with a carrier density of 10^{19} to $10^{20}/cm^3$ provided by Cu vacancies (Kryzanavskii[35]). An indirect band gap of 1.2 eV exists at 300°K (Marshall and Mitra[36]) and there is a direct band of 1.8 eV at 300°K according to Abdulla et al.[37]

The optical absorption spectrum has been measured by numerous workers including Eisenmann[38]; Sorokin et al.[39]; Shiozawa, Sullivan, and Augustine[40]; and Selle and Maege[41]. A number of the results have been summarized by Shiozawa et al.[15]

The phase diagram of Cu_2S has been investigated quite intensely because of the mineralogical importance of Cu_2S and its potential as a thermoelectric material. The stable form of Cu_2S at room temperature is very complex, containing 96 molecules of Cu_2S per unit cell. The material has several possible phases at room temperature:

Chalcocite (Cu_2S), orthorhombic structure at 300°K, transforms hexagonal at 104°C.

Djurleite ($Cu_{1.96}S$), orthorhombic or pseudo-orthorhombic at 300°K, transforms to tetragonal at 86°C, and to cubic at 100°C.

Diginite ($Cu_{\sim 1.8}S$), pseudo-cubic at 300°K, transforms to cubic at 78°C.

A good review of existing data is given by Cook in reference 15.

Singer and Faeth[42] found a preferred orientation between Cu_2S grown on CdS with the a and c axes aligned. Sizable CdS crystals may be transformed into oriented polycrystalline Cu_2S by the dipping method. A good discussion on this point is given by Cook, et al.[43] who describe the relationship between the $Cu_{2-x}S$ phases and CdS.

The lattice constants of chalcocite are a = 11.9 Å, b = 27.3 Å, and c = 13.5 Å. During crystalline modification the sulphur lattice

remains virtually unchanged while the Cu atom positions are altered (according to Heyne[44]). Examination of the lattice constants of CdS and chalcocite shows nearly integral relationships between them: 3 a(CdS) exceeds $a(Cu_2S)$ by about 4.5%, 2 c(CdS) is nearly equal to $c(Cu_2S)$ with about 0.4% difference, and 8 b(CdS) exceeds $b(Cu_2S)$ by 4.8%. A portion of this strain is relieved by cracking of the Cu_2S. A large density of interface states is expected to result from this lattice mismatch.

A comparison of the optical properties of Cu_2S, $Cu_{1.96}S$, $Cu_{1.9}S$ and $Cu_{\sim 1.8}S$ has been made in 1972 by Mulder[64].

1.2.4 Recent Models of the Cu_2S-CdS Cell

The processes involved in a photovoltaic cell include: (1) photoexcitation, (2) injection and charge separation, (3) loss (e.g., by recombination or reinjection), and (4) collection (usually through ohmic contacts). Initial research on Cu_2S-CdS system was concerned mainly with the first two processes. As models evolved, the proposed origin of the effective excitation changed from the Cu layer (by photoemission), to the CdS (with the Cu or Cu_2S layer playing a passive role), and finally back to an active Cu_2S layer. Consideration of loss mechanisms in the cell (other than simple optical reflection or absorption losses) became more sophisticated to include enhancement effects (Potter and Schalla[12]), a photoconducting layer (Shiozawa[40]), conduction band spikes (Lindquist[45]), and recombination at interface states (Gill[16,46]).

Most (but not all) researchers now agree on the following points:

(1) The active layer in which extrinsic* photoexcitation occurs

*We refer to energies smaller than the CdS band gap as extrinsic.

is $Cu_{2-x}S$, from which the electrons are injected into the CdS.

(2) The forward bias current flows through the junction by tunneling and/or recombination at interface states, rather than over the barrier into the Cu_2S conduction band.

(3) Diffusion of Cu into the CdS occurs during heat treatment and widens the depletion layer on the CdS side by compensation of CdS donors. This modification of the CdS plays an important role in determining the junction properties of the cell in virtually all the models proposed. Heat treatment is necessary for the production of good thin film cells.

(4) Long wavelength response is enhanced by short wavelength illumination. The response to simultaneous illumination by a long and a short wavelength light for example will be considerably more than the sum of the responses to the long and short wavelengths used alone. This nonadditivity is strongly increased by heat treatment of the cell.

(5) The dark and light forward-bias current versus voltage curves cross in the heat treated cell, rather than just being displaced by the amount of the short-circuit current as in the ideal photovoltaic cell.

(6) Long term loss of cell efficiency occurs due to a chemical reaction in the Cu_2S and/or Cu diffusion into the CdS.

A good comparative discussion of models prior to and including the Clevite model (Shiozawa[40], 1968) is given by van Aershodt et al.[47] (1971).

The major uncertainty remaining is over the mechanisms that control the magnitude of the injected photocurrent. Some of the proposed

mechanisms are:

(1) the presence of various phases of $Cu_{2-x}S$ with different quantum efficiencies for excitation,

(2) the direct control of injection by a spike in the conduction band of the Cu_2S at the junction interface,

(3) a series photoconductive layer of CdS:Cu with, for example, space-charge-limited-current control of short-circuit and dark forward bias current,

(4) recombination loss in bulk and/or interface states, and

(5) reverse tunneling through interface states.

The Clevite model and the Stanford model (due to Bube, Gill, and Lindquist) are perhaps most important currently. The basic features of the Clevite model (for front wall cells which have been heat treated at 250°C) are:

(1) Photoexcited carriers are injected from the Cu_2S layer where nearly all the light absorption takes place.

(2) The junction current is controlled by a series photoconducting layer of Cu doped CdS (i-CdS) which is insulating in the dark and weakly n type when illuminated. Optical quenching effects are associated with this layer.

(3) The important photovoltaic junction under illumination is between the Cu_2S and the i-CdS. There is no barrier to injection of carriers into the CdS.

(4) In the dark, the important junction is between the i-CdS and the n-CdS substrate with a potential barrier of $\sim$1.2 eV. This means that the i-CdS is slightly p-type in the dark.

(5) The crossing of the light and dark I_f-V curves is due to the change of the effective junction position from the i-CdS, n-CdS interface in the dark to the Cu_2S, i-CdS interface under illumination. Each junction has different transport properties.

(6) Under forward bias the current recombines through Cu_2S, i-CdS interface states which form a pathway through the junction. This current is probably space charge limited.

The principal features of the Stanford model are:

(1) Carriers are injected from the Cu_2S as in the Clevite model.

(2) Electron injection into the CdS is controlled by a spike in the Cu_2S conduction band at the Cu_2S-CdS interface, or by recombination through interface states (an alternative mechanism suggested by Gill[46]).

(3) On heat treatment, a partially compensated layer of CdS:Cu is formed with impurity levels at 0.3 and 1.1 eV above the valence band.

(4) Optically induced hole trapping at states in the CdS near the interface modulates the barrier profile with an accompanying change in junction capacitance. The barrier profile in turn controls injection and/or recombination. Shorter wavelengths of illumination increase hole trapping, narrowing the barrier and increasing cell current (enhancement). Long wavelengths or thermal emptying makes the charge on these states more negative, increasing the barrier width and decreasing cell current (quenching).

(5) The forward bias current is dominated by tunneling through the barrier via interface states. Since the width of the barrier is modulated by light, the crossover of the dark and light I-V characteristics is expected.

(6) The enhancement of long wavelength short-circuit current response by short wavelength illumination is due to the effect on the conduction band spike of the enhancement and quenching described in item 4.

(7) After the enhancing light is turned off, enhancement persists over time periods of hundreds of seconds at room temperature and for very long times at low temperatures (at least hours and perhaps stable at 105°K).

(8) Heat treatment widens the Cu doped CdS layer, increasing the significance of the above effects.

Other recent models include contributions by Duc Cuong and Blair[10] and Balkanski and Chone[50] (both 1966) who suggested that the effective photoexcitation is from interface states rather than either the Cu_2S or the CdS. Massicot[51] (in 1972) and Böer, et al.[52] (1970) proposed a three-layered structure of Cu_2S, $Cu_{1.96}S$*, and CdS. The $Cu_{1.96}S$ (Djurleite) interlayer with effective band gap assumed to be 1.8 eV, forms a potential barrier which controls the injection of electrons of energy less than 1.8 eV from the Cu_2S. The Djurleite layer forms chemically by diffusion of Cu into the CdS and can be restored to Cu_2S by a photochemical process involving ionization of Cu vacancies by trapping electrons created by illumination with short wavelength light. The vacancies move by field

*Reported by Massicot as 2-x = 1.93 and by most other workers as 2-x = 1.96.

assisted diffusion into the Cu_2S layer changing the Djurleite into Cu_2S thus explaining the enhancement effect. While such a layer might be able to control the cell output, this model does not explain the increase of junction capacitance by near intrinsic light which accompanies the enhancement effect. The creation of the Djurleite layer of the Massicot-Böer model would eventually exhaust the Cu supply of the Cu_2S and make further "enhancement" impossible. It has been observed, however, that enhancement and quenching can be recycled indefinitely without change in the cell properties.

Miya[48] (1970) proposed two quite different heterojunction models for cells formed on the a and b faces of the CdS crystal, one of which included a p-type CdS layer. A model in which the barrier height is controlled by interface state charging by hole injection from the Cu_2S into the CdS was proposed by Lindmayer[49] in 1970.

None of the above models includes the thermally-restorable optical-degradation effect studied in this investigation.

Chapter 2

THEORY

"God made truth with many doors to welcome every believer who knocks on them" - Kahlil Gibran

In this chapter we outline the basic theory of the homojunction and heterojunction diodes with respect to their use as photovoltaic cells. In particular we consider the tunneling-recombination mode of carrier transport through heterojunctions which have a large density of interface states. After discussing the theory of junction capacitance measurements we present a short discussion of photochemical reactions in CdS crystals.

2.1 The Basic p-n Diode and Photovoltaic Cells

The theory of both homo- and heterojunctions is well documented and we outline it here principally in order to define terms.

The p-n homojunction (where the materials making up the junction differ only in carrier type and density) is well explained by the Shockley diffusion model which assumes in part that (see Fig. 2-1):

(1) The electron and hole currents are controlled by diffusion and the built-in field.

(2) The junction barrier profile is given by the abrupt depletion layer approximation.

(3) No recombination or generation occurs in the junction region and the e' and h° currents are constant in the depletion layer.

(4) Boltzmann statistics apply.

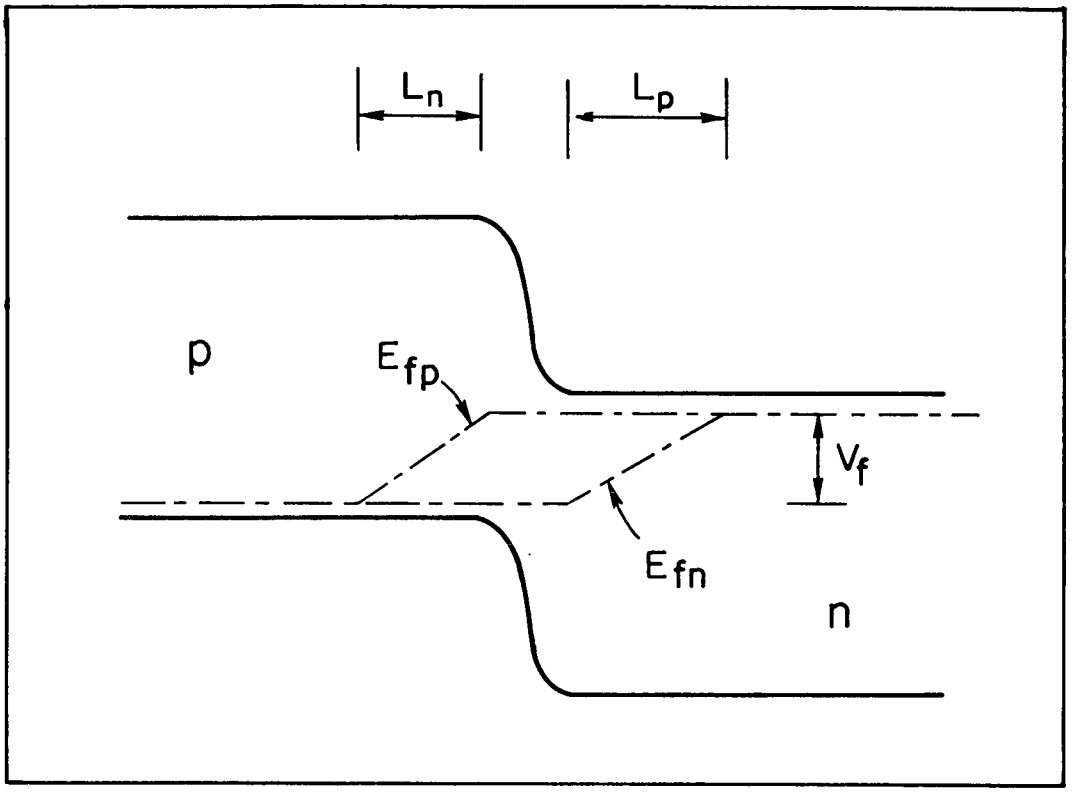

FIG. 2-1. Energy band diagram for a forward biased p-n homojunction.

(5) The injected minority carrier densities are small compared to the majority carrier densities so that their charge does not modify the band profile.

Such a model leads to the current-voltage relationship

$$J = J_o \left\{ \exp\ (qV_f/\eta kT) - 1 \right\}$$

where η is a numerical factor equal to one in this case. In real but close to ideal junctions $1 < \eta < 2$. J_o is given by

$$J_o = q \left\{ n_p L_n/\tau_n + p_n L_p/\tau_p \right\}$$

where n_p and p_n are the minority carrier densities in the p- and n-type

materials respectively and L_n and τ_n are the diffusion length and minority carrier lifetime for electrons in the p-type material. L_p and τ_p are the corresponding quantities for holes in the n-type material.

If we consider recombination at states in the forbidden band in the junction region, a term

$$J_R = \sigma_x v_t N_t w_d n_i \left\{ \exp(qV_f/2kT) - 1 \right\}$$

is added to the junction current where σ_x is the capture cross section of the recombination centers, N_t is their density, v_t is the electron's thermal velocity, w_d is the depletion layer width, and n_i is the intrinsic carrier density of the material. Note the temperature dependence of the log J_R versus V_f slope for this term is proportional to 1/2kT

In real devices we must consider the effects of series and shunt resistances. Although these are distributed parameters their effects are well represented in most cases by an equivalent circuit such as shown in Fig. 2-3 (omitting the current source). For $V_f \gtrsim 2R_s I_o \exp(qV_f/\eta kT)$, the series resistance R_s (arising mainly from the contacts and the bulk material of the diode) will dominate the I versus V_f characteristic with a V_f/R_s dependence. In the low current region, the shunt resistance R_t (mainly due to leakage across the junction) dominates for $I \lesssim V_f/2R_t$, again giving a linear dependence of I on voltage. These effects are considered in Si solar cells by Stirn[102].

Formation of a quasi-insulating layer (by compensation of donors adjacent to one side of the junction for example) changes the basic diode to a so-called p-i-n structure. The forward characteristic isn't modified in general unless $w_i > L_a$, where w_i is the i-layer thickness

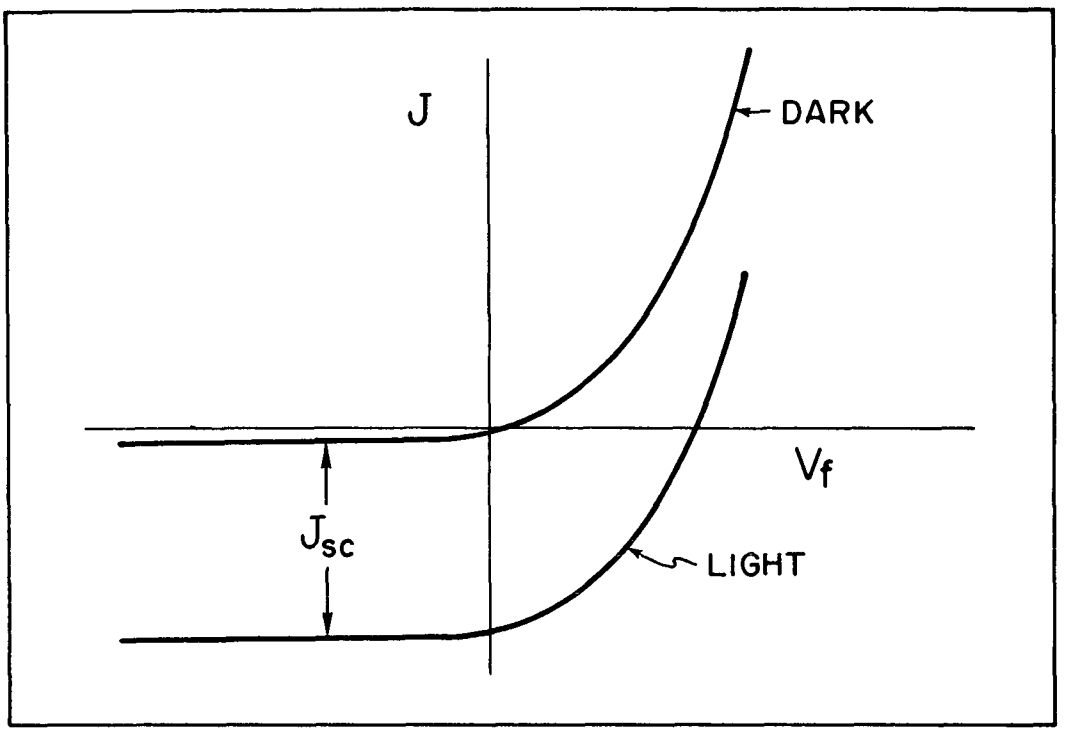

FIG. 2-2. Dark and light I-V characteristics for an ideal photovoltaic cell.

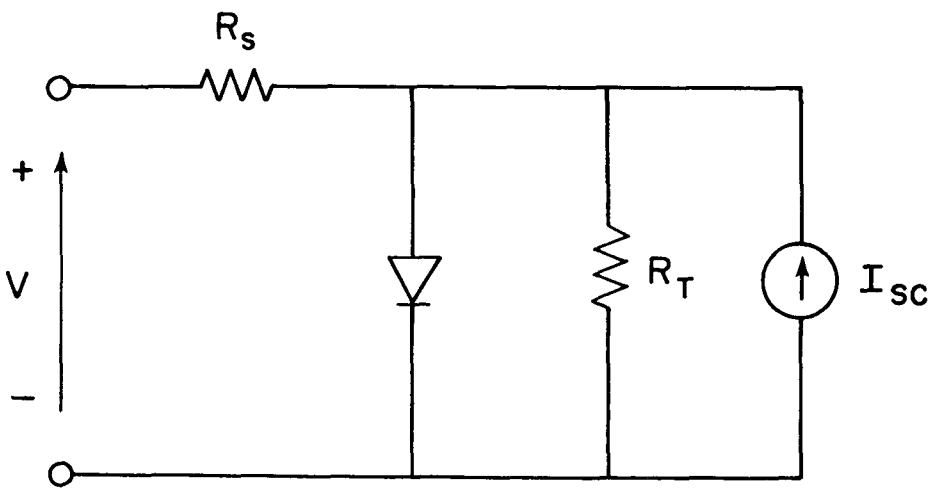

FIG. 2-3. Equivalent circuit for the photovoltaic cell.

and L_a is the ambipolar diffusion length in the region.* When $w_i > L_a$, the I-V_f characteristic may be dominated by space-charge-limited flow depending on whether single or double injection is occurring and on the presence of traps in the i-layer. This situation has been studied for the Cu_2S-CdS system with thick (>10μ) i-layers by Keating[9]. The presence of space-charge-limited current is usually indicated by a power law dependence of I_f on V_f.

For an ideal photovoltaic cell we assume the following:

(1) Uniform illumination.

(2) Uniform absorption of photons within a minority carrier diffusion length of the junction interface.

(3) Photoexcited carrier density negligible compared to the majority carrier density.

For these conditions the dark J versus V_f characteristic is just displaced by the short-circuit photocurrent, $J_{sc} = qg(L_p + L_n)$, for a volume generation rate g so that (see Fig. 2-2)

$$J = J_o \left\{ \exp(qV_f/kT) - 1 \right\} - qg(L_p + L_n).$$

Thus the short-circuit current is proportional to light intensity. The temperature variation of J_{sc} is that of L_p and L_n, so that for lattice scattering $J_{sc} \sim (L_p + L_n) \sim T^{-1/4}$, and for charged impurity scattering $J_{sc} \sim T^{5/4}$. For the open-circuit voltage V_{oc}, the temperature variation of J_o dominates and as the temperature goes to 0°K, V_{oc} approaches E_g/q, where E_g is the band gap of the material.

Consideration of the effects of series and shunt resistance leads to:

---

*Gill finds L_a = 3-5μ in un-HT cells[16].

$$I = I_o \left\{ \exp \alpha(V_f - IR_s) \right\} + (V_f - IR_s)/R_t - I_{sc}$$

where α is the diode factor. ($\alpha = qV_f/\eta kT$ for the Shockley diode.)

2.2 Heterojunctions

When semiconductors of two different materials are joined, a heterojunction is formed with differences in band gap E_g, electron affinity χ, work function ϕ, and crystal structure across the junction. In addition to the built-in potential (analogous to that in the simple homojunction diode), discontinuities are introduced in the conduction and valence bands by the differences in band gap and electron affinity of the two materials. The resulting band profile is shown in Fig. 2-4. This so-called abrupt junction model (which neglects interface states) developed by Anderson[54] and others is a straightforward modification of the homojunction diffusion model of Shockley.

In graded junction theory due to Van Ruyven and Williams[103] and others there is a more gradual change from one material to the other due to alloying with the result that the discontinuities are smoothed. However, according to Van Ruyven[61] the abrupt junction theory may be more appropriate for the Cu_2S-CdS cell since these materials do not form mixed crystals. Although considerable interdiffusion doping may occur, the solubility limits the proportion of Cu in the CdS for example, to a percentage which is too small to affect the CdS band gap. Thus the transition region from one band gap and electron affinity to the other is very thin. An excellent review of current thought on heterojunctions is given by Van Ruyven[61].

Heterojunctions can have several different configurations of course but the one in which we are particularly interested is shown in Fig. 2-4.

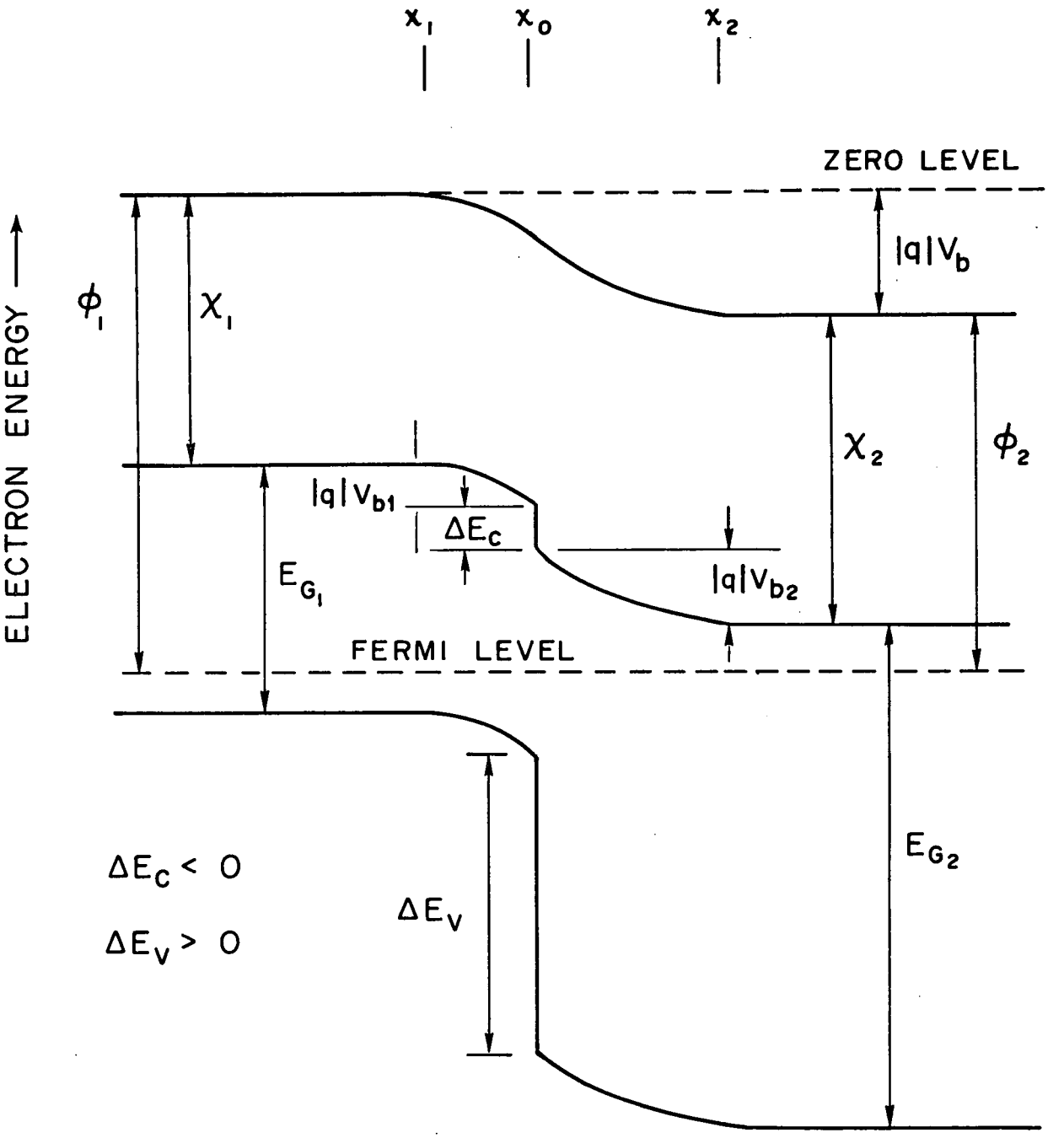

FIG. 2-4. Energy band diagram for an abrupt p-n heterojunction. The p-type material has an acceptor density N_{A1} and a permittivity ε_1 while the n-type material donor density is N_{D2} and its permittivity is ε_2.

The conditions imposed by our system, $E_{g1} < E_{g2}$ and $N_{A1} >> N_{D2}$, offer some simplification. The proportion of the barrier voltage, $V_b = V_{b1} + V_{b2}$, appearing on either side of the junction is given by $V_{b1}/V_{b2} = N_{D2}\varepsilon_2/N_{A1}\varepsilon_1$ for zero bias so that in the Cu_2S-CdS cell V_{b1} is very small. The other condition, $E_{g1} < E_{g2}$, implies (given the doping of our materials) that the barrier for holes traveling to the right is much larger than that for electrons traveling to the left and that the hole current can be neglected for most situations of interest.

Interface states formed as a result of lattice mismatch between the two crystal structures making up the junction may have a large effect on its electrical transport properties.*

For large lattice mismatches the density of interface states due to dangling bonds is large and they are confined to a thin region. For smaller mismatches it is energetically more favorable to spread the interface states over a thicker region. If a system with a given lattice mismatch is graded the number of interface states is not reduced. Oldham and Milnes[56] estimate the surface density of interface states of most heterojunctions of interest to be at least $5 \times 10^{13}/cm^2$.

Defect states near the interface formed by interdiffusion doping may play a role similar to that of the interface states and in practice it may be difficult to distinguish the two kinds of states.

Interface states can play two roles in the heterojunction: (1) they may have a large effect on junction current transport by acting as recombination and/or tunneling centers and (2) they may modify the band profile in the junction region by trapping charge.

---

*The possibility of interface dipoles is not considered here because the simpler model is sufficient to explain the results.

One treatment of current transport through interface states suggested by Oldham and Milnes[56] and Donnelly and Milnes[104] involves the assumption of a metal-like layer of recombination centers between the two semiconductors. The carriers are thermally excited over Schottky barriers to the recombination layer as shown in Fig. 5-2. Because of the thermal excitation the model would be expected to lead to a current-voltage dependence proportional to $\exp\{AV_f/kT\}$ where A is a constant. Since the recombination centers are treated collectively forming the quasi-metallic layer, assumptions must be made about the minority carrier transmission coefficient of the layer as well as about the position of the quasi-Fermi levels there.

A treatment involving both tunneling and recombination through individual interface states is proposed by Riben and Feucht[58] to account for the temperature independence of the log I versus V_f slopes and the absence of minority carrier injection observed in many heterojunctions. They propose a qualitative model involving recombination from the conduction band to states near the junction interface followed by tunneling to the valence band of the other material (or vice versa). Such a model had been used by several workers to explain the excess current in Esaki tunnel diodes (Chynoweth et al.[105], Sah[106]). Figure 5-8 is appropriate. Riben and Feucht's model assumes:

(1) Tunneling is the rate limiting process.

(2) Tunneling takes place through the base of a triangular energy barrier with the current density given by

$$J = BN_t \exp\left\{-4(2m^*)^{1/2} E_b/3q\hbar F\right\}$$

where B is a constant, N_t is the density of interface states, m* is the effective mass of the electrons, E_b is the barrier height and F is the electric field.

(3) The electric field (represented by the slope of the band edges) is given by a maximum approximation for a standard constant donor density depletion layer:

$$F \simeq \left\{2qN_{D2}(V_b - V_f)/\varepsilon_2\right\}^{1/2}$$

(4) The barrier height is given by $q(V_b - V_f)$ and thermal excitation to tunneling levels higher than the bulk conduction band level is not considered.

Such a model leads to the following relationship for the dark, forward-bias current:

$$J = BN_t \exp\left\{-\alpha(V_b - KV_f)\right\}$$

$$\alpha = \frac{4}{3\hbar}(m^*\varepsilon_2/N_{D2})^{1/2}$$

and $K = 1/(1 + N_{A1}\varepsilon_1/N_{D2}\varepsilon_2)$ expresses the proportion of the applied voltage appearing on the n-type side of the junction ($K \simeq 1$ in our case).

According to this model the slope of the ln J versus V_f characteristic is independent of temperature. At constant bias voltage the current depends on the variation of V_b with temperature. If the band gap of the Cu_2S is assumed to vary linearly with temperature (with a coefficient, A) then, to a first approximation, the constant bias current varies as $\exp(+AE_{g2}T/q)$.

Since theoretical values of α were higher than those obtained experimentally, Riben and Feucht modified their model to use a staircase tunneling pathway involving several centers within the forbidden band[59].

Lindquist[17] treated a similar problem for Cu_2S-CdS heterojunctions in which the tunneling and recombination were assumed to be through a layer of interface states with a uniform distribution in energy, and thermal excitation to levels higher than the bulk conduction band level was included. The resulting expression for the dark, forward-bias current could not be integrated exactly. However, an approximate integration yields

$$I \simeq \frac{A}{(q/kT - 2\beta\eta)} \exp\left\{-2\beta\eta(V_b - V_f)\right\}$$

for $q/kT > 2\beta\eta$ and with $\beta = (1/\hbar)(m^*\varepsilon_2/N_{D2})^{1/2}$ where A and η are constants. This expression again gives a ln I versus V_f slope which is almost independent of temperature.

Modification of the junction band profile by charging of interface states is the other major effect of these states on the junction transport properties. Oldham and Milnes[56] found that in n-n Ge-Si heterojunctions a charged layer of interface states moved the band edges with respect to the Fermi level producing a double depletion layer which controlled current transport. The best evidence for such a double depletion layer is a reversal in sign of the photovoltaic current generated by such junctions as the wavelength of the illumination is changed. The conduction band edge slopes downward on both sides of the interface. Thus photon energies just larger than the smaller band gap produces current of one sign. Photon energies greater than the larger band gap cause

photoexcitation on the other side of the interface and a current of opposite sign which dominates the total current. This has been observed by Van Ruyven, et al.[98] in n-n Ge-GaP heterojunctions and by Van Opdorp and Vrakking[99].

In the Cu_2S-CdS junction the movement of the band edges with respect to the Fermi level due to interface state charging is effectively limited on the Cu_2S side by the large acceptor density there. Thus most of the change effected by trapping of charge at interface states occurs on the lightly doped CdS side.

Gill[16] and Lindquist[17] proposed such trapping effects as a mechanism for control of current transport in the Cu_2S-CdS cell. Certain states could be optically charged by short wavelength illumination and the resulting positive charge density decreased the width of a conduction band spike to enhance the cell photocurrent. These effects were interpreted as being due to defect states in the CdS near the metallurgical interface but characteristic of the bulk CdS. Decreasing the positive charge (and the cell current) can also be accomplished optically. Details of these effects in Cu_2S-CdS cells are given in Sections 1.2.4 and 4.3.7.

2.3 Junction Capacitance

When a junction is formed between semiconductors with different work functions, ϕ_1, ϕ_2, a redistribution of charge takes place. This redistribution forms an extended dipole layer which supports the barrier voltage resulting from the alignment of the Fermi levels. In each material the necessary charge is provided by the formation of a depletion layer whose width adjusts itself according to the available free carrier

density so that overall charge neutrality is maintained. The relation between barrier voltage, junction capacitance, and the free carrier densities follows directly from the solution of Poisson's equation and the requirement of overall charge neutrality.

An excellent treatment of the basic theory is given by Gossick[62], and Van opdorp has derived the C-V relations for many common doping profiles[92].

For uniform doping on both sides of a p-n heterojunction, the capacitance per unit area, C, is given by:

$$1/C^2 = \frac{2}{q}\left\{\frac{\varepsilon_1 N_{A1} + \varepsilon_2 N_{D2}}{\varepsilon_1 \varepsilon_2 N_{A1} N_{D2}}\right\}(V_b - V_f)$$

where $V_b = (\phi_1 - \phi_2)/q$ is the barrier voltage, V_f is the forward bias voltage, N_{A1} and N_{D2} are the net acceptor and donor densities of the p- and n-type materials respectively, and ε_1, ε_2 are their permittivities. For $N_{A1} >> N_{D2}$ this reduces to

$$1/C^2 = 2(V_b - V_f)/\varepsilon_2 N_{D2}\, q \qquad (2\text{-}1)$$

and the depletion layer is almost entirely on the lightly doped side. (We shall henceforth let $\varepsilon_2 \approx \varepsilon$ and $N_{D2} = N_D$). Note that N_D is the total positive charge density in the depletion region which may include filled hole traps as well as ionized donors. Extrapolation of the linear $1/C^2$ versus V_f curve to $1/C^2 = 0$ gives the barrier voltage and the slope of the curve gives N_D. In general data for forward biases greater than $\sim V_b/2$ is unreliable because of carrier injection effects.

If N_D is a function of distance from the interface, $N_D = N(x)$, the $1/C^2$ versus V_f curve is no longer a straight line but for $N_{A1} >> N(x)$ we

can still obtain N(x) from the slope of the curve. We obtain

$$N(x) = \frac{dV_f}{d(1/C^2)} \quad \frac{2}{q\varepsilon} \tag{2-2}$$

For each bias voltage the depletion layer width is given by $x = \varepsilon/C(V_f)$. The barrier voltage, however, can no longer be determined simply by extrapolation of the high reverse bias slope.

One approach to the incorporation of the effects of interface states into the junction capacitance relationships is to consider the case of an intermediate layer of a different donor density than the bulk of the n-type material. If its width is w_i and its donor density is N_i we obtain

$$w_d^2 = \frac{\varepsilon^2}{C^2} = w_i^2 \left(1 - N_i/N_D\right) + \frac{2\varepsilon}{qN_D} \left(V_b - V_f\right)$$

for $N_A >> N_D, N_i$. The value of N_D is still given by Eq. (2-2) for $w_d \geq w_i$ but the extrapolated barrier voltage V^* is now

$$V^* = V_b + \frac{q}{2\varepsilon} \left(N_D - N_i\right) w_i^2$$

For $N_i = 0$, this reduces to the expression obtained by Bethe for the p-i-n diode.

A more complete description of the capacitance of a heterojunction with interface states and dipoles which includes the dependence on the frequency of the ac test signal is given by Donnelly and Milnes[93]:

$$1/C^2 = \frac{\left[\frac{2(\varepsilon_1 N_{A1} + \varepsilon_2 N_{D2})}{q\varepsilon_1\varepsilon_2 N_{A1} N_{D2}}\right] \left(V_b - V_f - \delta - BQ_{IS}^2\right)}{\left[1 + \frac{f(V)}{1 + (\omega\tau_Q)^2} \frac{dQ_{IS}}{dV} + \frac{1}{1 + (\omega\tau_\delta)^2} \frac{d\delta}{dV}\right]^2} \tag{2-3}$$

with

$$B = [2q(\varepsilon_1 N_{A1} + \varepsilon_2 N_{D2})]^{-1}$$

where Q_{IS} is the surface density of interface states, δ is the magnitude of the interface dipole, τ_Q and τ_δ are the relaxation time constants for Q_{IS} and δ, dQ_{IS}/dV is the contribution to C due to the differential change in interface charge, $d\delta/dV$ is the differential change in the dipole, and f(V) is a factor depending on the magnitude and sign of dQ_{IS}/dV.

Since trapping times related to the photocapacitance effect are long we can neglect the dynamic term. The $1/C^2 = 0$ intercept is now given by

$$V^* = V_b - \delta - BQ_{IS}^2$$

and N_D may be obtained from the slope of the curve as before. Lindquist found some frequency dependence for the zero bias photocapacitance in heat-treated Cu_2S-CdS cells for $f < 10^3$ Hz but only a small (10%) change from 10^5 to 10^6 Hz and concluded that the test frequency used for $1/C^2$ versus V curves (1 MHz) the trapped charge was not responding to the test signal in a dynamic manner.

In summary, the effect of interface state charging is to change the intercept voltage of the $1/C^2$ versus V curve without changing its slope. Although an estimate of the total interface charge can be obtained, additional input is required to discriminate between dipoles and a surface or volume charge layer and to determine the thickness of such a layer.

2.4 Photochemical Reactions

The term photochemical reaction (PCR) has been given to certain slow changes in the electronic properties of crystals induced by exposure to light while the crystal is held above some threshold temperature. The changes are irreversible until the crystal is heated above another characteristic temperature.

The concept of PCR appears to have originated as an explanation for changes in the optical transmission spectrum of alkali halide crystals on exposure to light. The effect was attributed to the optically assisted agglomeration of certain crystal defects forming electron trapping centers. (F centers): An electron optically removed from one F center is trapped at another F center thus producing two oppositely charged F centers. To bring together the defects required a diffusion step which accounted for the necessity of a threshold temperature for the "optical" process. Since the diffusion distances are of the order of 10 to 100 Å, however, the temperatures can be quite low. Annealing at a higher temperature dispersed the defects and destroyed the agglomerate. PCR effects have been investigated extensively in the alkali halides and the above model has been confirmed in KCl (Compton and Rabin in 1964[66], also see Van Doorn[107]).*

---

*It is interesting to note that the essential characteristics of PCR are quite similar to those involved with the phenomena of photocrystallization in amorphous Se (p-type) observed by Dresner and Stringfellow[85]. In that process bonds in the chains of amorphous Se are broken by the absorption of light. Holes are trapped which then accelerate the growth of crystallites due to an electric field at the crystalline-amorphous boundary. Since the growth rate under illumination increases rapidly with temperature (following an $\exp\{-\Delta E/kT\}$ law), a characteristic temperature can be defined analogous to T_p below which photoexcitation is no longer able to assist in the agglomeration of chain fragments to form a crystallite. In this case the agglomerates are macroscopic and the melting point corresponds to the annealing temperature (or TSC peak) of the PCR.

Apparently the first suggestion of a type of PCR in CdS crystals was as an explanation for slow decreases of photoconductivity at constant light intensity observed by Böer, Borchardt, and Borchardt[67] in 1954. Woods[68], in 1958, again used the PCR to explain certain changes in the thermally-stimulated-current (TSC) curves in CdS due to illumination at various temperatures. PCR in alkali halides may, of course, be a basically different phenomenon than PCR in CdS. These have been two different ways of observing PCR.

In the study of TSC curves the usual procedure is to anneal the crystal at a higher temperature T_A and then cool it with illumination present below some temperature, $T_I \leq T_A$, to a low temperature (usually 77°K). On subsequent heating at a constant rate in the dark a complex set of characteristic peaks in the conductivity versus temperature (TSC) curve appear. As T_I is decreased toward some threshold temperature T_p, some of the TSC peaks disappear--those not associated with traps that are formed by PCR between T_I and T_p.

In the study of the decrease of photoconductivity under constant illumination, the crystal is annealed at a higher temperature T_A, cooled in the dark to T_I (now in a sensitive state) and held there while being exposed to light. The photoconductivity slowly decreases to a minimum corresponding to an insensitive state providing that T_I is above the threshold temperature, T_p. Thus the TSC method examines the creation of traps by PCR while the photoconductivity decrease method deals with the effect of PCR on the recombination centers affecting the photoconductivity lifetime. Whether the same, related, or different defects are involved in these two kinds of effects is not unambiguously known.

Additional investigations of the photoconductivity decrease effect in CdS have been carried out by Böer[70] who showed that the decrease in photoconductivity was due to a decrease in carrier density (i.e., carrier lifetime). Borchardt[71,72], using a variety of impurities, found a range of T_p from ∿240°K for undoped material to ∿400°K for Cu doping.* He ascribed the decrease of photoconductivity to optically assisted thermal diffusion of sulfur vacancies and the effect of the centers thus created on recombination kinetics in the crystal. In 1961, Albers[73] attributed the effect to sulfur vacancies diffusing from the surface into the bulk of the crystal (a concept later contested by Tscholl).

Most recent work on PCR in CdS has been done using the conductivity decay method. Bube in 1957[76] and 1959[77] and Bube and Barton[78] (1959) observed similar effects but attempted to find an alternative to the PCR interpretation. Nicholas and Woods[79] (1964), in an excellent survey, discussed six trapping levels in CdS prepared with excess sulfur with depths ranging from 0.05 to 0.83 eV using other work as well as their own. Only the 0.83 eV level (with TSC peak at 290°K) was associated with the PCR and this was discussed more fully in another paper by the same authors[80]. Korsunskaya et al.[81] also studied PCR in CdS with excess S which is particularly interesting because the PCR produced an increase in photoconductivity (due to new sensitizing centers) rather than a decrease as seen by other workers.

Bube et al.[82] in 1966 found a trapping level at 0.73 eV in CdS-CdSe which obeyed monomolecular kinetics and could only be filled at $T \geq$ ∿180°K. Rather than a PCR explanation, they initially proposed that

*The values of T_p found by Borchardt are much higher than those found in this work (∿200°K for Cu doping).

the trap was surrounded by a coulomb repulsive barrier. In 1970, Im, et al.[84] (1970) using CdS with excess S measured the wavelength dependence of trap filling for the equivalent trap and found that it could not be explained by the coulomb repulsive model.

Cowell and Woods[83] in 1969 identified two traps in CdS:S with depths of 0.63 eV (with a TSC peak at 310 to 320°K) and 0.85 eV (TSC peak, ∿280°K) with a PCR effect and found $T_p \simeq 185°K$ and 245°K respectively. They suggested that the traps were an aggregate of Cd vacancies.

Tscholl in 1968 presented an excellent paper[69] in which he surveys earlier work and presents a model based on the photo-agglomeration of crystal defects. According to this model T_p is controlled by the diffusion of the defects. He suggests that a single set of defects is responsible for the whole group of traps seen above ∿100°K, their energy being varied by the distances between the defects in the crystal. Tscholl's experiments done with CdS:Cu include the effects of additions of isovalent Ni. He argues against the repulsive barrier theory of Bube, et al.[82] (which requires a double acceptor). Although Tscholl was mainly concerned with general changes in a total TSC curve, we can find a TSC peak at 350°K with a T_p between 230 and 270°K in his data for a CdS:Cu sample with a Cu concentration of $\sim 10^{19}/cm^3$. Tscholl notes that in what he calls a condition of "good compensation" (i.e, the majority of the recombination centers occupied by electrons in the dark) the filling of the traps formed by PCR is accompanied by an increase in the density of vacant recombination centers and hence a decrease in photoconductivity lifetime.

Most recently, Kanev, et al.[74] in 1969 observed a photoconductivity decrease in highly Cu doped CdS crystals and suggested a model in which

certain slow recombination centers are converted (by the irreversible loss of an electron to a peculiar trap) to faster recombination centers by the action of light. He found $T_p \simeq 220°K$ and that the effect began with a Cu concentration of $\sim 4 \times 10^{18}/cm^3$ and increased in magnitude with higher doping levels. Kanev, Fahrenbruch, and Bube[75] in 1971 found that similar effects exist in heat treated Cu_2S-CdS photovoltaic cells and have a large effect on their output.

Chapter 3

EXPERIMENTAL METHODS

3.1 Preparation of Samples

All experiments were performed on samples cut from the same CdS crystal boule grown in the Stanford Center for Materials Research Laboratories[100]. Using resublimed 99.999% pure starting material the crystal was grown by vapor transport in an evacuated quartz ampoule employing a method described by Piper and Polich[101]. The crystal had a donor density (probably due to excess Cd) of about $0.4 \times 10^{16}/cm^3$ as determined from four point conductivity measurements (assuming an electron mobility of 400 cm^2/volt sec). The boule was optically clear and free of visible imperfections. Laue back reflection photographs used to align the boule showed it to be a single crystal.

The CdS crystal was diced into samples about $4 \times 2 \times 1.5$ mm^3 with the c-axis normal to the large faces. A short etch in dilute HCl was used to identify the crystallographic polarity (on etching the b-face becomes diffusely reflecting).* Ohmic contacts of pure In were applied by pressure to both end faces and the samples were annealed in H_2 at 200-250°C for several minutes. The large faces were then optically polished using γ alumina (0.03μ) as the last polishing agent.

After cleaning in boiling TCE, acetone, deionized H_2O and finally methanol the samples were mounted on glass slides and masked to expose only one surface using Lacomit (T. M., an excellent maskant manufactured

---

*a-face (Cd, (0001)); b-face (S, $(000\bar{1})$).

by W. Canning and Co. Ltd., Birmingham 18, England).* Generally the samples were etched (if required), rinsed, and stored in H_2O until dipping.

The epitaxial Cu_2S layer was formed by an exchange reaction at 75°C in an aqueous solution of Cu^+ ions according to the reaction

$$CdS + 2Cu^+ \rightarrow Cu_2S + Cd^{++} \qquad F°(298°K) = -29.6 \text{ kcal/mole.}$$

The reaction rate is discussed in Section 4.1.

The dipping reaction was carried out in a temperature controlled "resin reaction flask" shown in Fig. 3-1. Pure argon flowing through a porous glass bubbler during the dipping provided an inert atmosphere and stirred the solution. The H_2O was previously boiled in the flask for 20 minutes with Ar flowing to eliminate dissolved oxygen after which 19.8 g/l of CuCl, 37.3 g/l of KCl, and 13.9 g/l of hydroxylamine hydrochloride** were added without appreciably disturbing the Ar blanket. A small amount of HCl was added until a pH of ∿3 was obtained. The solution was clear and colorless and the undissolved CuCl was grey-white. After the reaction proceeded for the allotted time (usually ∿30 min) the samples were withdrawn quickly, rinsed in H_2O, polished with soft tissue to remove clinging CuCl, and demounted in acetone. The solution was colorless at the end of the dipping reaction except longer dipping times when it appeared slightly blue-green.

---

*Several other maskants were tried (including black wax) but they produced an invisible film across the crystal surface which inhibited film nucleation for short dipping times.

**Hydroxylamine hydrochloride (NH_2OH HCl) reacts with any Cu^{++} ions present according to $NH_3OH + Cu^{++} \rightarrow 1/2\ N_2 + Cu^+ + H_2O$ to prevent oxidation of the Cu^+ to Cu^{++} during the dipping reaction.

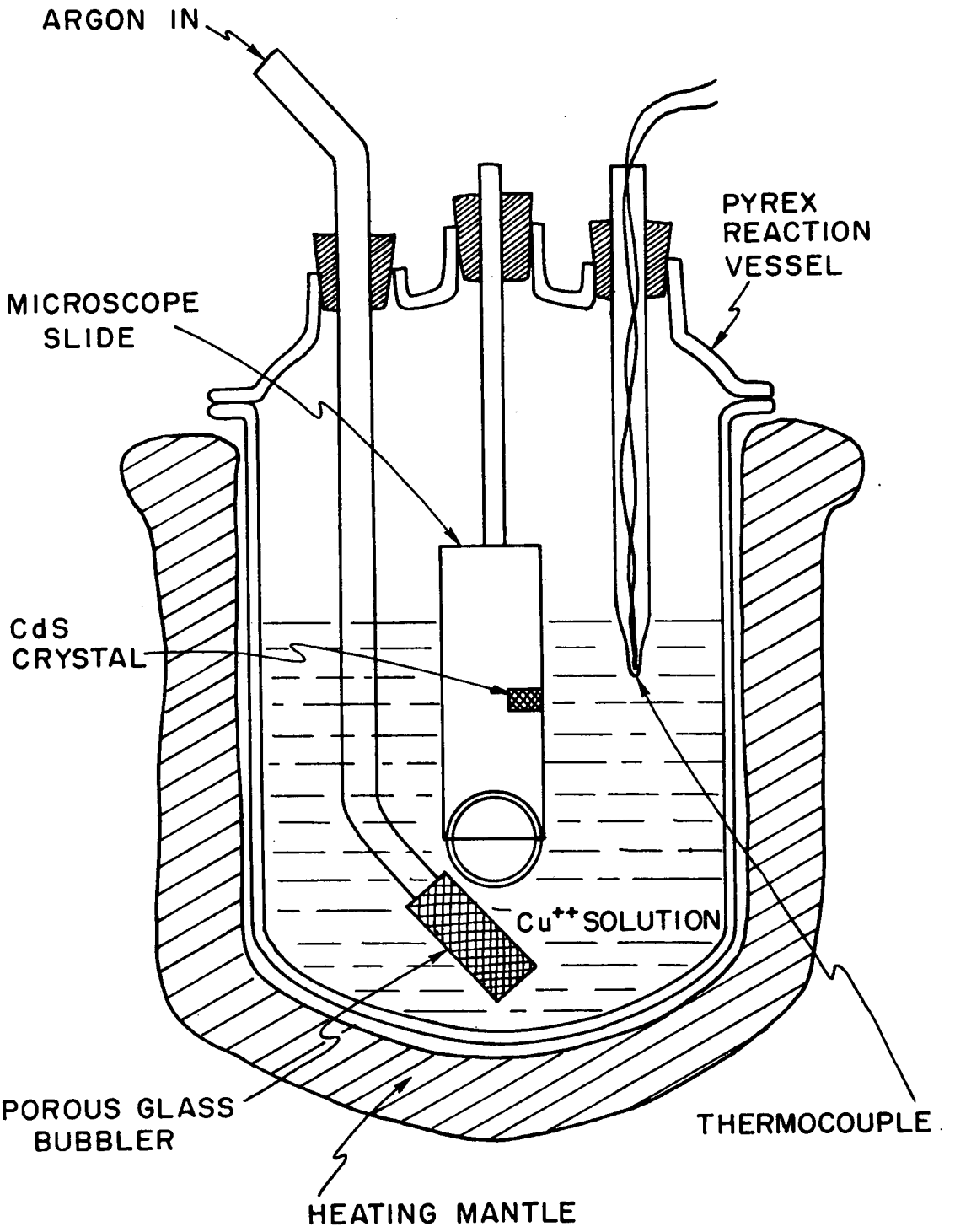

FIG. 3-1. Reaction vessel for dip forming Cu_2S layer.

To determine the Cu_2S film thickness the samples were mounted on their sides in glycol phthalate (m.p. 70 to 120°C), ground and polished and measured with a metallurgical microscope to $\sim$0.5μ. Thus these cells have been heat-treated for several minutes at temperatures not over 120-130°C. Finally the Cu_2S was contacted with Ga-In alloy* and the electrical properties of the cells were measured.

Several cells were made in the usual manner described above with special care to avoid any heat-treatment above the dipping temperature of 75°C during preparation. The resulting cells were very uniform and had a high short-circuit current density J_{sc} and open-circuit voltage V_{oc}:

$J_{sc} = 12$ mA/cm^2 at 280 mW/cm^2, white tungsten light

$J_{sc} = 5$ mA/cm^2, $V_{oc} = 0.43$ V } in normal sunlight

Except for a somewhat higher J_{sc}, these cells were identical with those having undergone the 120°C heat treatment.

Several homogeneously Cu doped single crystal photoconductors were made from the same CdS boule as the above cells. After polishing the 4 x 2 x 1.5 mm^3 CdS samples a layer of Cu sufficient to give the required doping level was evaporated on two opposite surfaces. The crystals were then annealed at $\sim$730°C in a sealed quartz ampoule containing about 1/2 atmosphere of H_2 for 26 hours. This rather severe anneal resulted in vapor transport of about 10% of the volume of the crystal to the ends of the ampoule but gave homogeneous doping. The crystals were noticably

*Ga-In alloy was used rather than Cu or Ag paint contacts because of the slower diffusion rate of the former elements.

darkened by the Cu doping but were still transparent. They were then polished on all sides and ohmic contacts of In-Ga alloy applied as in previous work. Sample #94 with an estimated Cu concentration of $5 \times 10^{17}/cm^3$ and a dark conductivity of less than $10^{-10}/\Omega cm$ was used for the experiments reported here.

The samples used in the work reported in this thesis are listed below:

Sample #	Type	Cu_2S Thickness, μ	Area, mm^2
36	b-face cell	9	$\sim$4
61	a-face cell	10	3.51
62	a-face cell	10	3.57
81	a-face cell	12	4.07
89	a-face cell	$\sim$10	$\sim$4
94	CdS:Cu photo-conductor	(length $\sim$4 mm, cross sectional area $\sim$1 mm^2)	

3.2 Apparatus

For electrical measurements the experimental apparatus shown in Fig. 3-2 was used for both the cells and the photoconducting crystal. This apparatus provided a vacuum, H_2, or air environment over a temperature range of 90°K to 600°K, with primary and secondary photoexcitation sources. All measurements were made in situ and thus sample transfer in the light was eliminated. The two light beams were directed at the sample at the bottom of an evacuable chamber immersed in liquid N_2. A bifilar chromel winding on a copper sample holder mounting supplied heat and a brass thermal resistance was connected to the base which was in thermal contact with the liquid N_2. This system was capable of a cooling time of 20-25 sec from 200°C to 60°C. Because of the exponential

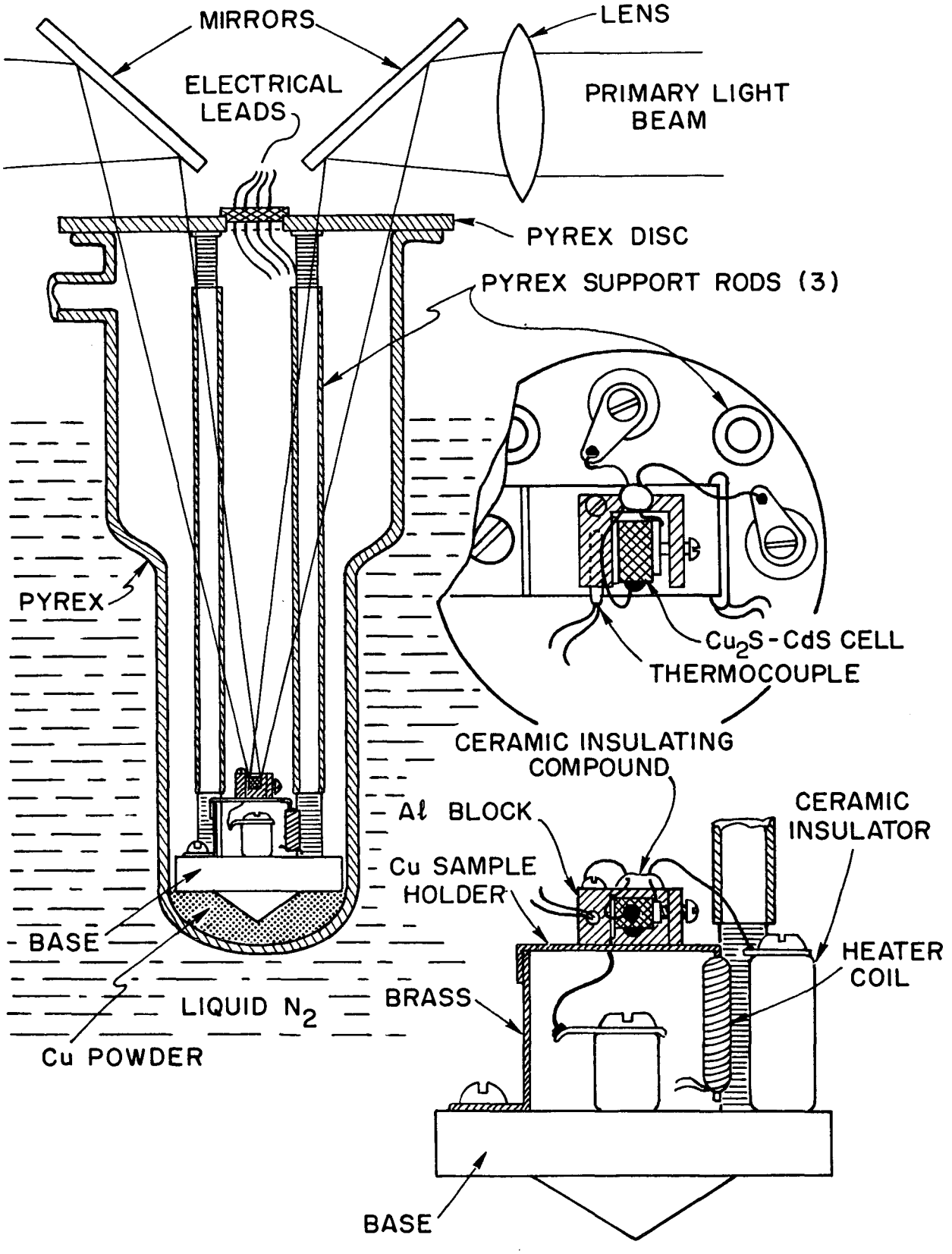

FIG. 3-2. Sample environment.

dependence of the restoration process on 1/T, this actual cooling rate corresponds to only about 2 to 4 sec of effective changes in cell properties.

The thermocouple was mounted in a well drilled directly into the aluminum sample holder block which surrounded the sample on three sides to insure thermal equilibrium (a fourth side of the sample was adjacent to the copper mounting). Thermal contact with the mounting block was maintained with a thin layer of a high thermal conductivity silicone compound. The cells were mounted so as to receive backwall illumination (through the CdS).

A Bausch and Lomb 500 mm grating monochromator with tungsten ribbon source was used as a primary (wavelength sweeping) light source and another Bausch and Lomb 250 mm grating monochromator provided the secondary (or bias) light. Both were filtered when appropriate with Corning 2-64 and 7-56 filters to eliminate the higher order spectra. The energy flux was measured at the sample location with a Perkin-Elmer thermopile.

Electrical connections using a shielded two lead system connected to ground only at the current meter permitted very low level measurements ($<10^{-10}$ A). The current measurements were made using a Hewlett-Packard 425A microvoltmeter connected across precision resistors such that the maximum voltage drop was either 1 mV or 0.1 mV. Voltage measurements were made on a Keithley 610A electrometer with an input resistance $\sim 10^{14}$ ohms. Meter outputs were connected to an X-Y recorder. The electrical system is shown in Fig. 3-3.

Junction capacitance measurements were made on a 1 MHz Boonton 75D capacitance bridge with a 1000x range extender. The signal level was adjusted to $\sim$20 mV. Series resistance corrections were made using resistance

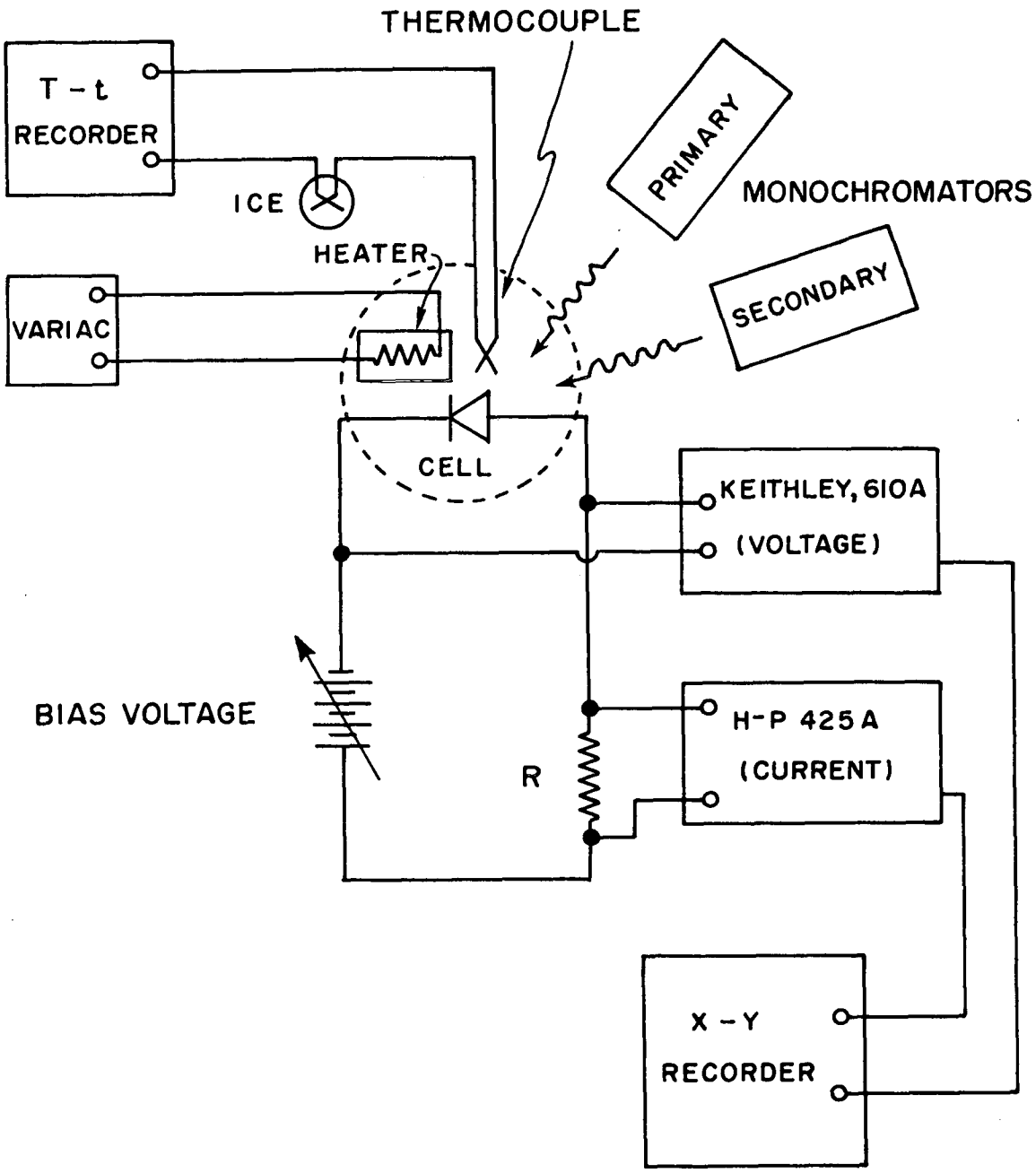

FIG. 3-3. Schematic diagram of electrical measurement circuit.

values determined from pulsed forward-bias current measurements for biases up to 10 volts (pulse length 10 μsec at a repetition rate of ~20/sec).

Chapter 4

EXPERIMENTAL RESULTS

"Never does nature say one thing and wisdom another" - Juvenal

The results section is divided into three parts in order to put the data into better perspective:

4.1 A discussion of Cu_2S layer growth on CdS single crystals, the effect of pre-etching the CdS on cell properties, and of the diffusion of Cu into CdS.

4.2 The thermally restorable optical degradation effect in cells and CdS:Cd:Cu photoconducting crystals.

4.3 Junction properties, where the detailed characteristics of individual states of the cell and the photoconductor are investigated to provide a knowledge of the actual structure of the junction and its influence on cell output.

Because of the frequent use of the following terms, their acronyms are used: HT, for heat treatment; BHT and AHT, for before and after HT; and TROD, for thermally restorable optical degradation (either the total effect or the degradation aspect in particular).

4.1 Junction Formation

4.1.1 Growth of the Cu_2S Layer

The topotaxial formation of the Cu_2S film on oriented single crystals of CdS by dipping appears to be a reaction-rate limited process. Furthermore, under the conditions of small thicknesses and low temperatures, the progress of the reaction is strongly affected by difficulty in nucleation.

Generally, the nucleation rate is proportional to $\exp(-\Delta G/kT)$, where ΔG, the free energy change, contains two terms, one less than zero dependent on the bulk or volume change in free energy, and the other, usually greater than zero, which is dependent on the surface energies involved. The surface energy term depends on the preparation of the substrate and it is decreased considerably at scratches induced by polishing, etch pits, and other surface defects. After nucleation, a transformed portion of the CdS tends to become larger (smaller) if it is greater (smaller) than a critical size such that the bulk energy changes begin to dominate the effect of surface energy changes.

Evidence for this nucleation difficulty comes from the observation of nucleation only on polishing scratches but no where else for short dipping times. The nucleation for the a-face is more difficult than for the b-face. Occasionally the b-face thickness of Cu_2S will exceed that of the b-face on the same sample (dipped simultaneously), even though after nucleation the a-face growth rate is 3 times the b-face rate.

Examination of cells with noncontinuous Cu_2S layers reveals evidence of antinucleation behavior in regions of crystal damage due to polishing scratches. In some cases the scratch itself was polished away leaving a track of damaged material. Although these damaged regions were invisible at 400x in reflected light, a track about 8μ wide failed to nucleate by the time the rest of the film was 2-3μ thick. Examination of a visible scratch showed that sufficient polishing damage was present to prevent nucleation up to about 5μ from the scratch edge. Nucleation occurred in the scratch mark itself however. The radius of antinucleation is consistent with the radius to which the dislocation density is

appreciably increased by surface scratches as observed by other workers. This result is surprising since the increased number of dislocations present near the scratch should strongly aid nucleation.

After nucleation is accomplished the layers grow at a constant rate as shown in Fig. 4-1. Extrapolation of these curves fits the data of Lindquist[17] quite well showing a growth rate linear in time up to a layer thickness of over 200μ with the a-face rate being 3 times that of the b-face.

4.1.2 CdS Substrate Etching and Surface Roughness Effects

The results of an investigation of the dependence of cell properties on the pre-dipping surface treatments given to the CdS single crystal substrates are summarized briefly here[86]. It should be pointed out here that there is a definite dependence of cell properties on the thickness of the Cu_2S layer, presumably resulting from the lattice mismatch between Cu_2S and CdS, as found by Lindquist[17].

Surface treatment effects may be conveniently separated into (1) geometrical effects depending on the interface shape and texture, and (2) chemical effects arising from the introduction of impurities and defects into the materials forming the junction.

The geometrical quality of the interface can be altered by polishing, etching, or other chemical action during substrate preparation and dipping. The resulting interfacial effects include:

(a) a change in the light absorption coefficient due to multiple reflections

(b) exposure of crystal planes other than c faces to film formation (which may have different electrical properties)

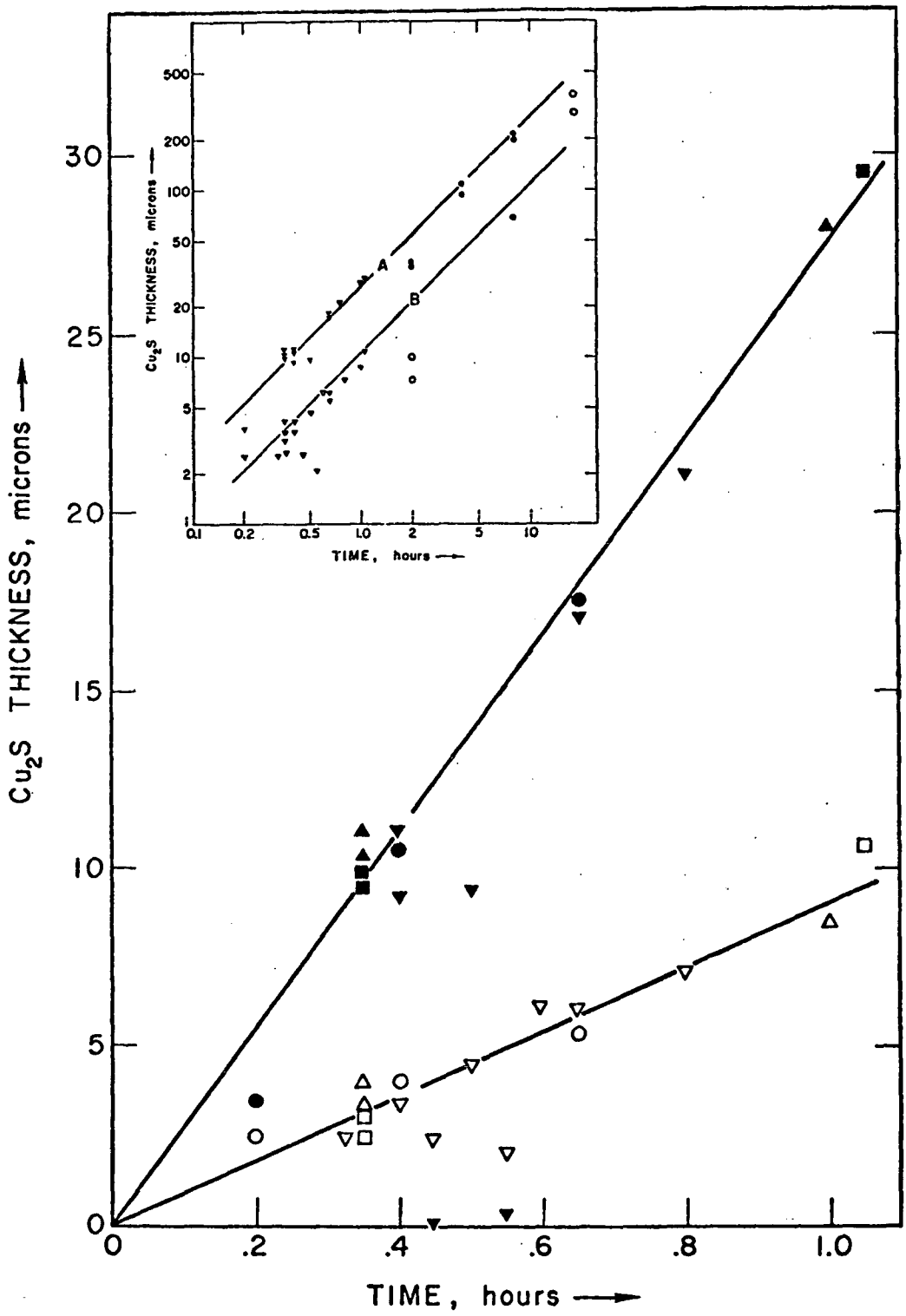

FIG. 4-1. Cu_2S layer thickness versus dipping time at 75°C. Pre-dip etches are: ○ HCl, □ HI, △ HBr, and ▽ none. The same linear growth rates are compared with Lindquist's data[17] in the inset (●○, Lindquist's data; ▼▽, data from figure below).

(c) the effect on lattice mismatch strain at the interface

(d) the presence of residual polishing strain fields

(e) changes in the grain size and defect density of the Cu_2S layer.

For example, b-face cell interfaces are generally much smoother and the film thicknesses more regular than are those of a-face cells. A typical interface profile is shown in Fig. 4-2. Macroscopic surface roughness of the CdS substrate is retained at the outside (Cu_2S-dip) surface as the CdS is transformed, while the Cu_2S-CdS interface profile is altered during its travel into the crystal by growth processes. In particular, the cracking or channeling behavior of the Cu_2S gives rise to a

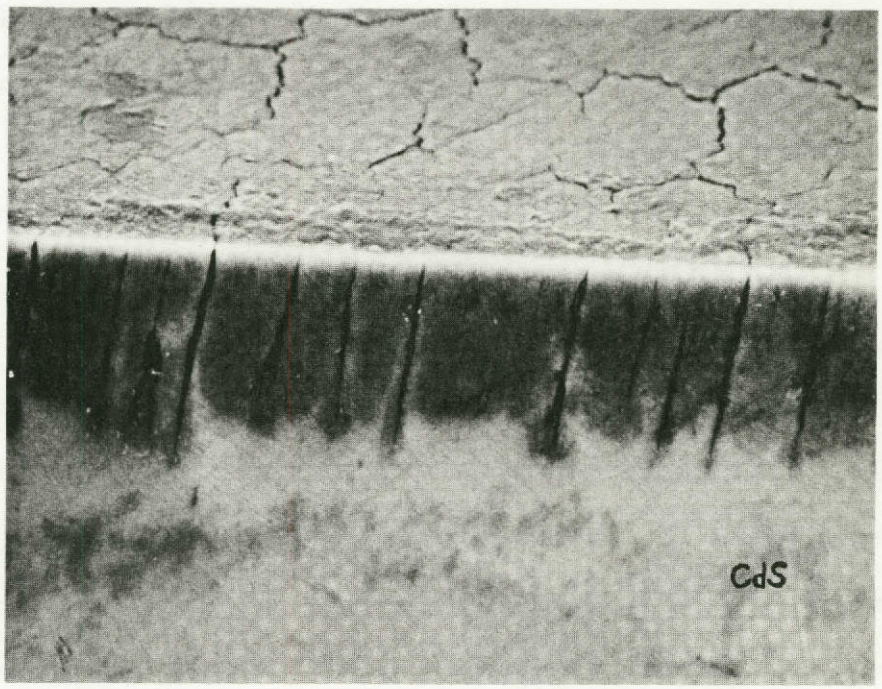

FIG. 4-2. Scanning electron microscope photograph of Cu_2S-CdS cell at 2000x. Cu_2S (about 10μ thick) appears as dark band (SEM photograph by Loren Anderson).

characteristic scalloped interface. This may result from either or both of the following effects: (1) the channeling aids movement of the Cu^+ ions from the dipping solution to the interface and (2) the maxima of the interfacial stress field are centered around the intersection of these cracks with the Cu_2S-CdS interface. The latter reason is favored since growth rate is controlled to rather large thicknesses (>100μ) by the choice of a or b face (the a-face growth rate being ∿3 times the b rate), thus implying that growth is controlled at the interface rather than by transport through the bulk of the Cu_2S. This is also implied by the linear dependence of layer thickness on time shown in Fig. 4-1.

Chemical influences include:

(a) the introduction of foreign defects by the halogen impurities remaining from the etching step

(b) changes in stoichiometry of the Cu_2S due to interfacial stress, the choice of a or b face, or the presence of Cu^{++} ions in the dipping solution

(c) residual Cu^+ or Cd^{++} concentrations in the layer when the cell is removed from the dipping bath.

It is expected that the first of these effects would be greater for thinner Cu_2S layers. Since the dipping reaction takes place in a Cl^- ion environment, the chemical role of an HCl etch should be small unless chemisorption of the Cl^- ion is increased by the etching step.

Fourteen cells with ∿10μ Cu_2S thickness and three cells with ∿2μ thicknesses were prepared. By keeping the thickness of the layer the same between samples, we eliminated variables such as lattice mismatch strain and change of interface profile during growth. The pre-dipping surface treatments used included mechanical roughening of the surface,

and etching with HCl, HBr and HI. Measurements were made at room temperature and included J_{sc} and V_{oc} in white light, dark I-V curves, spectral response of J_{sc} and V_{oc}, zero-bias capacitance and optical transmission of the 2μ cells.

All of these cells received a short heat treatment (1 to 2 min at 100°C to 130°C) during embedding for the polishing necessary to measure the Cu_2S layer thickness. It is thought that this HT does not affect the validity of the results which follow.

The results show that any differences in cell properties with variation in etching and mechanical polishing preparation of the substrate are a relatively subtle effect, comparable to statistical variations in cell behavior of uncontrolled origin. The fact that nonetched samples tended to have comparable electrical properties, suggests that any etching differences that are observed are the result of differences in the geometrical profile of the interface and in film thickness caused by the use of these etchants rather than any chemical effect.

Differences were detected between a and b face cells however. These include:

(1) b-face samples have the highest V_{oc} and usually have the largest J_{sc}

(2) dark reverse bias current is smaller by a factor of 10 for the a-face cells (at -5 volts)

(3) in general the a-face cell of an etchant pair had higher values of the factor α in the diode relation $J_f = J_o (\exp \alpha V - 1)$ than its b-face counterpart, while the values of J_o were lower. (All cells showed a break in the $J_f - V_f$

curve at 0.2 to 0.4 volts so there were two α's and two J_o's involved in this comparison for each cell.)

4.1.3 Cu Diffusion into CdS

It is well founded that the increase of depletion layer width on HT of Cu_2S-CdS cells is due to the diffusion of Cu and the resulting compensation of donors in the CdS. Many workers have studied the diffusion of Cu into CdS[15,22,27,87] (both from Cu films and from Cu_2S layers) and have found diffusion coefficients differing by as much as a factor of 100. Of these, Sullivan's work[27] using a compensated i-layer capacitance method seems most complete and reliable as well as giving the lowest value of diffusion coefficient.

Normally the width of the zero bias depletion layer, w_d, exceeds the width of the compensated, nearly intrinsic layer, w_i. Their difference becomes relatively smaller with increasing w_i (as is discussed further in Section 4.3.8) and w_d becomes a good approximation to w_i for values of >0.5 μm in these cells.

If we assume a diffusion model in which the surface concentration of Cu, $[Cu]_o$, is held constant by the solubility of Cu in CdS then

$$[Cu]\ (x,t) = [Cu]_o \left\{1 - \mathrm{erf}[x/2(Dt)^{1/2}]\right\} \qquad (4.1)$$

and, for constant values of concentration, x plotted against $t^{1/2}$ should have a slope proportional to the square root of the diffusion constant, D. As complete compensation of the CdS donors is approached, the conductivity decreases very rapidly and the value of x for which the Cu concentration approximately equals N_D can be identified with $w_d \simeq w_i$. Data for the HT of a cell is shown in Fig. 4-3 where w_d from capacitance

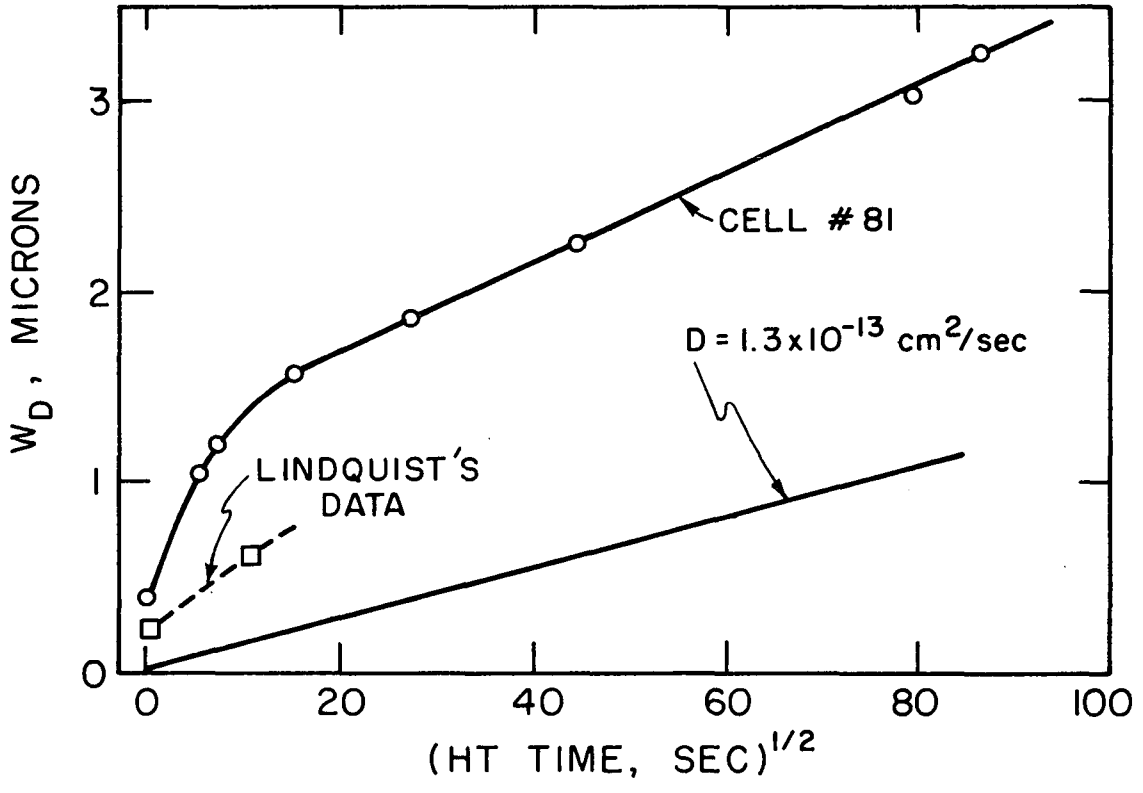

FIG. 4-3. Depletion layer width w_d versus the square root of HT time for cell #81.

measurements is plotted against the square root of the time of HT.* Using a solubility of 3 x $10^{17}/cm^3$ at 200°C from Sullivan[27] and a donor density in the CdS of 4 x $10^{15}/cm^3$ (from $1/C^2$ versus V measurements) we can calculate a value for D. These data indicate rapid diffusion up to $\sim$1μ with D ≃ 120 x 10^{-13} cm^2/sec which then slows to a constant value of 4.6 x 10^{-13} cm^2/sec for greater diffusion depths (in good agreement with D = 1.3 x 10^{-13} cm^2/sec at 200°C from ref. 25). These data suggest that diffusion is more rapid initially because of the effects of the rough interface (typically 0.5μ peak to valley in these cells) and due to the presence of dislocations due to interface strain. The variation of capacitance as the actual interface area decreases toward the geometrical (projected) area during HT predicts that the curve of Fig. 4-3 should be concave upward. However, the variation of effective diffusion rate with interface roughness would have the opposite effect and contribute to the decrease of the diffusion constant as seen in Fig. 4-3. This is particularly true in view of Sullivan's data showing a diffusion rate in the direction $\perp$ to the c axis about 30 times faster than that in the direction $\parallel$ to the c axis.

Also shown in Fig. 4-3 for comparison is a slope calculated from Sullivan's value of D using the donor and Cu surface concentrations as above. Two points from Lindquist's work[17] are shown as well.

---

*The value of w_d actually changes as the state of optical degradation and/or enhancement of the cell is changed (this is discussed in Section 4.3.8). We presume that the diffusion data from capacitance measurements given in the literature for the Cu-CdS system is for the optically degraded and quenched state since this is the normal, equilibrium state at room temperature after exposure to room light for some time. Thus the data presented here is for the degraded, quenched state as well. The cell was HT at 200°C, then cooled to 300°K and degraded before capacitance measurements were made. Diffusion is parallel to the c axis in the CdS.

F

4.2 Thermally-Restorable Optical Degradation

In this section we describe the phenomena involved in thermally-restorable optical degradation (the TROD effect) and show the similarities between its effects in Cu_2S-CdS photovoltaic cells and those in CdS:Cd:Cu photoconducting crystals. These slow transients have been called photochemical reactions (PCR) because of their low rate and quasi-irreversible nature[69,71,72,73,74,84]. Optical degradation leads irreversibly to a degraded state (D state) which is stable until the device is thermally restored to its other stable state (R state). These states are independent of the enhancement and quenching effects observed in such samples in that both the R and D states are subject to enhancement and quenching. We discuss here the time and temperature dependence and the dependence on wavelength of the degrading radiation for optical degradation as well as the temperature dependence of restoration.

4.2.1 Time Dependence of Optical Degradation

When a cell (or photoconductor) is exposed to light of suitable wavelength for optical degradation, the short-circuit current (or photocurrent) rises quickly to a peak (called here the TROD maximum) and then falls slowly. The current plotted against time, called a TROD curve is shown schematically in Fig. 4-4(a).

The falling portions of the TROD curves shown in Fig. 4-4(b) show strikingly similar decay forms for both the cell and the photoconductor.

A phenomenological equation derived in terms of a recombination model (see Section 5.5) gives an excellent fit for the cell over a wide range of conditions including degradation with white light at 300°K and

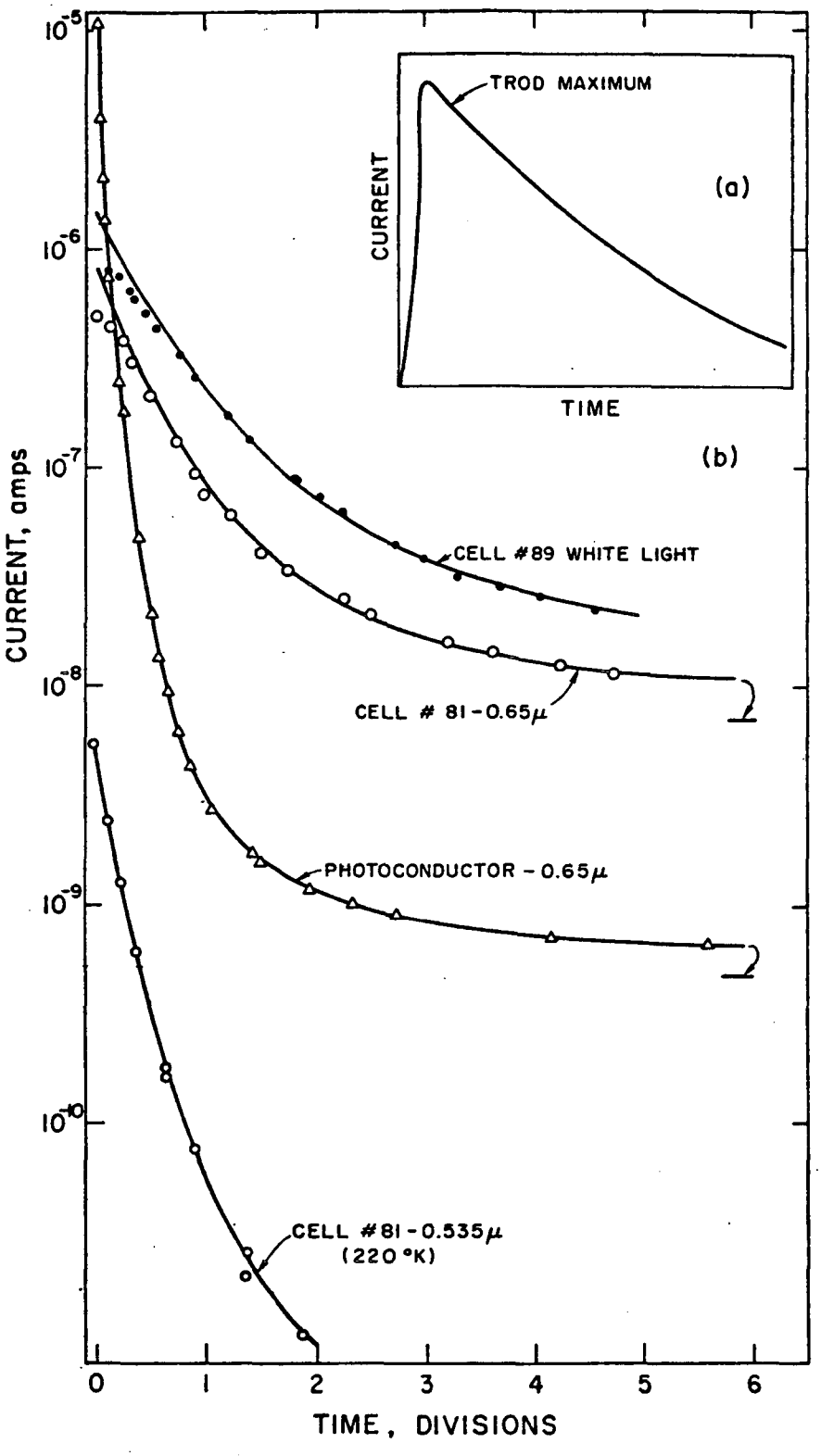

FIG. 4-4. (a) Schematic TROD curve. (b) Short-circuit current and photocurrent versus time during optical degradation. The wavelength of the degrading light is noted on each curve and the time scales are as follows:

Cell #89 white light	200 sec/division
Cell #81 0.65μ	4000 sec/division
Photoconductor 0.65μ	4000 sec/division
Cell #81 0.535μ	100 sec/division

All curves are at 300°K except as noted and the fully degraded values of current are shown at right for two of the curves.

degradation with monochromatic light at 200°K (with variation of parameters of course):

$$I_{sc} = I_m \exp\{-A\,[1 - \exp(-\delta(T)t)]\} \qquad (4.2)$$

where I_m is the maximum current, A is a constant, $\delta(T)$ is the rate of degradation at temperature T, and t is the time. The factor in the square brackets is proportional to the number of recombination centers activated by the optical degradation process.

The first part of the cell data are expected to lie below the curve because of the equilibration of enhancement when the light is turned on; the current rises rapidly to a maximum within 50 sec (called the TROD maximum). The photoconductor curve appears to be of the same nature (i.e., a decay curve when plotted on a semilog graph) but does not fit the above equation well. The curve through the cell data points is plotted from the phenomenological equation while the photoconductor curve is merely drawn as a best fit to the points.*

4.2.2 Temperature Dependence of Optical Degradation

Since optical degradation occurs only above temperatures of 200 to 250°K we conclude that it is both thermally and optically activated. The dependence of the rate of degradation on temperature was measured in terms of the current excited by a low intensity "probe" light. The degree of degradation must be probed at a single temperature since the degree of enhancement varies with temperature. To eliminate the possibility of degradation during probing and to make use of the largest

*The "220°K" curve is degraded at 200°K but it is measured in terms of short-circuit current excited with 0.70μ light in the quenched state at 150°K (see Section 4.3.4).

possible variation in current from restored to degraded state, the samples were probed at 150°K. It is also necessary to standarize the degree of enhancement in some way. For the cell, the maximally quenched situation was chosen as a standard state. This situation is produced by the simultaneous use of quenching light and reverse bias, as demonstrated by Lindquist[17]. The measurement was made in the same manner as the "transient" measurements discussed in Section 4.3.4. For the photoconductor, the equilibrium degree of quenching under 0.65μ illumination was chosen as a standard state.

Thus the degradation of the cell and the photoconductor were measured using the following procedure:

(1) The sample was completely restored.

(2) The sample was cooled to 150°K and:

  (a) after the cell had been quenched with 0.95μ light and 5.0V reverse bias, the initial response to a 0.65μ probe light (11 $\mu w/cm^2$) was measured or,

  (b) the stable response of the photoconductor to 0.65μ light was measured.

(3) The sample was degraded with 0.535μ light of constant intensity at a temperature, T, for 25 sec.

(4) The sample was cooled to 150°K and step 2 repeated.

(5) The sample was again restored and the above steps repeated for a different temperature.

The results are shown in Fig. 4-5 where the data are analyzed in terms of an exponential curve:*

*For small degradation times this equation is a good approximation to Eq. (4.2).

$$I = I_m \exp(-\delta t)$$

where $\delta = \delta_o \exp(-\Delta E/kT)$,

I_m = maximum cell current (restored),

δ = thermally activated degradation rate (δ_o includes the photon flux of the degrading light as a factor).

A plot of $\log_{10} \log_e(I_m/I)$ yields an activation energy for the process of 0.44 eV for the cell and 0.40 eV for the photoconductor. Another method of analysis is to take equivalent degradation times from a plot of current versus time during degradation (such as Fig. 4-4) taken at a median temperature in the range being considered. These times are directly proportional to the rate of degradation for any form of decay law in which δt appears as a product. This procedure yields the same activation energies as the model above.

For the cell optical degradation begins at ∿200°K and is virtually complete at ∿230°K for a 25 sec exposure to 0.535μ light of ∿300 $\mu w/cm^2$ intensity. Under the same conditions degradation in the photoconductor begins at ∿250°K and is virtually complete at ∿330°K.

The similarity between the cell and the photoconductor is clear and the offset in temperature can be attributed to a difference in rate constant, δ_o, such that the rate for the cell is greater by a factor of 160.

4.2.3 Wavelength Dependence of Optical Degradation

The relative effectiveness of various wavelengths of light for optical degradation was studied at room temperature by the following procedure:

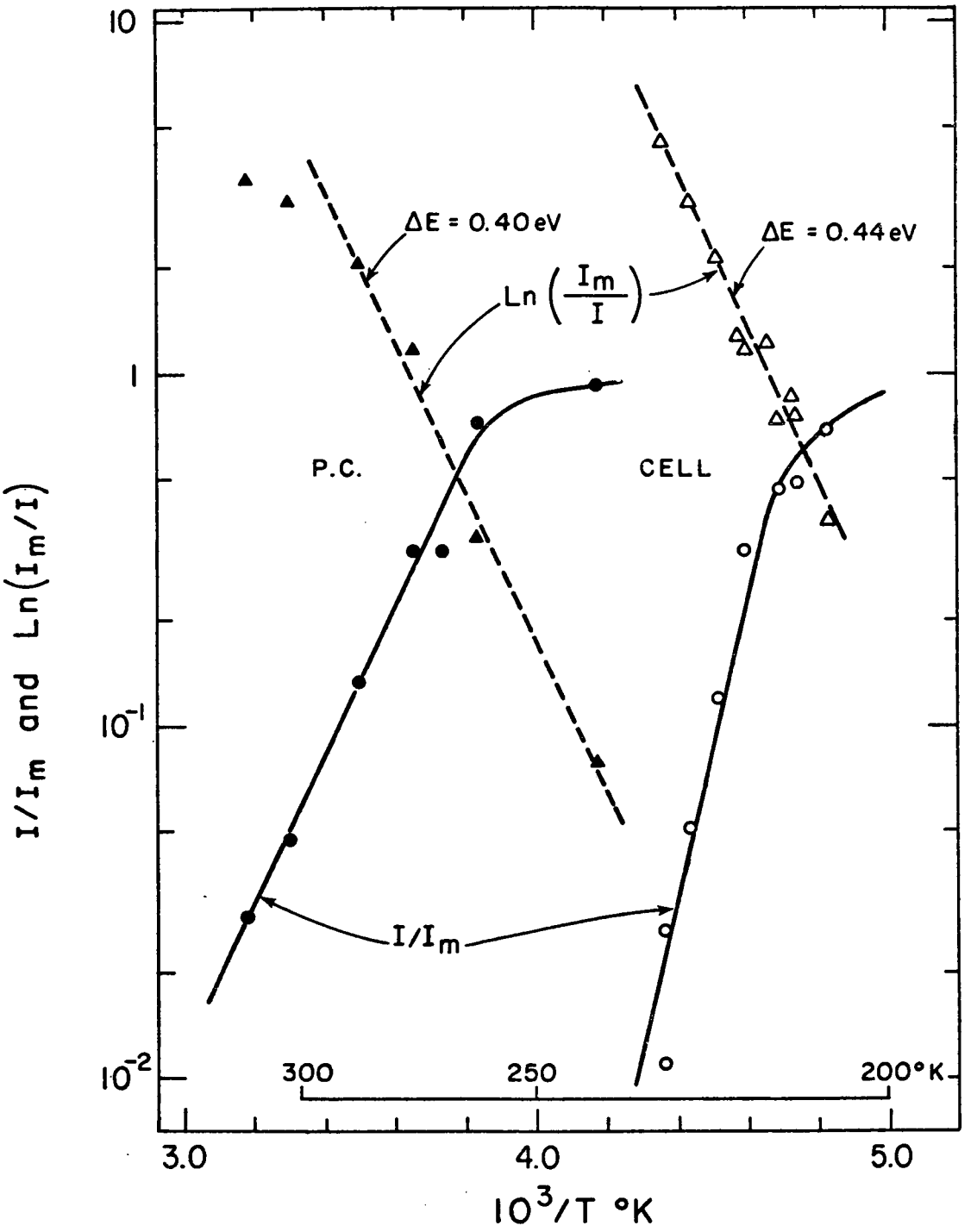

FIG. 4-5. Optical degradation versus reciprocal temperature for cell #81 and the photoconductor #94 relative to the fully restored state. The degree of restoration is probed with 0.65μ light at 150°K (probe current is I with fully restored value I_m).

(1) Probe with weak, white light until the short-circuit current reaches an equilibrium to get I_o.

(2) Degrade with monochromatic light for 25 sec.

(3) Repeat (1) to get I_1 and go on to the next wavelength in step 2.

We assume the approximation of simple exponential decay for the degradation curve that was used in Section 4.2.2 so that Ln I_1/I_o is proportional to Dt. This measurement was carried out over a single degradation cycle using the longer wavelengths first (i.e., the cell was not restored between degradations). The total amount of degradation was limited to decreasing the photocurrent by a factor of 13 to make the above approximation reasonable. We further assume that the degradation rate, D, is proportional to the photon flux in order to normalize the result with respect to photon flux at each wavelength.* Then the effectiveness, η_d, of optical degradation should be proportional to

$$\frac{1}{Ft} \ln (I_1/I_o) \qquad (4.3)$$

at each wavelength, where F is the photon flux, and t is the time of exposure. η_d may be proportional to the cross section for the optical transition involved in the degradation mechanism.

η_d was also calculated on the basis of equivalent degradation times using a white light degradation versus time curve as in Fig. 4-4. The results of both methods of calculation are shown in Fig. 4-6 where η_d is arbitrarily fixed at 1 for 0.535μ light.

---

*Experiments by Kanev, et al.[74] indicate that the degradation rate is proportional to photon flux.

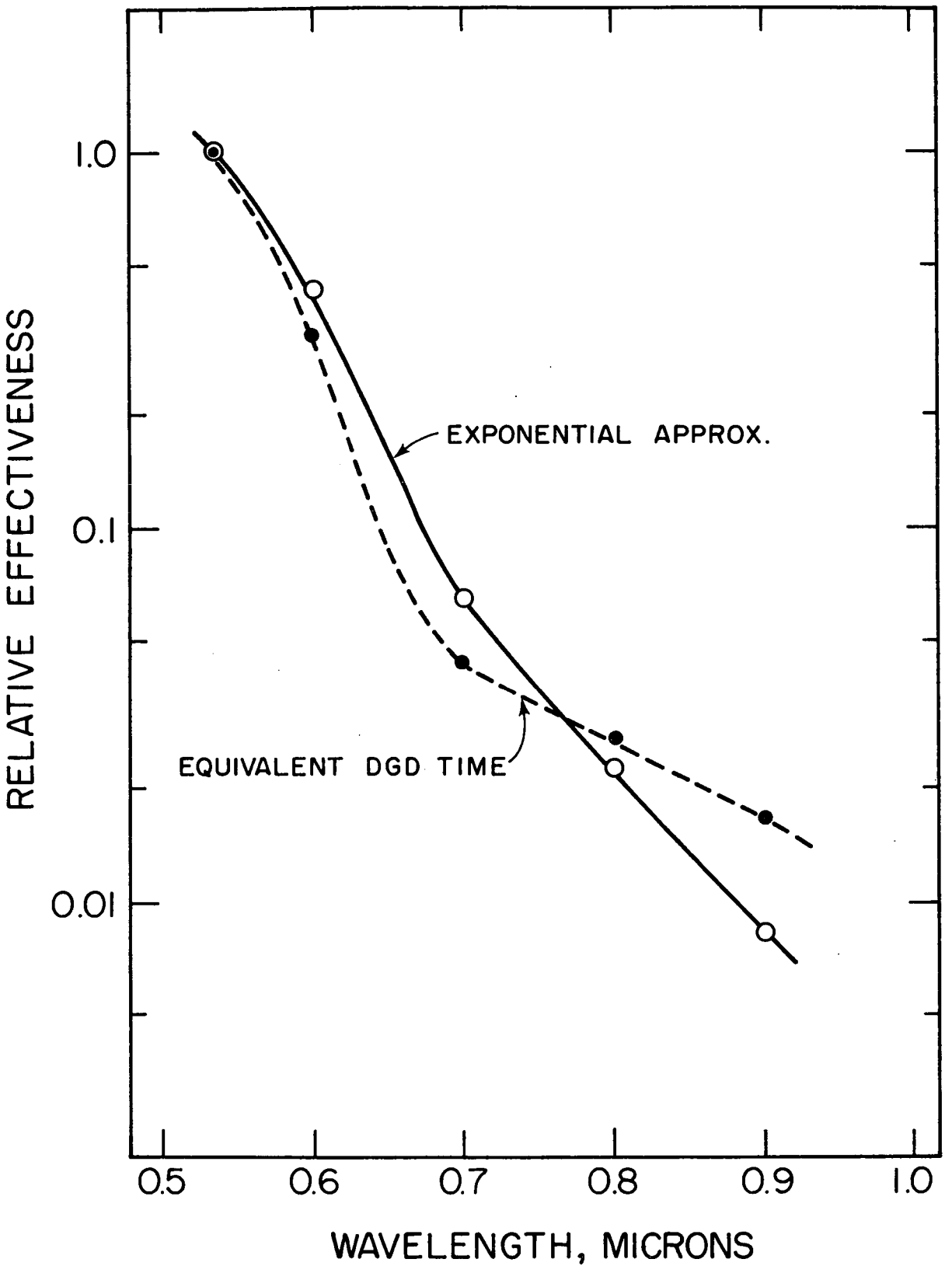

FIG. 4-6. Effectiveness of optical degradation versus wavelength of the degrading light at 300°K. Curves have been normalized with respect to photon flux (8×10^{14} photons/sec cm^2 at 0.535μ).

This measurement is reported as an estimate for η_d and should be considered only as an approximation to the true wavelength dependence, which should be measured with equal photon fluxes for each wavelength, and complete restoration between the degradations at each wavelength.

4.2.4 Temperature Dependence of Thermal Restoration

To measure the temperature dependence of the restoration effect, a cell with extensive previous HT was selected (cell #89 with over 100 minutes of HT).*

Measurements were made as follows:

(1) Full degradation of the cell in white light.

(2) Measurement of cell short circuit current under a constant white light of about 14,000 $\mu w/cm^2$. ($\sim$800 $\mu w/cm^2$ for the photoconductor.)

(3) HT at temperature, T, for 1 min.

(4) Equilibration to room temperature.

(5) Measurement of the TROD curve maximum, I, when exposed to the constant white light.

The current maximum, I, at each temperature relative to the fully restored value, I_m, is plotted again 1/T°K in Fig. 4-7 (solid curves).

The value of the activation energy determined from the above data is dependent on the model used to describe the restoration effect. Thus we cannot expect to simply plot ln I versus 1/T and obtain an activation

*Early in the previous treatments of this cell, a thin film of Cu had been evaporated on the Cu_2S to provide a better contact; after some 90 min of HT the Cu had completely diffused into the Cu_2S. The resulting cell showed stable optical degradation, restoration, and photocapacitive behavior like other cells with less HT and without the Cu film.

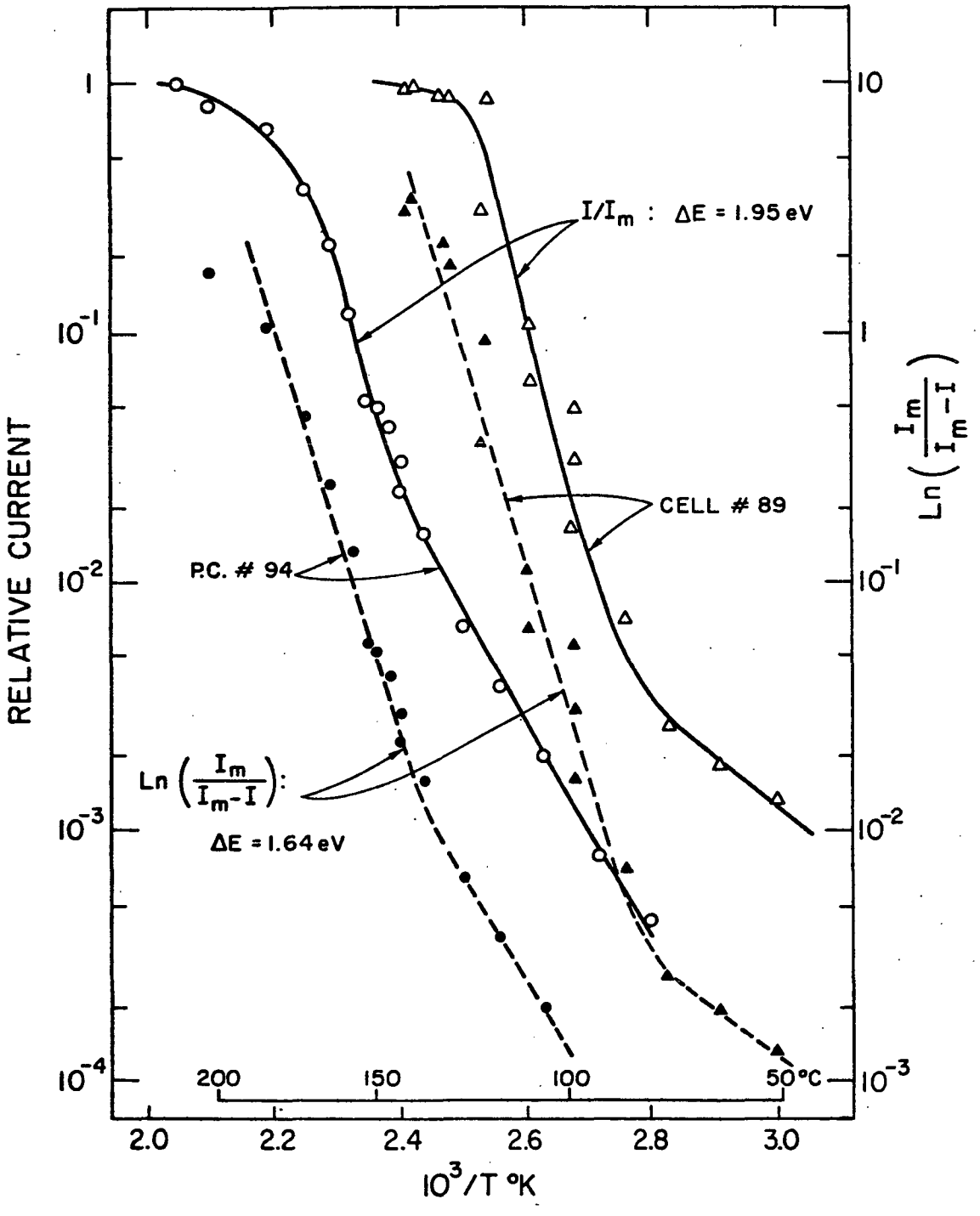

FIG. 4-7. Thermal restoration versus reciprocal temperature for cell #89 and photoconductor #94 relative to the fully restored state. Degree of restoration is probed by TROD curve maximum, I, at 300°K using white light (fully restored current I_m).

energy truly descriptive of the process. The choice of such a model is not obvious. However, we present here a model chosen for its simplicity:

$$I = I_m [1 - \exp(-Rt)]$$

where I_m is the fully restored value of maximum current, and $R = R_o \exp(-\Delta E/kT)$ is the thermally activated restoration rate. A plot of $\log_{10} \{\log_e [I_m/(I_m - I)]\}$ versus $1/T$ yields an activation energy of 1.64 eV for both the cell and the photoconductor (dashed curves of Fig. 4-7). This is to be compared with an activation energy of 1.95 eV obtained from the plots of I versus 1/T (solid curves).

Despite the difficulty with the choice of model, Fig. 4-7 shows the similarity between the cell and the photoconductor. The displacement along the 1/T axis can be attributed to a difference in rate constant, R_o, such that the rate for the cell is greater by a factor of 270. Thus both the rates of degradation and restoration for the cell exceed those of the photoconductor by about two orders of magnitude.

Since both the completely restored and completely degraded values of current remained nearly constant despite more than 35 restorations during this experiment, the independence of the TROD effect and changes in the Cu concentration profile due to diffusion during the restoration is clearly shown. For the temperatures encountered in restoration the rate of Cu diffusion (in a cell with long HT) is so slow that it causes no appreciable changes in cell properties during restoration.

4.3 Junction Properties of the Heat Treated Cell

4.3.1 Relationships of the R, D, E, and Q States

Both the enhanced (E) and quenched (Q) states exist in either the restored (R) or the optically degraded (D) condition of the cell. The same is true for the photoconductor. In the cell, the resulting four states are stable and reproducible at low temperatures and metastable at room temperature, where the E state decays to Q thermally and the R state decays to D optically.

Intermediate states also exist and thus the specification of the state of a cell requires that both the degree of degradation and the degree of quenching be known. Such a state is apparently unique and all states lying on the plane bounded by the points DQ, RE, DE, and DQ are attainable.

The relationship of these states is shown in Fig. 4-8, a symbolic plot of short-circuit current, I_{sc}, for 0.70μ light versus the degree of degradation of the cell. The current values for each state were obtained from the spectral response curves given in the next section. The extent of degradation is a qualitative parameter whose meaning is unambiguously defined only at the end points. Thus we can only say that a sample is completely degraded or completely restored without resorting to some definition for the intermediate points.* Operationally, the extent of degradation is measured in terms of the integrated flux of the degrading light (starting from the restored state; as in Fig. 4-4 or Fig. 4-14) or

*For example, if we select a hypothetical model in which optical degradation is caused by the conversion of a particular crystal defect, Y_R, to another defect, Y_D, then an appropriate definition of the percent of degradation in terms of the concentration of these defects would be $100\ [Y_D]/([Y_D] + [Y_R])$.

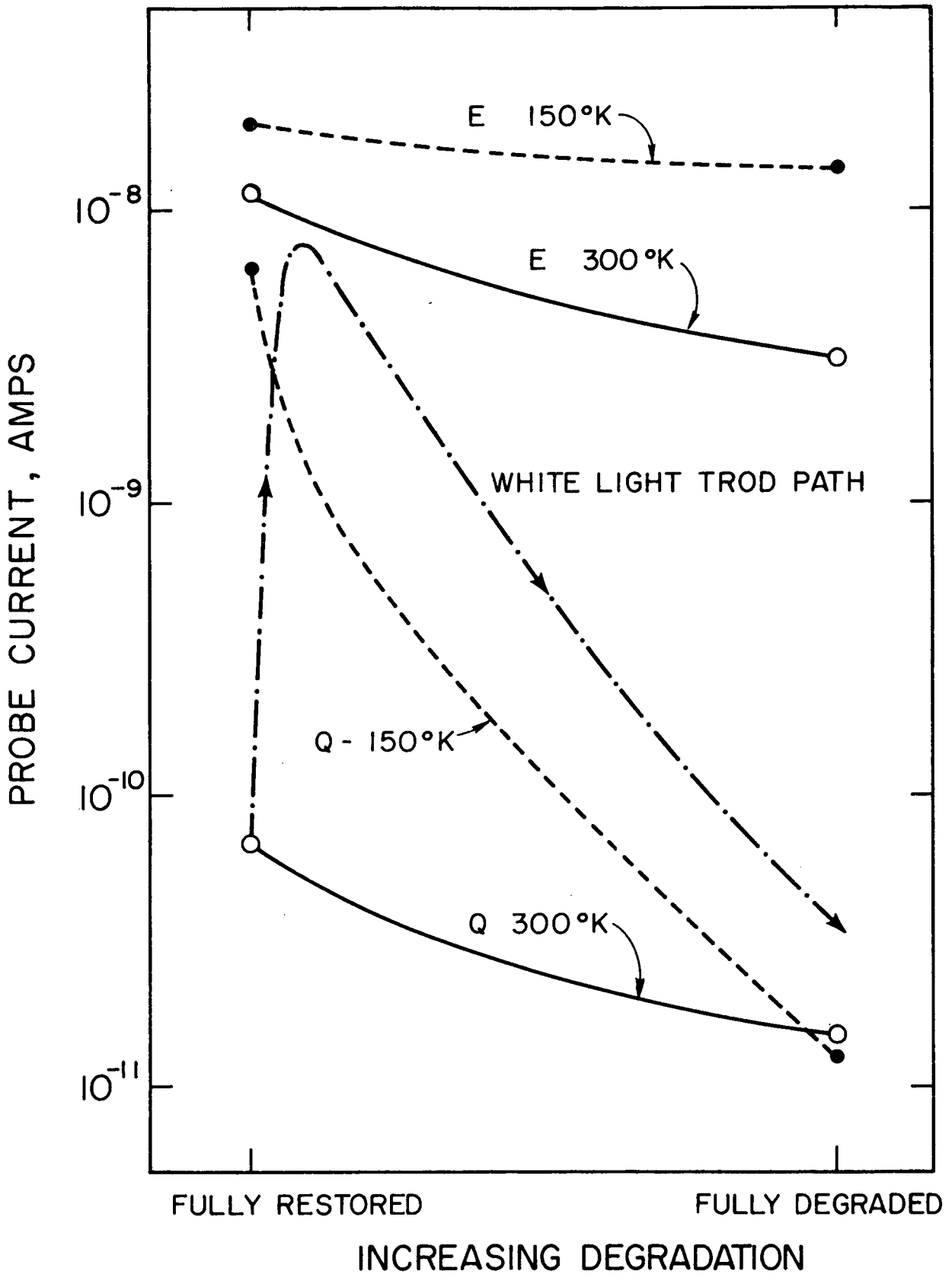

FIG. 4-8. Symbolic plot of low intensity probe short-circuit current (at 0.70μ) versus degree of optical degradation in the enhanced (E) and quenched (Q) states for cell #81. The path of degradation process by white light at 300°K is also shown.

in terms of the time and temperature of restoration (starting from the degraded state). Both of these measures are expected to be nonlinear. The obvious result of degradation is a decrease in I_{sc}. Thus the extent of degradation can be defined in terms of the decrease I_{sc} itself.

4.3.2 Effect of Heat Treatment on Short-Circuit Current

To study the decrease of short-circuit current with HT an "a" face cell (#81) was chosen, with higher than average I_{sc}, and a previous history of only mild HT (100°-130°C) during fabrication. The cell was mounted with a Ga-In alloy contact to the Cu_2S to reduce the effects of diffusion from the contact that would occur with an Ag or Cu contact. This cell was then heat treated for short times up to a cumulative total of 125 min at 200°C. White light was used to determine the TROD curve maximum (as in Fig. 4-4a) as well as the stable short-circuit current, I_{sc}, after degradation. A low intensity white "probe" light was used to measure I_{sc} in the restored state to avoid optical degradation. Since both enhancing and quenching wavelengths are present in white light the cell attains a degree of enhancement appropriate to its state of restoration (more will be said of this in Sections 4.3.5 and 4.3.6). The junction capacitance was measured in the DQ state since this is the equilibrium state at room temperature and thus these data are comparable with the results of other workers. These data are presented in Fig. 4-9.

The current for the restored state reaches a stable value after a short HT ($\sim$1 min) and remains relatively constant for further HT, even though the capacitance and the degraded value of current continue to decrease. Thus there is a large increase in the influence of the TROD effect as heat treatment is continued.

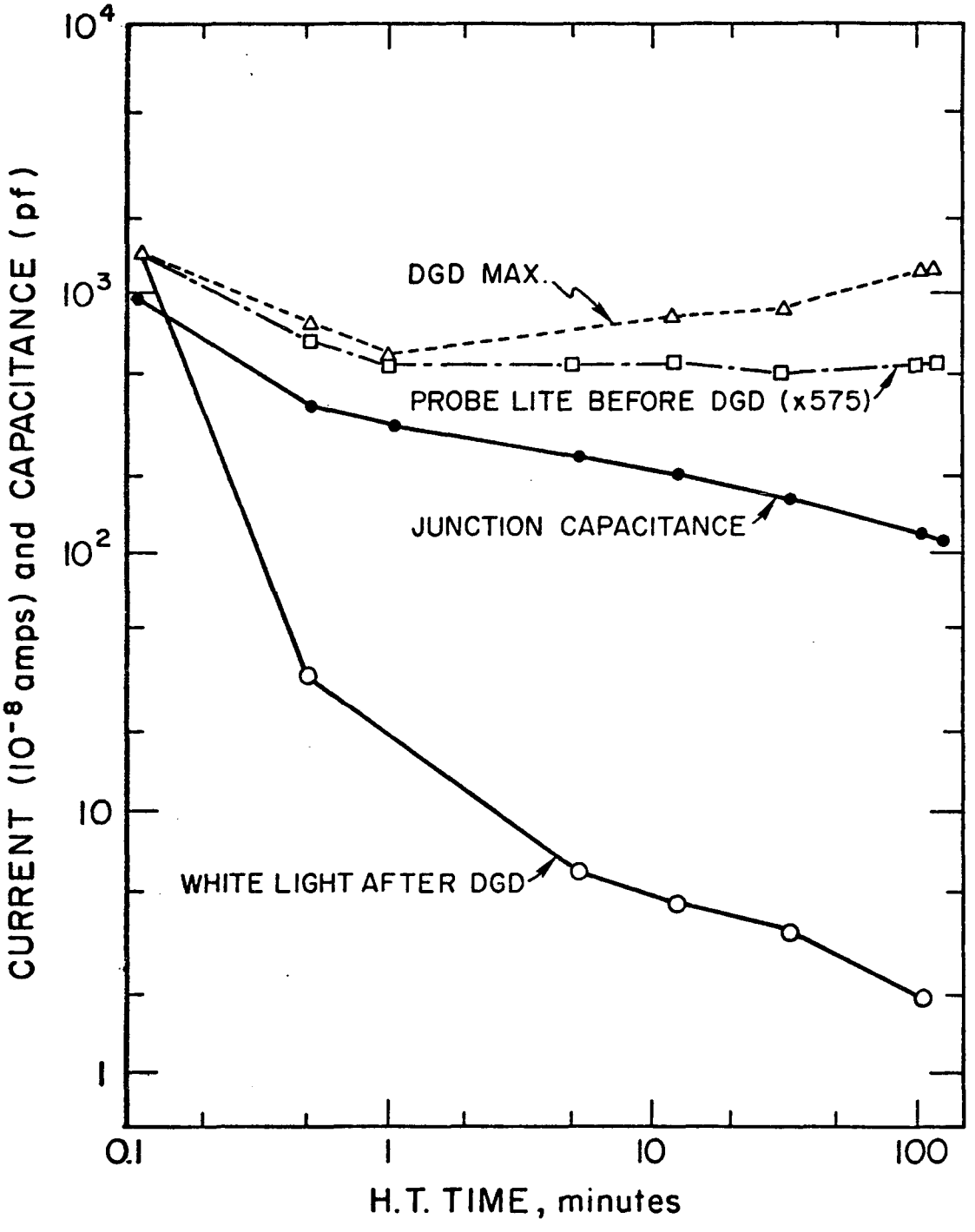

FIG. 4-9. Properties of cell #81 versus cumulative HT time. TROD curve maximum and the current after full degradation is measured with white light (14,000 $\mu w/cm^2$). Probe light current measured with white light (24 $\mu w/cm^2$, down by a factor of 575) in the restored state.

On turning on the probe light after heat treatment, the current rises from a very small value (less than 10^{-10} amp) to its equilibrium value with a rise time of about 5 min. This rise is attributed to the slow attainment of the equilibrium degree of enhancement under weak illumination.

The ratio of enhanced I_{sc} to quenched I_{sc} in the degraded state increases rapidly with HT; from $\sim$3 before HT, to 50-200 after 6.25 min, and finally to 10^3 after 60 min. This effect is discussed in greater detail in Section 4.3.6.

4.3.3 Effect of HT on the Dark Current-Voltage Curves

The behavior of the dark I-V curves with heat treatment is quite complex and there is considerable variance from cell to cell. An example of the behavior is shown in Fig. 4-10 where log I versus forward bias voltage in the DQ state at RT is plotted before HT (but after the usual 1-2 min of 120°-130°C HT during fabrication), after 1-1/2 years of storage in dry air at 300°K, and finally after 6.25 min of HT at 200°C in air. The shelf storage has had the same effect as is seen for short HT at about 100°C. Typically the low bias current rises with short HT and then falls again for longer HT while the high bias (>0.4 volts) current always falls with HT. The values of α for the diode relation $I = I_o$ [exp αV - 1] are also shown on the figure. Lindquist[17] observed the same behavior.

In general the curves consist of 2 straight line segments with no sign of resistive or V^2 behavior until the current becomes limited by the series resistance of the device (due to contacts and the bulk resistance of the CdS and Cu_2S--usually 80-250 ohms); this always occurs at a

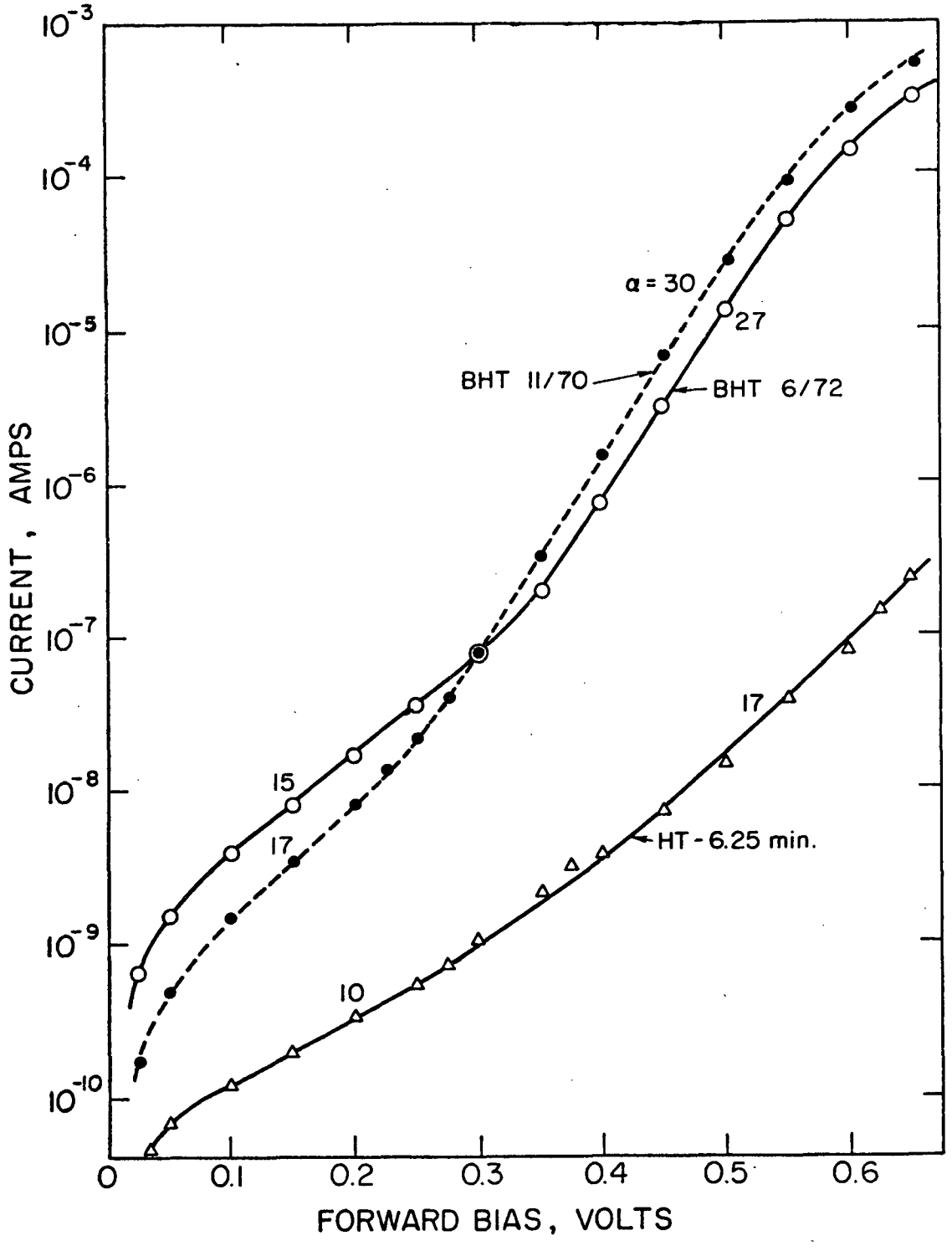

FIG. 4-10. Dark current-voltage curves for cell #61 at 300°K in the DQ state. Values of α from the diode relation $I = I_o(\exp\alpha V_f - 1)$ are noted on the curves (α = 38.6/volt for a perfect Shockley diode at 300°K).

voltage above V_{oc}. The break point between the straight line portions of the curve usually occurs at 0.3-0.4 volts but may increase to 0.5 volts after HT.

4.3.4 Spectral Response of Short-Circuit Current

Cell Results

While the magnitude of the short-circuit current, I_{sc}, of the cell changes by as much as a factor of 10^3 between the various R, D, E, and Q states, the relative spectral response changes very little.

The measurement of the spectral response is complicated by the transient nature of the states involved. At 300°K the enhanced state decays rapidly toward its equilibrium (Q) state. At 150°K the situation is reversed and even a weak enhancing light quickly destroys the maximally quenched state. Thus we must take the measurement in such a manner that both the decrease of enhancement and the effect of the probe light itself may be accounted for. With these facts in mind we examine several of the methods of obtaining spectral response curves:

(a) Transient: By observation of the transient response to a weak probe light after enhancement or quenching we can obtain the sensitivity in a constant state. This is illustrated in Fig. 4-11. The cell is enhanced with 0.535μ light until equilibrium is reached, the light is turned off, and after a small time delay the probe light at some wavelength, λ, is turned on. The current rises rapidly to a maximum and then falls as the probe light quenches the cell in this case. By extrapolation of the falling part of the curve back to the time when the probe light was turned on, the enhanced state

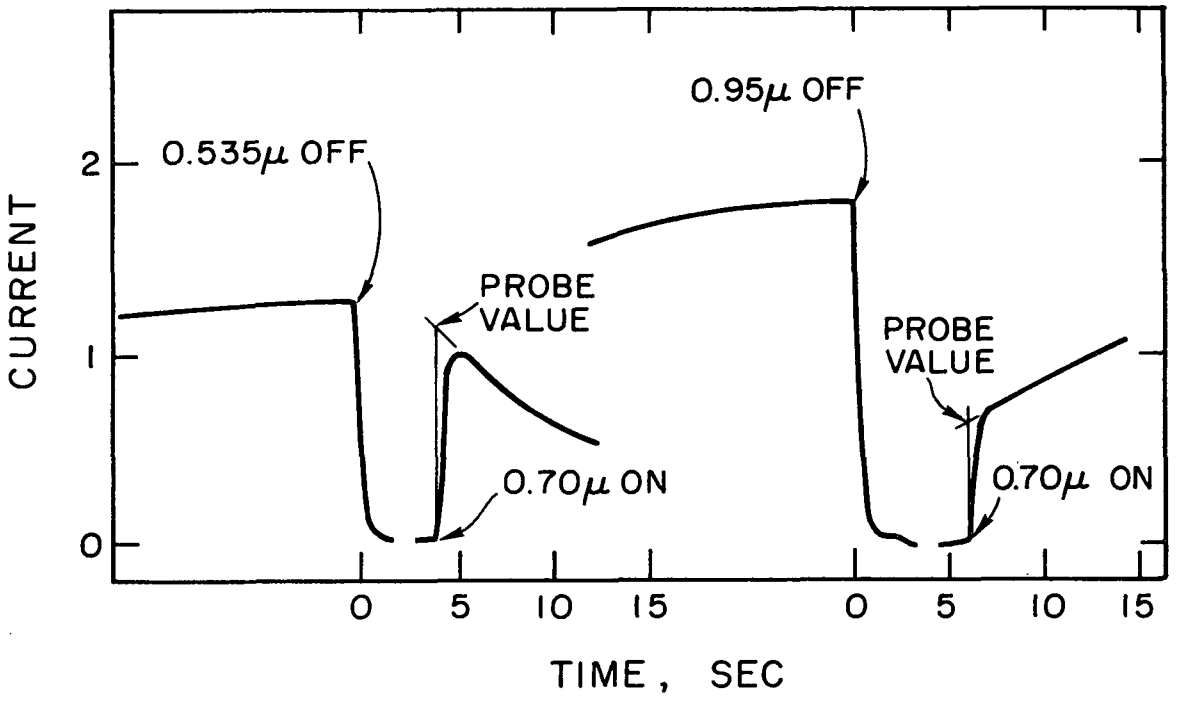

FIG. 4-11. Typical transient measurements for the enhanced-first and quenched-first cases. The current scales are as follows: 0.535μ light, 10^{-7} amp/div; E probe, 10^{-8} amp/div; 0.95μ light, 10^{-8} amp/div; Q probe, 10^{-9} amp/div.

response is obtained for λ. The procedure is repeated for each wavelength. The same method is used for the quenched state except that in this example the probe light is enhancing the cell and the current increases slowly after its initial fast rise. Delay times between the excitation of enhancement and the probe value as short as 2 sec were experimentally feasible.

(b) Stable: The current, and the degree of enhancement, is allowed to equilibrate at each wavelength. Thus this measurement represents the response for a continuously varying state of enhancement.

(c) Fast Scan Cycle: In this method the cell is cycled from short wavelength to long and back in a time of the order of 1 to 2 min. During this time the degree of enhancement changes somewhat and by examination of the hysteresis a qualitative estimate of both stable behavior and the transient response is obtained.

(d) Bias Light: In this measurement the response to a variable wavelength primary light is monitored while a bias light of constant wavelength necessary for enhancement or quenching is simultaneously incident on the cell. The results may be dependent on the relative intensities of the two light sources and on nonlinear response and thus may be ambiguous if a qualitative interpretation is attempted. (See, for example, Gill[16].)

In summary, a measurement is desired with a characteristic time longer than the rise time of the photoexcited carrier level in the Cu_2S

(<0.1 sec) and the instrument response time (∿0.5 sec) but shorter than the transient time for the rise or decay of enhancement (5 sec to 100s of sec) and the decay time of optical degradation (10s of sec to 1000s of sec).

In measuring the spectra for the cell, shown in Fig. 4-12, the transient method was used for all curves except the before-HT one which is a "stable" response curve. Some curves are not complete since the currents were too low to measure or the rate of E or Q was too fast to separate from the other rise times. When this latter condition obtained some small perturbation can be expected which would produce a relative decrease in long wavelength response in all cases (particularly for the Q states at 150°K and the E states at 300°K). A response curve for the same cell before-HT (except for the very small HT occurring during fabrication) is shown for comparison. After taking into account the transient behavior, the curves are in substantial agreement with the data of Gill[16] and Lindquist[17].

These data indicate that the shape of the transient spectral response curve is unaffected by the state of the cell or by the fact that its white light response has been reduced by a factor of 100 by extensive HT. Apparent large differences in steady-state spectral response are caused by enhancement or quenching effects introduced by the process of making the measurement. Further, several of the curves lie above the one taken before HT. We may conclude that excitation in the Cu_2S layer is not appreciably affected by extensive HT or by the state of the cell and that the important photoexcitation remains in the Cu_2S.

A small shoulder near 0.7μ appears in all the curves taken at 150°K. Since the direct bandgap of Cu_2S is at 1.2 eV while the indirect

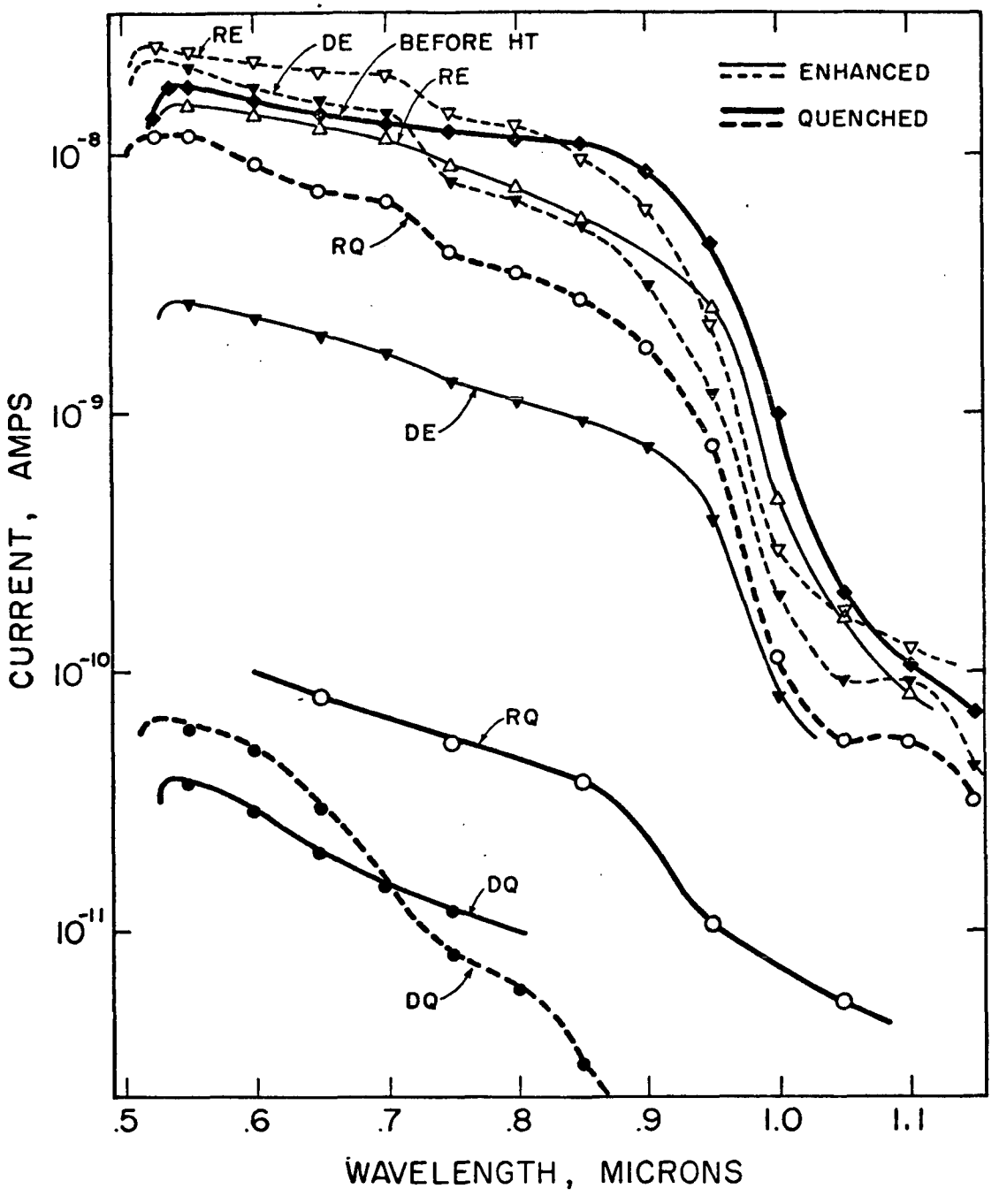

FIG. 4-12. Short-circuit current spectral response for cell #81 at 300°K (full lines) and 150°K (dashed lines). Enhancing light of 0.535μ (∿290 μw/cm^2) and quenching light of 0.85μ (∿580 μw/cm^2) were used. The data are normalized with respect to a probe light intensity of 9.3 μw/cm^2 at 0.70μ.

band gap is 1.8 eV[66] (0.69μ), this shoulder may be due to the decrease of indirect absorption as the phonon population is reduced at low temperatures and the phonon absorption contribution to indirect photon absorption is reduced.

Photoconductor Results

The fast scan spectra for the CdS:Cd:Cu photoconductor (#94, whose properties are described in Section 3.1) shown in Fig. 4-13 indicate little extrinsic photoconductivity in the degraded state compared with the restored state. In the degraded state little persistent enhancement is seen even at 150°K where a similar fast scan for the cell would show a large hysteresis.

In the photoconductor the rise and decay times of the carrier density are much larger than in the cell presumably because of the presence of a large density of traps. Since the majority carriers are replenished at the contacts of the photoconductor the current depends only on the effective carrier lifetime and may in some cases have a decay time of 10s of sec after the light is turned off. In the cell, however, the supply of carriers to the CdS interface is cut off very rapidly when the light is turned off and they cannot be replenished at the contact (in this case the Cu_2S). Thus transient measurements are much more difficult to make and to interpret in the photoconductor case because the carrier density growth or decay cannot be distinguished from the quenching transients. This topic is explored further in Section 4.3.7.

4.3.5 Effect of Optical Degradation on the Cell

As implied by the spectra of Fig. 4-12, the effect of degradation on the short-circuit current produced by monochromatic excitation (in

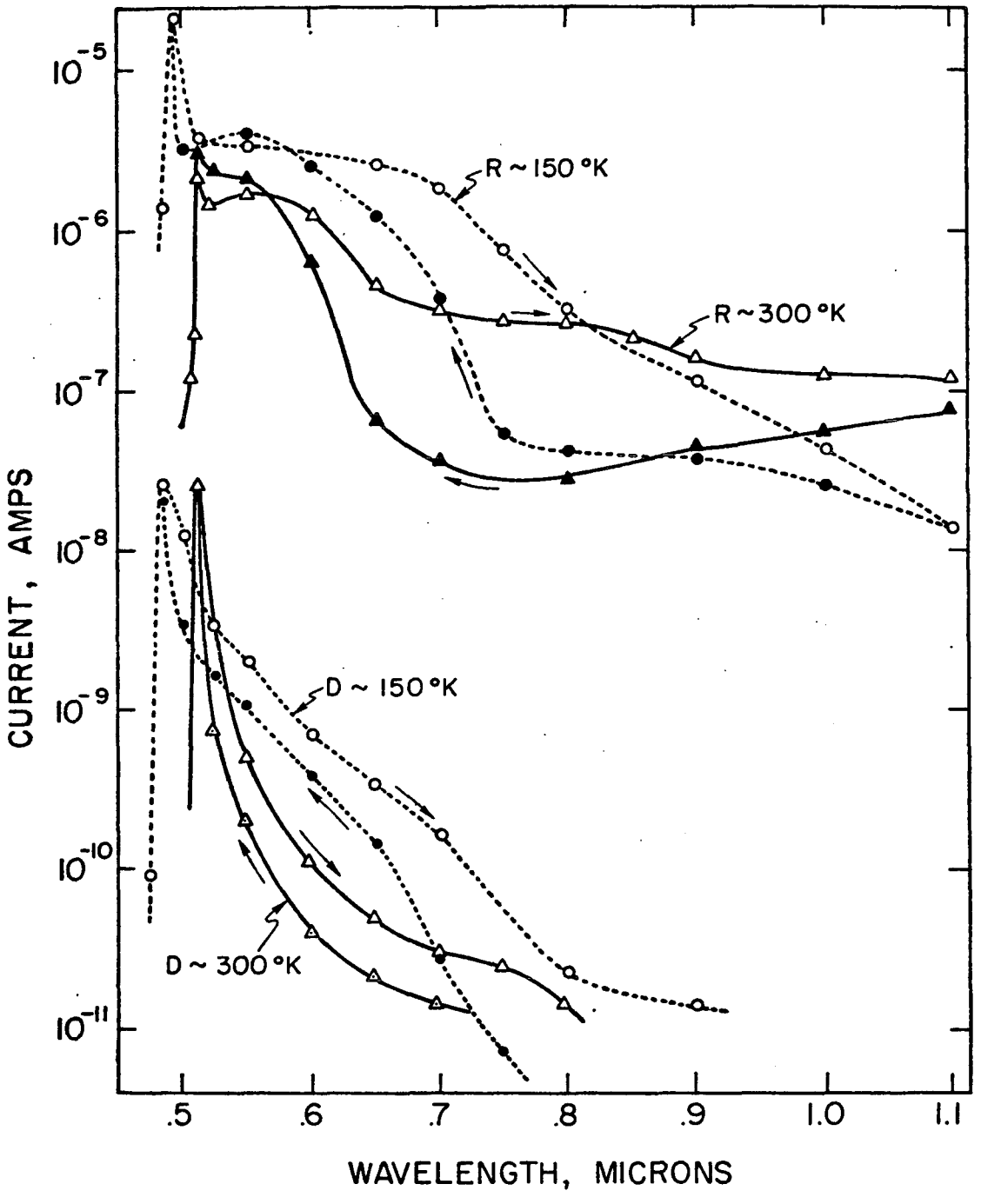

FIG. 4-13. Fast scan spectra for the photoconductor crystal at 300°K and 150°K in the restored and degraded states. Cycle time from low λ to high λ and back is two min. Curves are normalized with respect to intensity of 9.7 $\mu w/cm^2$ at 0.70μ. Electric field is 14.4 V/cm and the cross-section is 0.011 cm^2.

either the E or Q states) is not large compared to the effect of enhancement or quenching per se (except for the Q state at 150°K). To show the relative magnitude of these effects more directly, the probe (small intensity) short-circuit current, I_{sc}, at 300°K for both E and Q states is shown in Fig. 4-14 as a function of cumulative time of exposure to a degrading light. The cell is fully restored on the left and degraded on the right, the degradation being interrupted at various times to take these measurements. Also shown here are the junction capacitances, C(E), C(Q), and their difference, ΔC, the photocapacitance increment. These data were measured in the same manner as the spectra except for C(E), where the enhancing light was left on during the measurement because of the longer time required for measurement of capacitance.

In earlier work[88] it was found that degradation or restoration did not affect ΔC appreciably. The apparent contradiction between these two sets of data lies in the method of measurement. The earlier data were measured with the E light off so that the cell's enhancement had been reduced considerably by thermal quenching. The value of ΔC reported here is still not large, however, compared to that of the restored state at 150°K where values of $\Delta C > 1000$ pf were measured for this cell (see Section 4.3.9).

These changes in $I_p(E)$ and $I_p(Q)$, measured with monochromatic light, are small compared with degradation in white light or some wavelength such that both enhancement and quenching occur simultaneously. In the latter case the current decreases by a factor of 75-100 for this cell. This difference is explained by the observation that the balance between the rates of enhancement and quenching changes quite radically

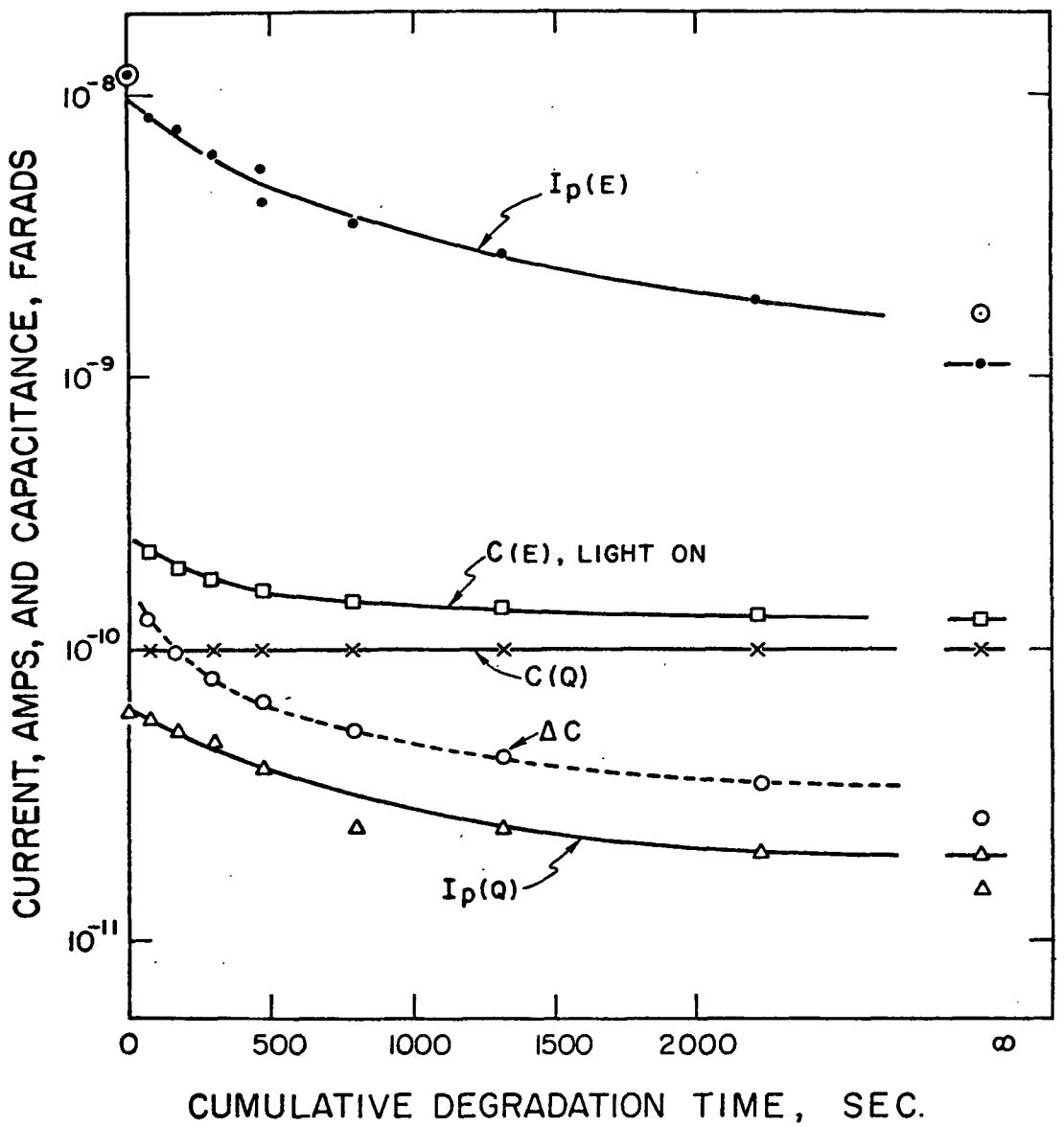

FIG. 4-14. Cell #81 parameters versus cumulative time of degradation at 300°K: probe light (0.70μ, 9.3 μw/cm^2) current with cell enhanced $I_{sc}(E)$ and quenched $I_{sc}(Q)$; junction capacitance, enhanced C(E), and quenched C(Q), and their difference ΔC. Completely degraded values are at right and circled points are taken from spectra of Fig. 4-13.

with degradation. Approximate data indicate that the ratio of the E rate to the Q rate may decrease by a factor of 20-30 during passage from the restored to degraded state.

4.3.6 Effect of Degradation on the Rates of Enhancement and Quenching in the Cell.

In addition to the decrease in magnitude of enhanced current, $I_{sc}(E)$, and ΔC during degradation shown in Fig. 4-14, there is also a variation in the rate of enhancement. In this section we will examine the growth and decay (i.e., quenching) of enhancement as a function of cell degradation. Although the photocapacitance is a more direct measure of cell enhancement, the time required to make capacitance measurements makes them difficult to use for determining decay rates. Instead we used the photocurrent as a measure of the cell enhancement at room temperature according to the following procedure:

(1) The cell was enhanced by exposure to 0.60μ light (19 $\mu w/cm^2$) and the growth curve was recorded until the equilibrium current was reached.

(2) The 0.60μ light was turned off and at the same instant a 0.95μ light (170 $\mu w/cm^2$) was turned on to quench the cell. The decreasing current was recorded until equilibrium was reached.

(3) The cell was degraded for a time, t, with 0.535μ light (290 $\mu w/cm^2$).*

*Since some small amount of degradation occurs with the 0.60μ light during step (1) (enhancement), step (3) was omitted for the first two points (3 and 6 sec) on Fig. 4-15b). The degrading effect of exposure to 0.60μ light during step (1) is expressed in terms of an equivalent time of exposure to 0.535μ light for these two points. These times were calculated using the ratio of intensities and efficiencies for degradation of the two light sources (from Section 4.2.3). The 0.535μ source was about 80 times more effective than the 0.60μ source.

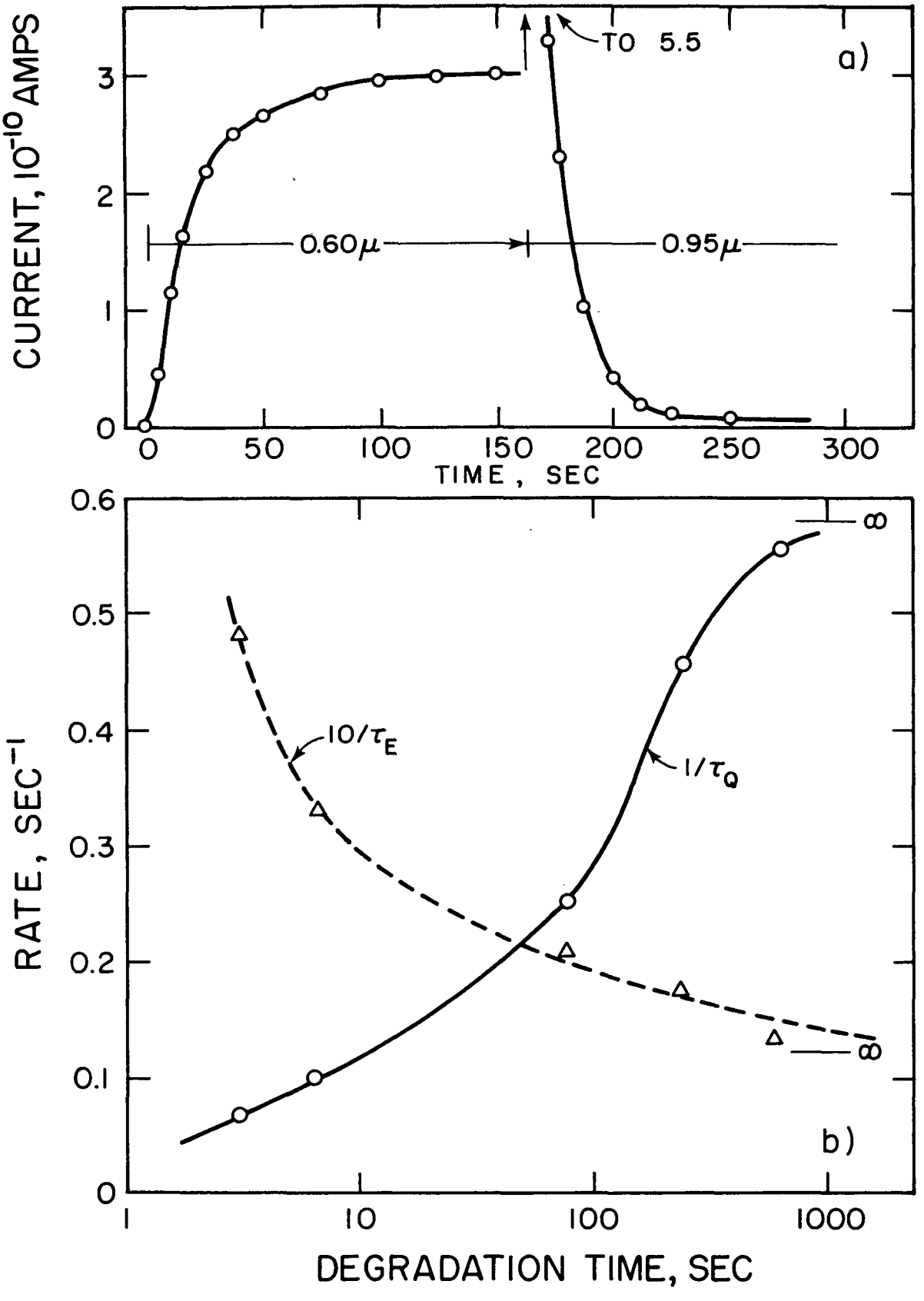

FIG. 4-15. (a) Typical curves of I_{sc} versus time during enhancement and quenching at 300°K for cell #81.
(b) Enhancement rate $1/\tau_E$ and quenching rate $1/\tau_Q$ versus cumulative degradation time at 300°K.

(4) The cell was then fully quenched with 0.95μ light and 5.0 V reverse bias to prepare for the next enhancement and the cycle was repeated.

An example of the growth and decay curves is shown in Fig. 4-15a. The exponential growth and decay laws, $I_{sc} = I_o[1 - \exp(-t/\tau_E)]$ and $I_{sc} = I_o \exp(-t/\tau_Q)$, fit the initial parts of the curves of Fig. 4-15a quite well and were used to calculate the rates, $1/\tau_E$ and $1/\tau_Q$, which are plotted versus cumulative degradation time in Fig. 4-15b. Although the curves are quantitatively approximate they clearly show the changes in the enhancement and quenching rates during degradation. These data may be compared with the rate of thermal quenching in the degraded cell at 300°K of ∿0.14 sec.

4.3.7 Enhancement and Quenching Effects in the Photoconductor

As was pointed out in the theoretical section, the enhancement and quenching effects seen in the cell bear some similarities to so-called infrared quenching effects seen in CdS photoconducting crystals. It is of interest to verify that the same effects (at least the ones pertinent to our investigation) take place in a highly Cu doped CdS photoconductor which shows the TROD effect.

In the cell, the normal equilibrium state is the quenched state, i.e., a cell left in the dark at RT will become quenched. Enhancing light charges states near the interface positively resulting in a change in junction capacitance, ΔC, of some 70% in a BHT cell. Accompanying ΔC are increases in the dark forward bias current and I_{sc} of about 300% which are presumably due to the change in depletion layer width. In short, ΔC is a direct measure of the state of enhancement.

In the photoconductor case quenching is usually considered in terms of a decrease in photosensitivity to near band gap illumination when a secondary, infrared light is turned on. Thus in the photoconductor the "enhanced state" is normal under near band gap illumination, while in the dark some other state--which we discuss here--is normal.

In the photoconducting crystal the measurement of a quenching spectrum is complicated by the slow decay of carrier density due to trap emptying. This decay time, τ_R, (on the order of a fraction of a second for a DQ or RQ state and up to 10 to 15 seconds for the RE state) is comparable to the time constants for the operations of enhancement or quenching. For some states spectra can be measured by the same probe technique used for those of Fig. 4-12 (e.g., probe spectra of the DE-150°K photoconductor agree well with the fast scan spectra of Fig. 4-13) but in the quenched state the probe current rises very slowly at first in an ogee shaped curve as the traps are filled and the carrier density builds up.

We consider here the transient measurement of photocurrent in three conditions: after illumination by enhancing light, after illumination by quenching light, and after equilibration in the dark. Examples of these situations are shown in Fig. 4-16a for a degraded sample at 300°K. In the first case the crystal has been enhanced by illumination from a high intensity 0.518μ light until an equilibrium current level of 5×10^{-7} amps is reached. When this light is turned off the dark current decays rather rapidly. Now when a probe light at 0.70μ is turned on some 40 seconds later, the probe photocurrent pulse "rides" on the decaying dark current level and decays to its own stable value. Thus it is difficult to separate the effects of decay of enhancement from the

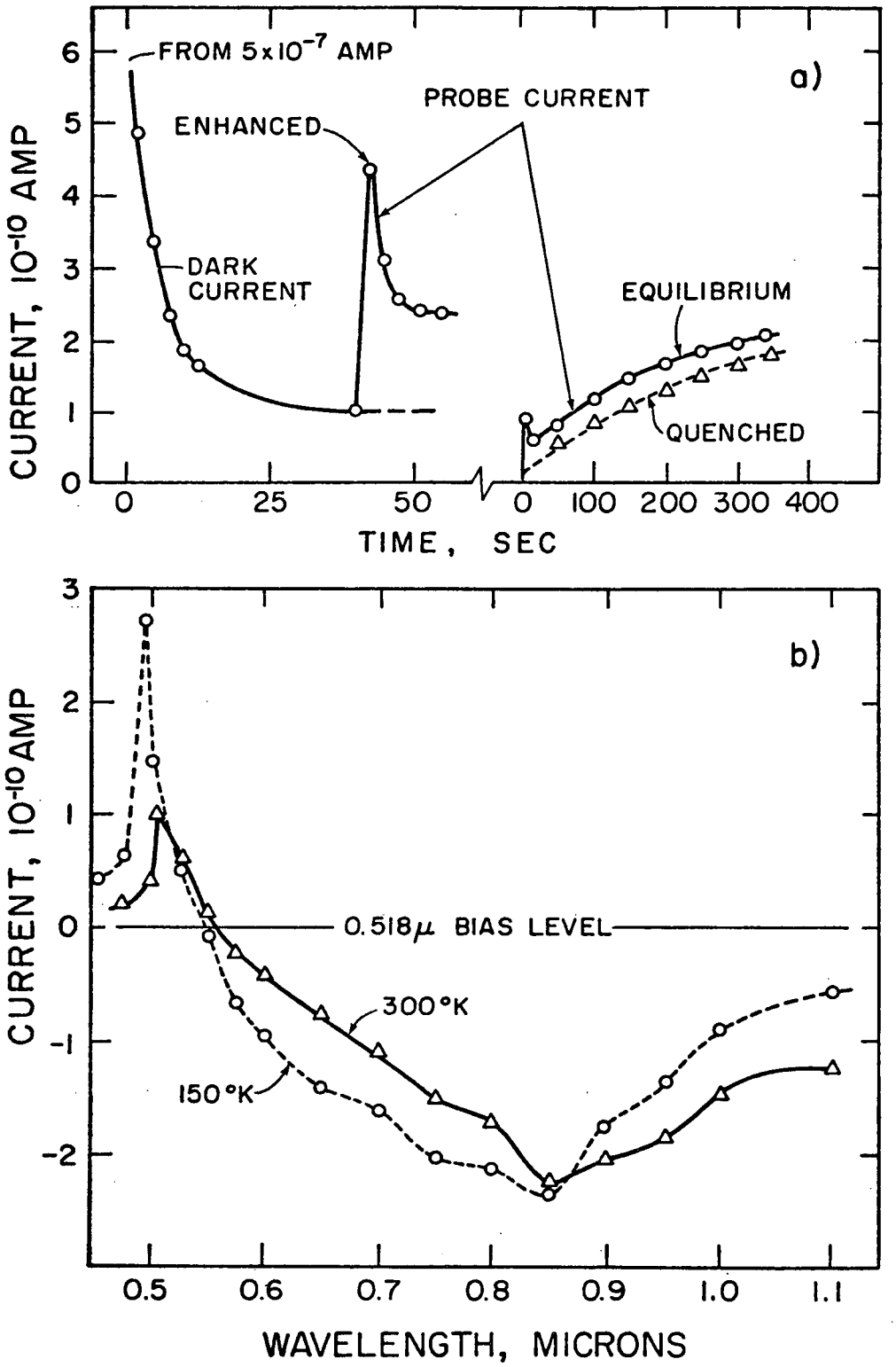

FIG. 4-16. (a) Probe photocurrent versus time at 300°K for the pre-enhanced pre-quenched, and pre-dark-equilibrated conditions. Probe light is 0.70μ (9.3 μw/cm^2).
(b) Probe photocurrent with simultaneous bias light versus wavelength of probe light. Bias light of wavelength 0.52μ (50 μw/cm^2) produces bias current level of 4.25 x 10^{-8} amp at 300°K and 4.85 x 10^{-8} amp at 150°K. Results are normalized to a probe intensity of 9.3 μw/cm^2 at 0.70μ.

decay of carrier density. If the photoconductor is quenched first using an intense 0.85μ light (to a level of 1.1×10^{-10} amps) and quickly (within 10 seconds) probed, the current starts at a very small value and slowly grows to its equilibrium value. For the third case the crystal was equilibrated (after enhancement) by 13 hours in the dark at RT and the probe current growth curve was obtained. This curve is similar in shape to the quenched case except for an initial cusp. For restored states similar curves are obtained but the range of current rise is much greater (for example, see Fig. 4-17 for the probe current growth from the RQ state). Thus the equilibrium growth curve and the quenched-first curve are very similar.

In order to determine the persistence of enhancement in the photoconductor, a number of experiments were done in which the photoconductor was probed after varying time delays following enhancement. Rather than the steadily decreasing peak of I_{sc} seen in the cell, the effect of increasing time delay is to slow the growth rate of the probe pulse which changes its form from the enhanced case in Fig. 4-16a to the quenched case in a continuous manner. These data suggest that enhancement is not persistent at low temperatures (ca. 150°K) in this material.

Figure 4-18 shows decay curves for the photoconductivity for this sample for some representative states. Clearly the response time is controlled by a large density of traps. The complexity of the system makes it difficult to measure trap depths and densities although we can get an estimate of the latter by using the approximation $n_t = n(1 + \tau_R/\tau_L)$ from Rose[89] where n_t is the density of traps, n is the carrier density with the light on, τ_R is the response time, and τ_L is the electron lifetime, about 10^{-3} sec for the RE-300°K case and 10^{-5} sec for the DE-300°K case.

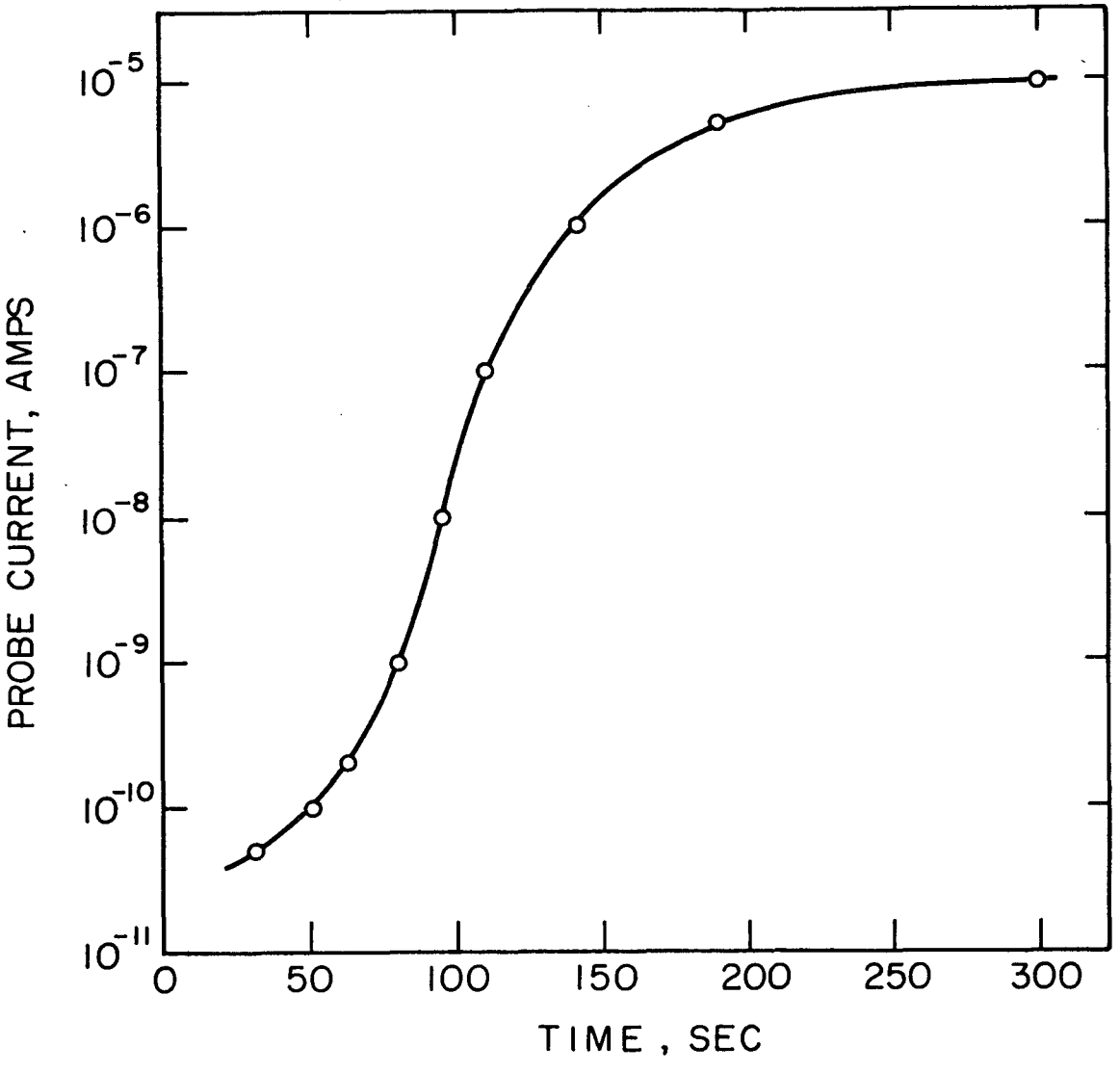

FIG. 4-17. Probe photocurrent (0.70μ at 9.3 μw/cm^2) versus time for the restored case at 150°K. Sample was maximally quenched with 0.85μ light before probing.

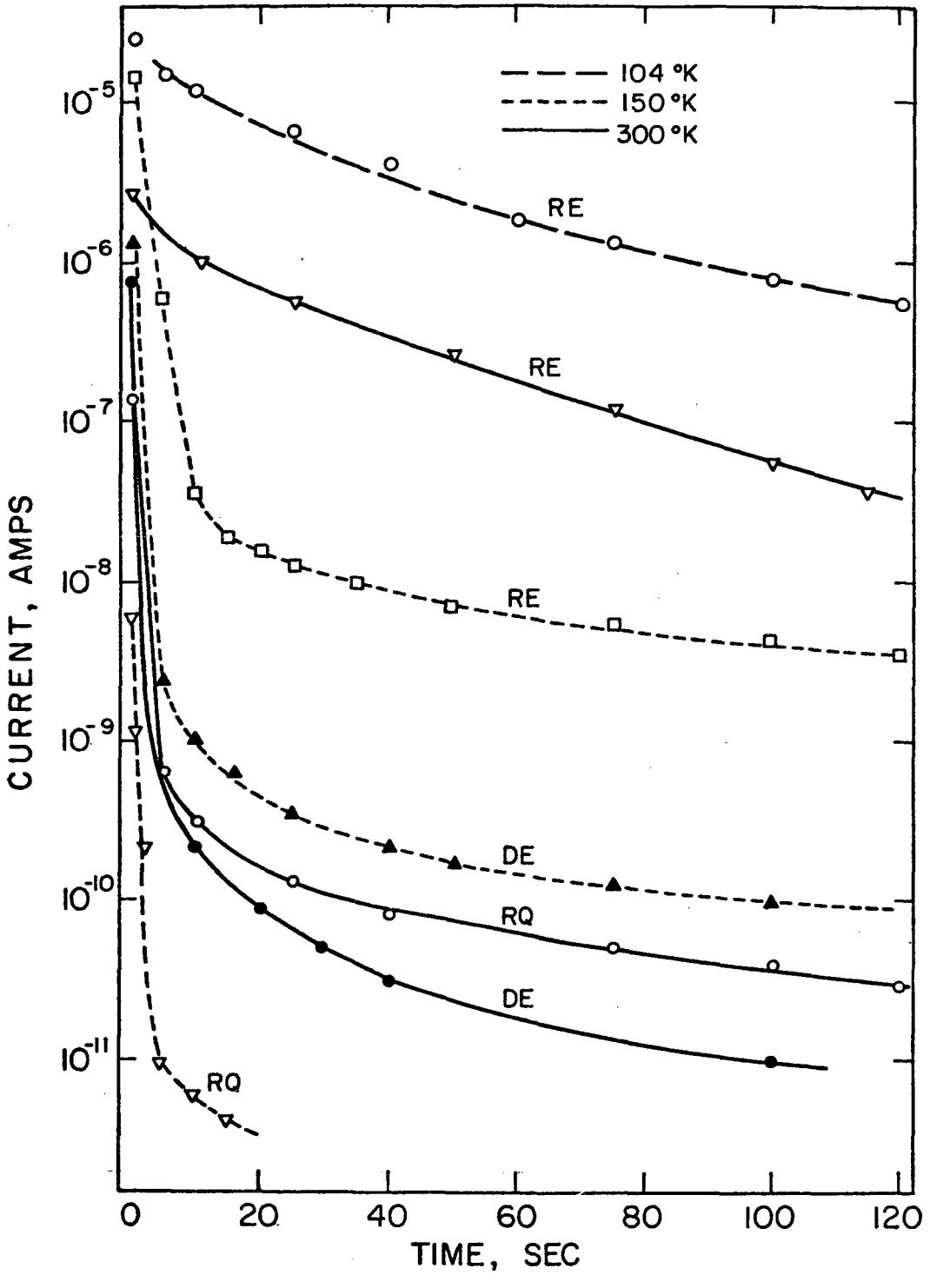

FIG. 4-18. Photoconductivity decay curves. Light sources (in descending order) are:

RE	0.70μ	9.3 μw/cm^2	104°K
RE	0.70μ	9.3 μw/cm^2	300°K
RE	0.70μ	9.3 μw/cm^2	150°K
DE	0.50μ	260 μw/cm^2	150°K
RQ	0.85μ	580 μw/cm^2	300°K
DE	0.52μ	265 μw/cm^2	300°K
RQ	0.85μ	580 μw/cm^2	150°K

Using the initial part of the decay curves, $n_t \approx 10^{15}/cm^3$ for both cases. The fact that the decay is much more rapid for the D and Q cases may be due either to the effect of increased recombination or a smaller number of traps or both.

We can get approximate quantitative data on enhancement and quenching despite the above difficulties by using fast scan spectra such as Fig. 4-14 or by using a bias light. To measure the quenching of photoconductivity sample #94 was illuminated by enhancing bias (secondary) light at 0.518μ (corresponding to the peak photocurrent). The crystal was simultaneously illuminated by a weaker primary light whose wavelength could be scanned. Although there was some hysteresis even for a very slow scan (5 to 10 min per cycle), the difference between the λ increasing and the λ decreasing curves was small enough for us to have confidence in the data. The photocurrent due to the primary light alone is subtracted from the result leaving the amount of quenching with respect to the constant bias light current level. This is plotted in Fig. 4-16b. Since the bias light is ∿5 times as intense as the primary light the quenching efficiency is quite large in the degraded state. A broad quenching band extending almost to the band gap energy of CdS is seen with a maximum near 0.85μ. This agrees well with both the quenching spectra of the cell as measured by Lindquist[17] and to quenching spectrums from published photoconductor data[90,91].

In the restored state case the measurement is further complicated by degradation by the bias light during the wavelength scan. When the measurement described above was attempted on a restored cell the peak current had dropped to half of its fully restored value before the cycle had been completed. Thus no quantitative results could be gained without

a stable primary light spectrum. However, the spectrum with bias light shows no appreciable deviations below the bias photocurrent level and it is concluded that quenching effects are much smaller for the restored state. Thus most of the hysteresis in the fast scan spectral response (Fig. 4-14) is probably due to the long response time in the restored state as illustrated by Fig. 4-18.

In summary we conclude:

(1) The quenching spectrum in this highly doped crystal which shows the TROD effect is substantially the same as seen in other more lightly doped CdS materials.

(2) The quenching spectrum in the degraded photoconductor is substantially the same as seen in the cell.

(3) The decay of photoconductivity in the photoconductor is very long and is dominated by trapping processes. This decay time is a function of the state of the cell; it is shorter for the degraded state than for the restored and it is shorter for the quenched state than for the enhanced state.

4.3.8 Junction Capacitance Measurements

Measurements of junction capacitance as a function of bias voltage were made on several cells in order to define the junction profile in the various cell states. In principle such measurements can be used to determine both the effective barrier voltage and the profile of the ionized donor or acceptor concentration (net) near the junction. However, the extrapolation of the $1/C^2$ versus bias voltage, V, to $1/C^2 = 0$ to determine the barrier voltage, V_b, depends sensitively on the presence of interface states, dipoles, and trapping effects as well as the grading

of the junction. Nevertheless, the determination of net donor density from the slope of the $1/C^2$ versus V curves is relatively insensitive to these effects[92,93,94,95,96]. Since the net acceptor density in the Cu_2S, $N_{A\ Cu_2S}$, about $10^{19}/cm^3$, is much larger than the net donor density in the CdS, $(N_D - N_A)$, we can write (following Van Opdorp[92])

$$\left|\frac{d}{dV}\left(\frac{A}{C}\right)^2\right|_{V=V_o} = \frac{2}{q\varepsilon\ (N_D - N_A)} \tag{4.4}$$

where A is the junction area, q is the electronic charge, and ε is the permittivity of the CdS ($10\varepsilon_o$). Most of the depletion layer width, $w_d(V)$, is on the CdS side of the junction since $N_{A\ Cu_2S} >> (N_D - N_A)$ and corresponding to each bias voltage, V_o, we have a junction capacitance given by

$$C(V_o) = \varepsilon A/w_d(V_o) \tag{4.5}$$

Thus we can obtain the value of $(N_D - N_A)$ as a function of the distance away from the metallurgical interface measured by w_d.

In Fig. 4-19 are presented $1/C^2$ versus V curves for cell #61 after a small HT ($\sim$2 min at 100-130°C).* These include curves measured at both room temperature and 150°K corresponding to the DQ state and to the DE state with 0.535μ light on during the measurement to maintain enhancement. They may be compared with similar curves for non-HT cells and cells with small HT measured by Lindquist[17] (Fig. 5-37) and by Gill[16] (Fig. 4-11). Before any HT the curves are linear and extrapolate to barrier voltages of 0.43 V to 1.1 V. After short HT the curves develop the upward convex "knee" shape seen here.

---

*The capacitance values have been corrected for cell series resistance.

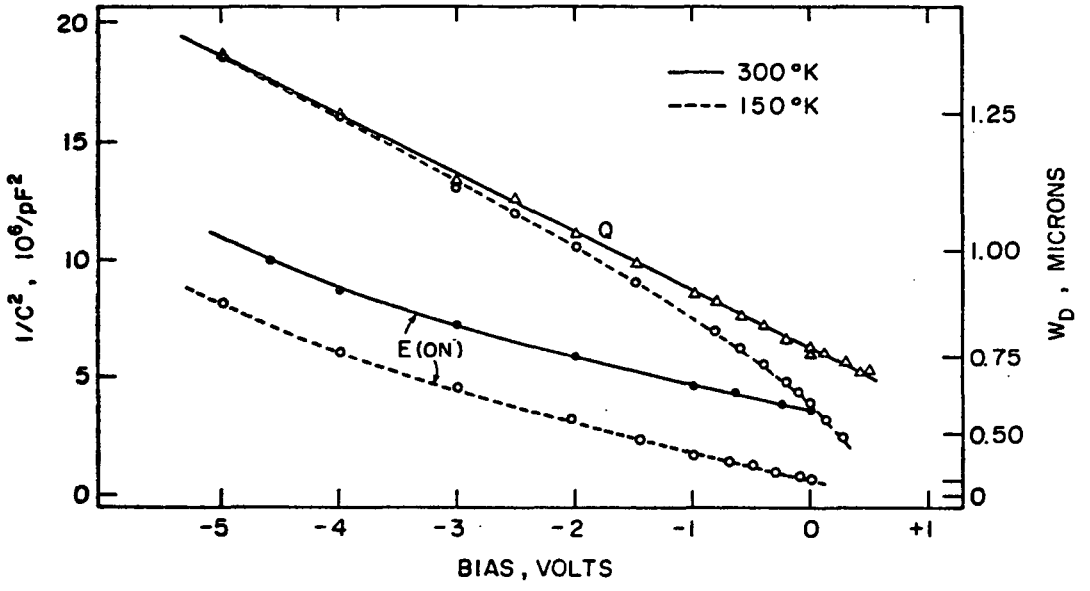

FIG. 4-19. Plot of $1/C^2$ versus bias voltage for cell #61 after small HT (∿2 min at 100 to 130°C). Depletion layer width is shown at right. "E (on)" denotes enhancing light (0.535μ at ∿290 μw/cm^2) is on during the measurement.

After extensive HT the knee develops into a linear segment which extrapolates to a voltage much higher than V_b. This is characteristic of a junction which includes a low conductivity layer (i-layer) which dominates the junction capacitance. For the extreme case when the i-layer is completely insulating, the width of the layer, w_i, is determined by the extrapolation of the high reverse bias $1/C^2$ curve to the barrier voltage (obtained by other means) where the capacitance value gives w_i from Eq. (4.5). Since it is determined by the doping profile near the junction, w_i is a constant for a given HT and is always smaller than w_d for a perfectly insulating layer.

The slope of the high reverse bias curve in Fig. 4-19 in the quenched case gives $(N_D - N_A) = 0.46 \times 10^{16}/cm^3$ which corresponds well with the value of $q(N_D - N_A)$ determined by conductivity measurements for the CdS crystal from which the cells were made. That measurement gave $0.4 \times 10^{16}/cm^3$ assuming a mobility of 300 cm^2/volt sec at room temperature. With the enhancing light on, the value of $(N_D - N_A)$ increases to $\sim 0.95 \times 10^{16}/cm^3$. This increase is probably due to photogeneration of electrons from deeper centers in the CdS leaving a net positive charge which adds to the apparent uncompensated donor density, i.e., the photocapacitance. After HT when w_i becomes larger, the i layer begins to dominate the measured capacitance and the effect of photocapacitance on the junction capacitance expected to become much smaller for the degraded cell.

The rise in the E-on (enhancing light on during the measurement) curves for large reverse biases may be due to either (1) reverse bias quenching, or (2) that w_d is approaching the end of the region of photoexcited centers and entering the region of the CdS which has not been

doped with Cu about 0.8μ from the Cu_2S-CdS interface. The second possibility is supported by the Q-150°K curve which shows a higher slope indicating a lower net donor density out to 0.6-0.8μ from the interface.

In Figs. 4-20 and 4-21 are shown similar curves for cell #61 after ∿6 min of HT. In these curves we can see a general increase in w_i, and the difference between R and D states becomes obvious. Note in particular the very small zero bias depletion layer width in the R-150°K and DE(on) states as compared with the remaining states at 150°K and 300°K. The value of w_d is virtually the same in the R-150°K states as it was before HT.

The net positive charge density, $N(x) = (N_D - N_A)$, profiles calculated from the $1/C^2$ versus V curves [using Eqs. (4.4) and (4.5)] are shown in Fig. 4-22 where the zero bias depletion layer widths have been marked on each curve. Because of bias current limitations and the unsuitability of the model for forward biases near V_b, the portions shown are the only accessible parts of the curves (with the exception of the DQ state where higher reverse biases show no appreciable change in slope). These data imply that restoration changes the i-layer (degraded) to a layer of fairly high conductivity even in the quenched state. Three distinct regions of $(N_D - N_A)$ develop, especially in the RQ-150°K case: a region adjoining the interface of increasing donor density, a broader region of minimum density, and a transition region to the bulk CdS.

Figures 4-23, 4-24, and 4-25 give similar data for cell #81 after a HT of about 1 hour. The i-layer is wider, of course, but the R state value of net donor density is still large. In the D state, the high reverse bias slope indicates a net donor density of about $0.3 \times 10^{16}/cm^3$ which again corresponds well with the conductivity donor density of the

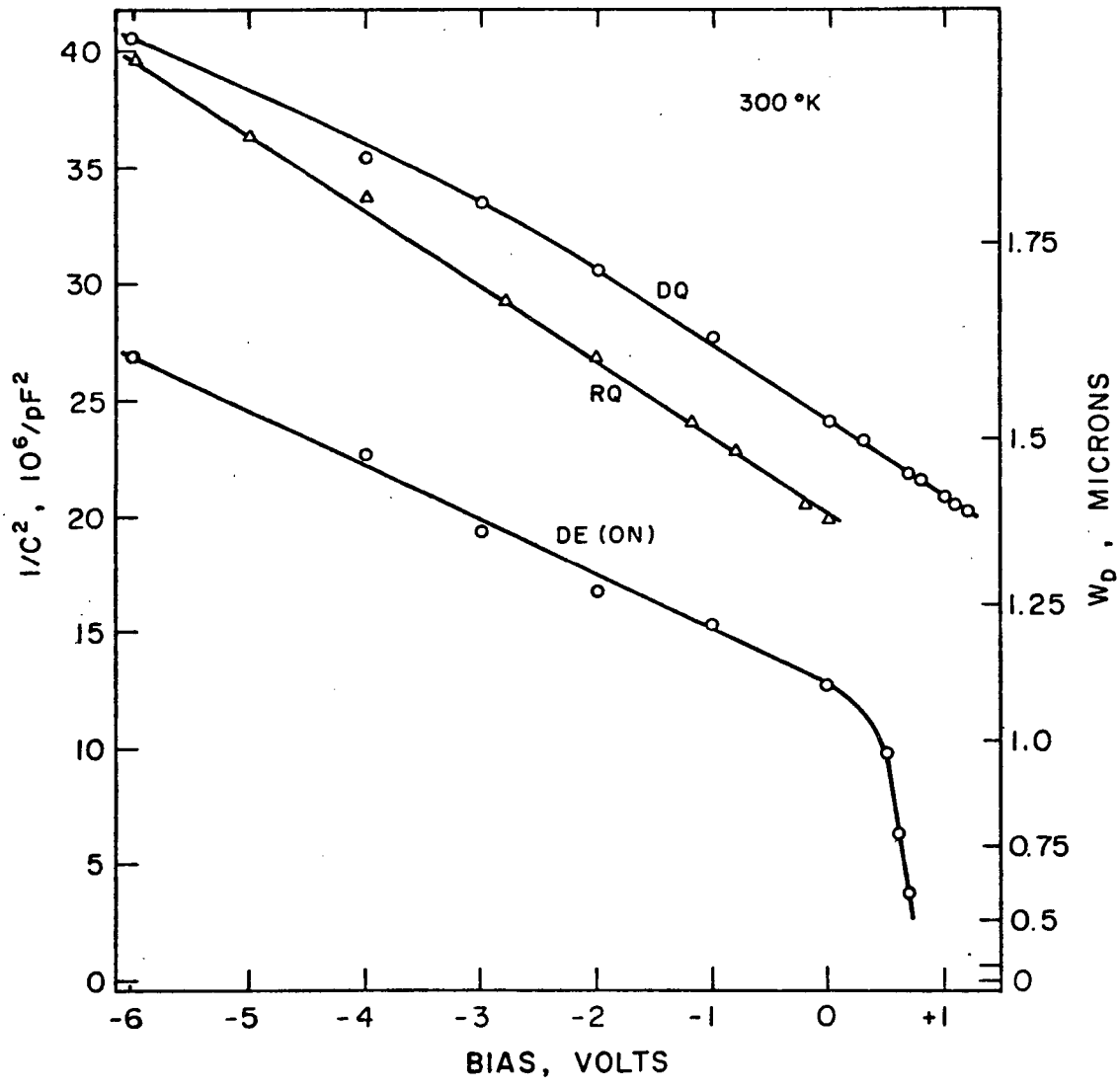

FIG. 4-20. $1/C^2$ versus bias voltage at 300°K for cell #61 after ∿6 min of HT.

B

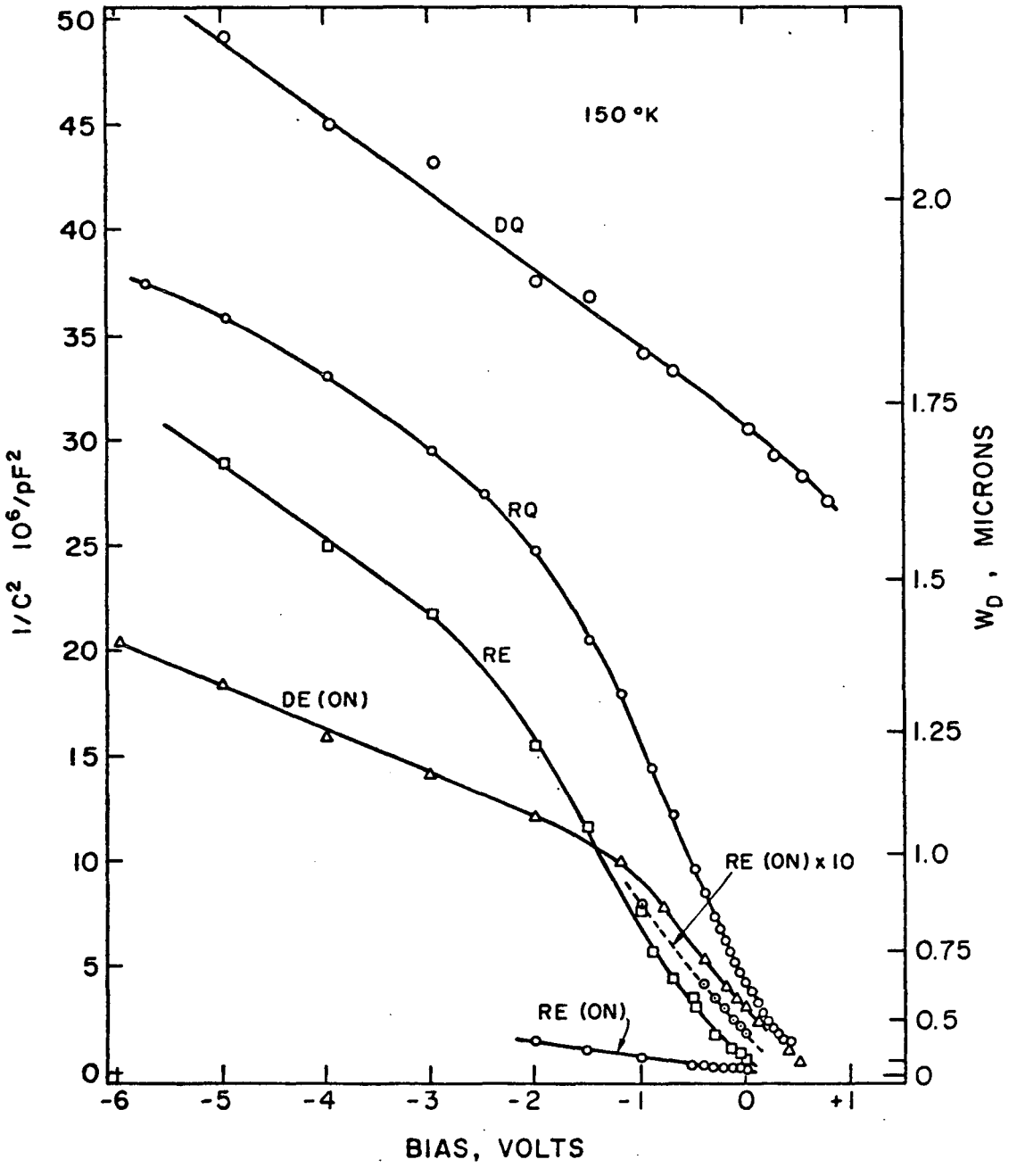

FIG. 4-21. $1/C^2$ versus bias voltage at 150°K for cell #61 after ∿6 min of HT.

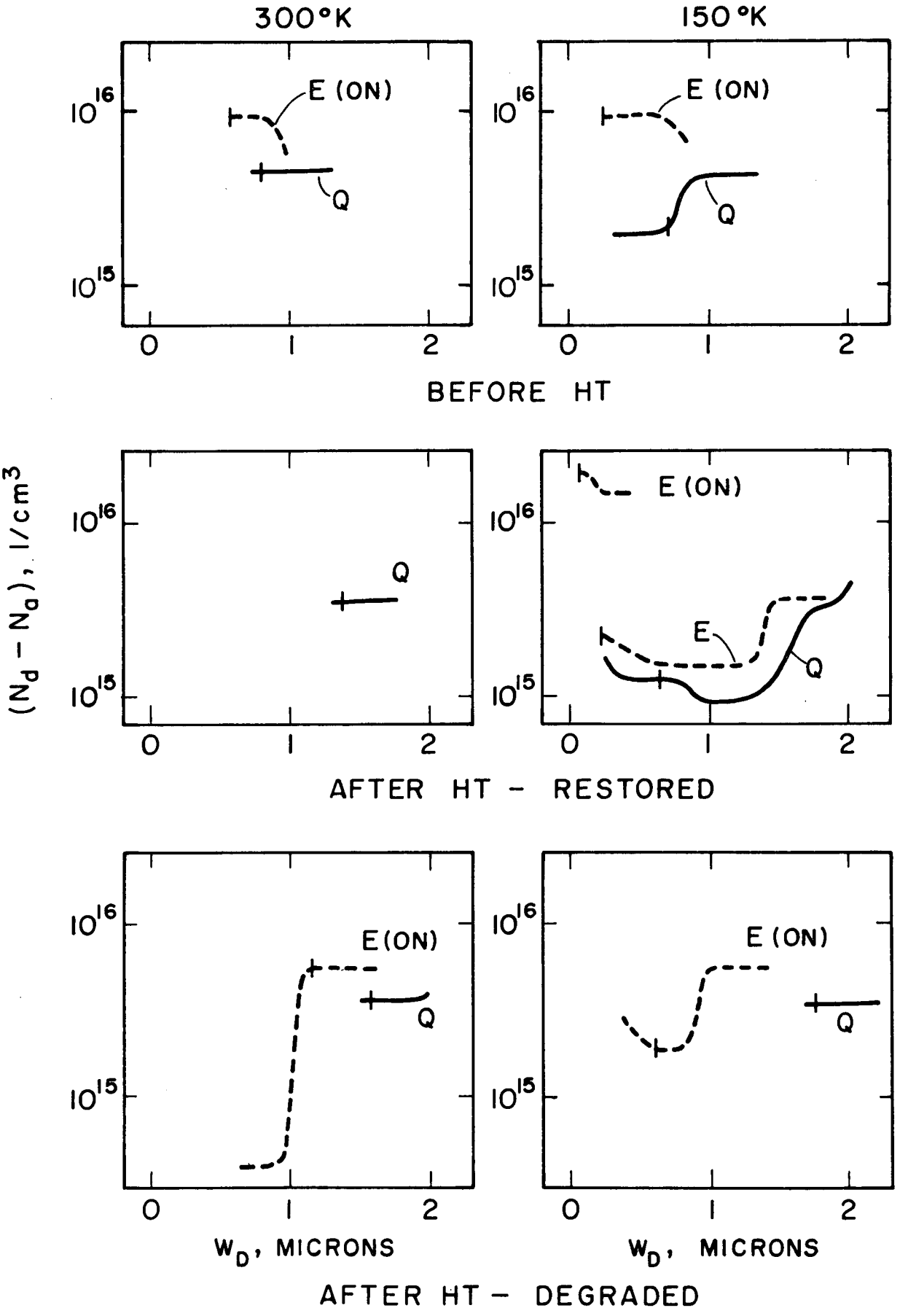

FIG. 4-22. Net donor density (N_D-N_A) versus depletion layer width w_d for cell #61. The zero bias value of w_d is marked on the curves.

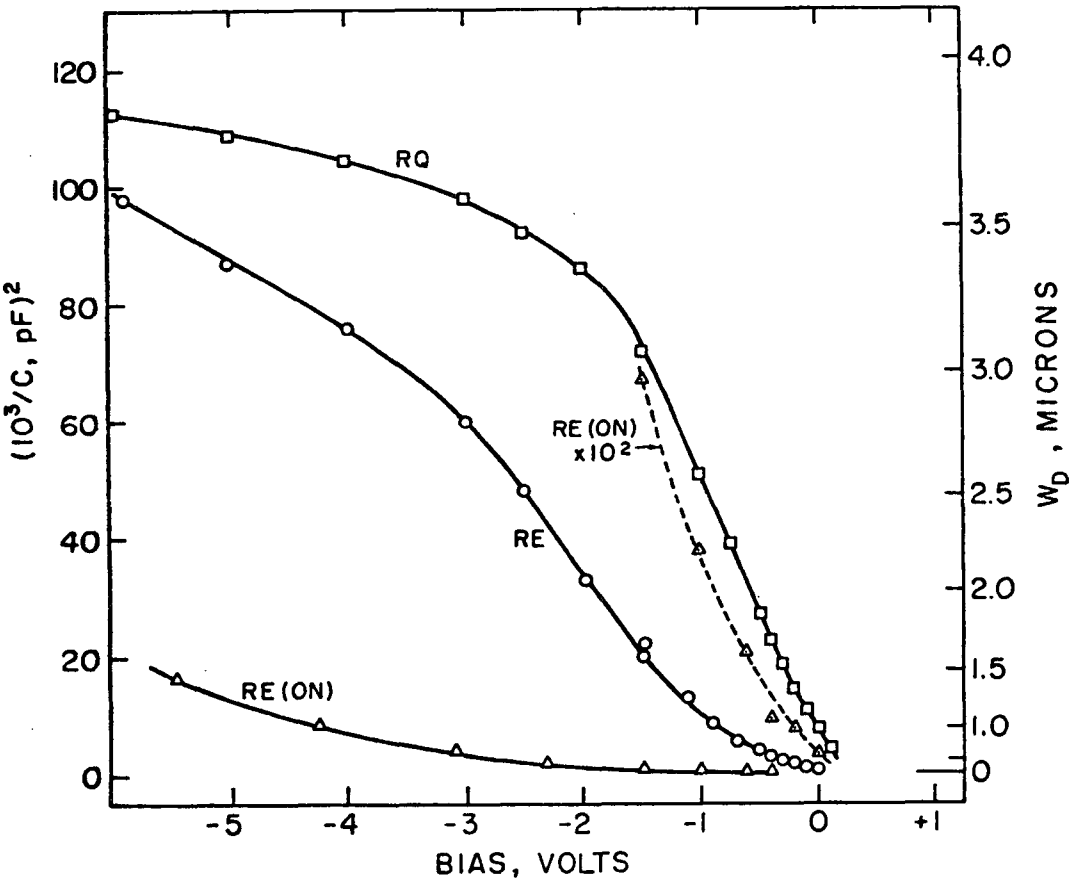

FIG. 4-23. Plot of $1/C^2$ versus bias voltage at 150°K for cell #81 in the restored state after ∿1 hour of HT.

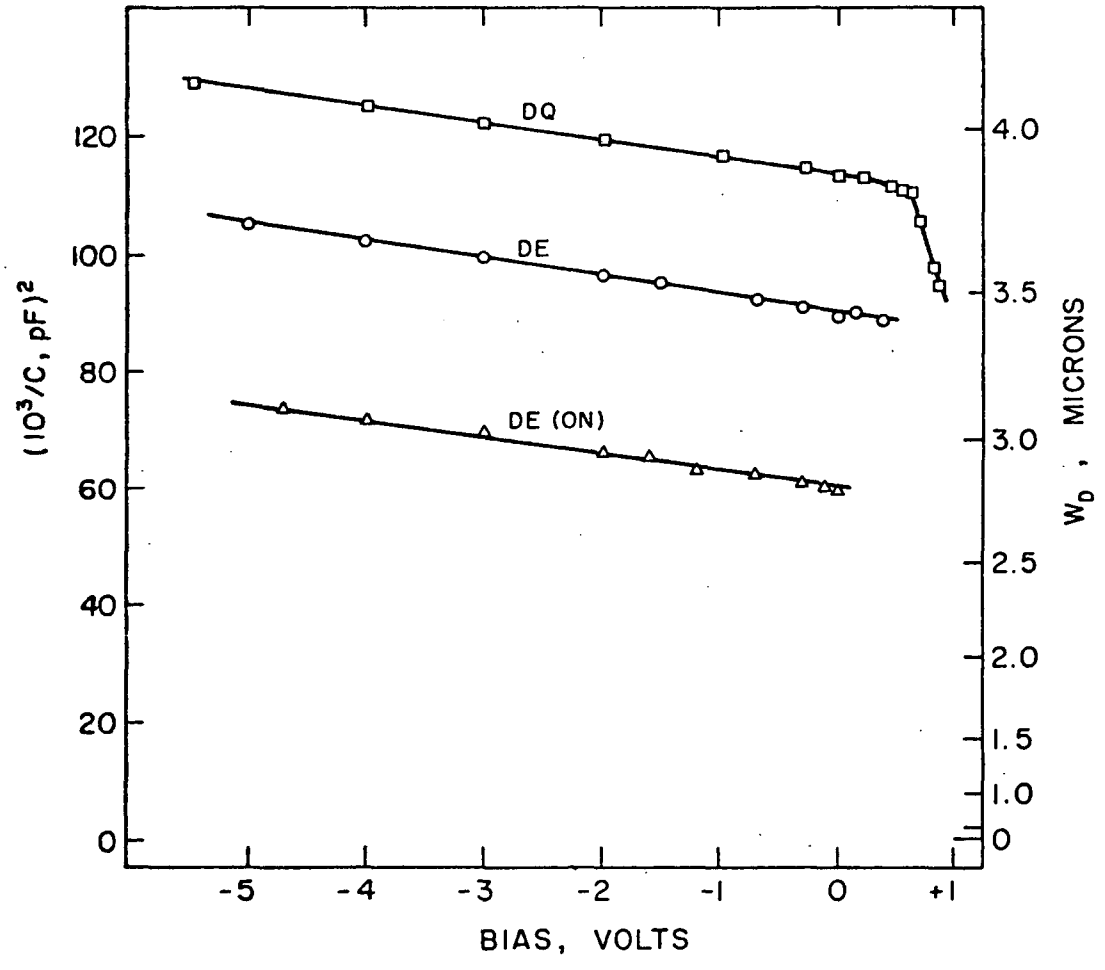

FIG. 4-24. Plot of $1/C^2$ versus bias voltage at 150°K for cell #81 in the degraded state after ∿1 hour of HT.

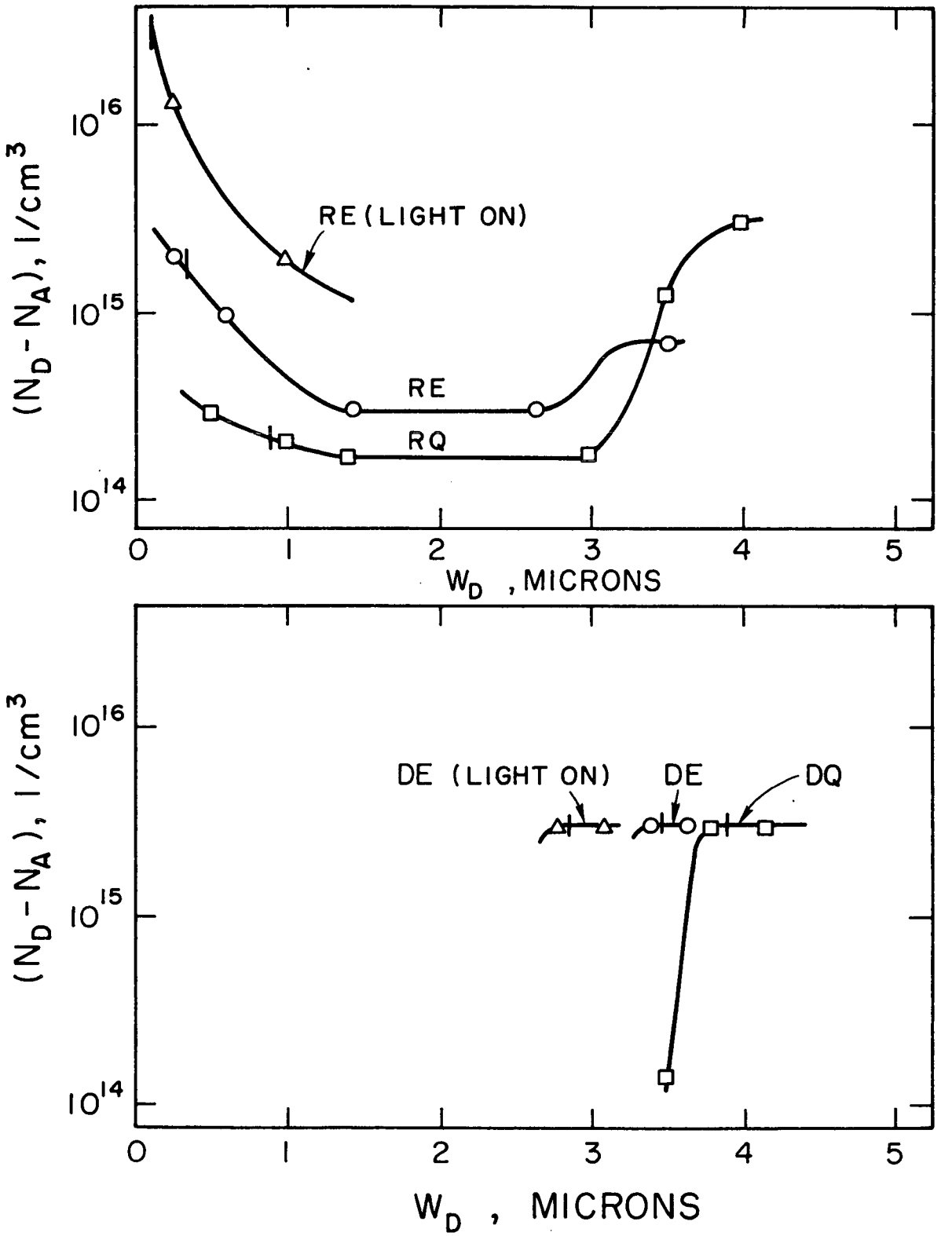

FIG. 4-25. Net donor density (N_D-N_A) versus depletion layer width w_d for cell #81 at 150°K. The zero bias value of w_d is marked on the curves.

starting material.

4.3.9 Effects of Depletion Layer Width on I_{sc}

In order to relate the short-circuit current of the cell to the junction profiles of the previous section, it is helpful to plot I_{sc} versus the zero bias depletion layer width, w_d. These data also demonstrate in a different way the effect of enhancement and quenching on I_{sc}.

Cell #81 was restored and cooled to 150°K where I_{sc} was measured over the range of currents obtainable by enhancement (with 0.535μ light at 290 $\mu w/cm^2$) and quenching (with 0.95 light at 570 $\mu w/cm^2$ plus 5 V reverse bias). The transient technique of Section 4.3.4 was used with weak probe light at 0.70μ (9.3 $\mu w/cm^2$) to excite I_{sc}. The junction capacitance was measured before each probe. The data are shown in Figs. 4-26 and 4-27 for several degrees of restoration and two HT times.

These data support the hypothesis that in the degraded state the capacitance is dominated by the width of the i-layer thus effectively masking any change in junction capacitance brought about by enhancement or quenching. These changes can only be seen in the restored cell where the Cu doped layer becomes conductive or in a degraded cell in which the i-layer is much thinner. Considering the fact that the width of the Cu doped layer is constant during this measurement the data imply that the width of this layer is not the major controlling factor for the photocurrent.

The end points on the curves show the limits of the values of I_{sc} obtainable by enhancement or quenching for the various states of restoration under these experimental conditions.

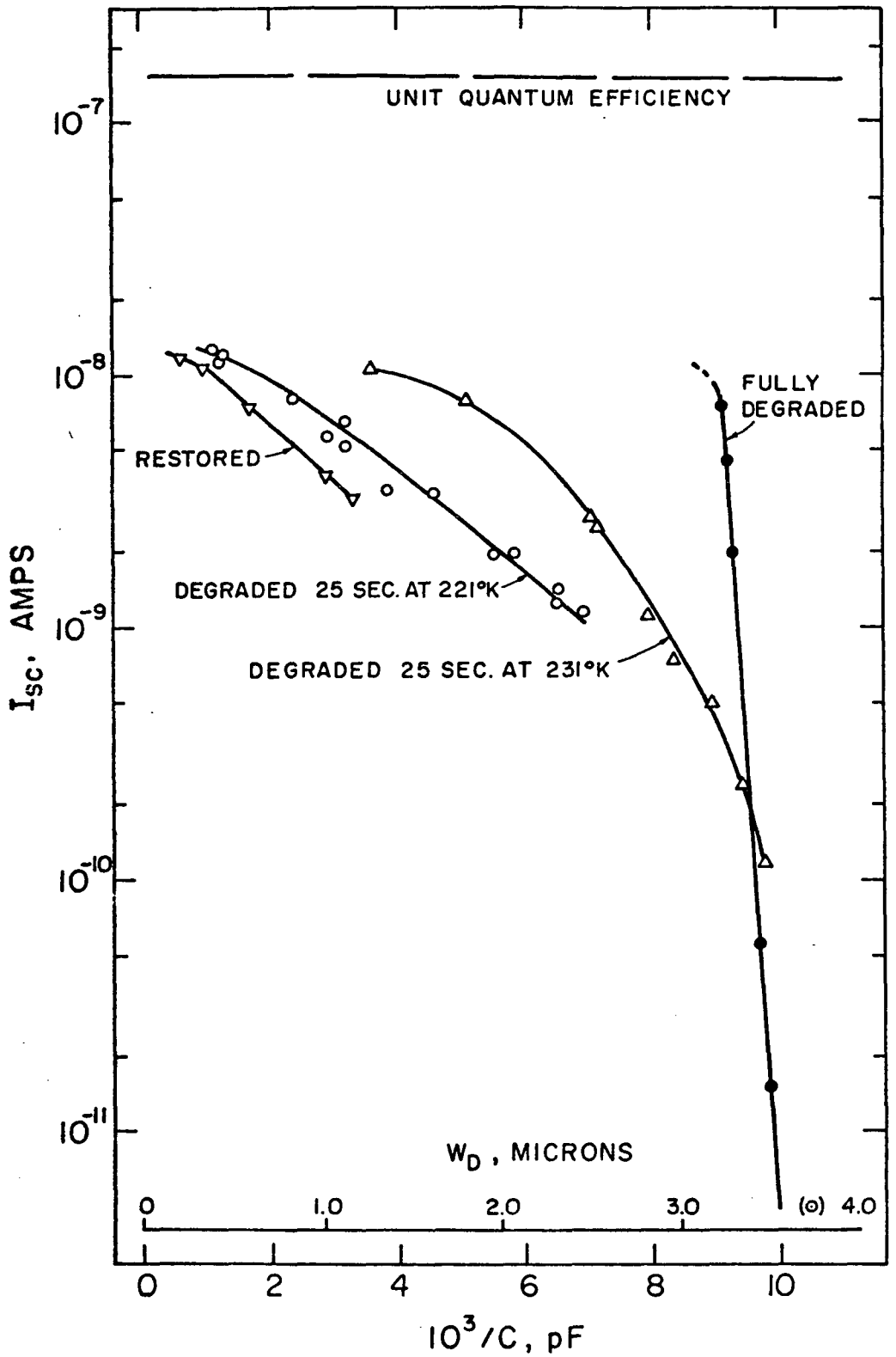

FIG. 4-26. Short-circuit current versus reciprocal capacitance for cell #81 (∿1 hour of HT) at 150°K. The cell was degraded for times and temperatures shown with 0.535μ light.

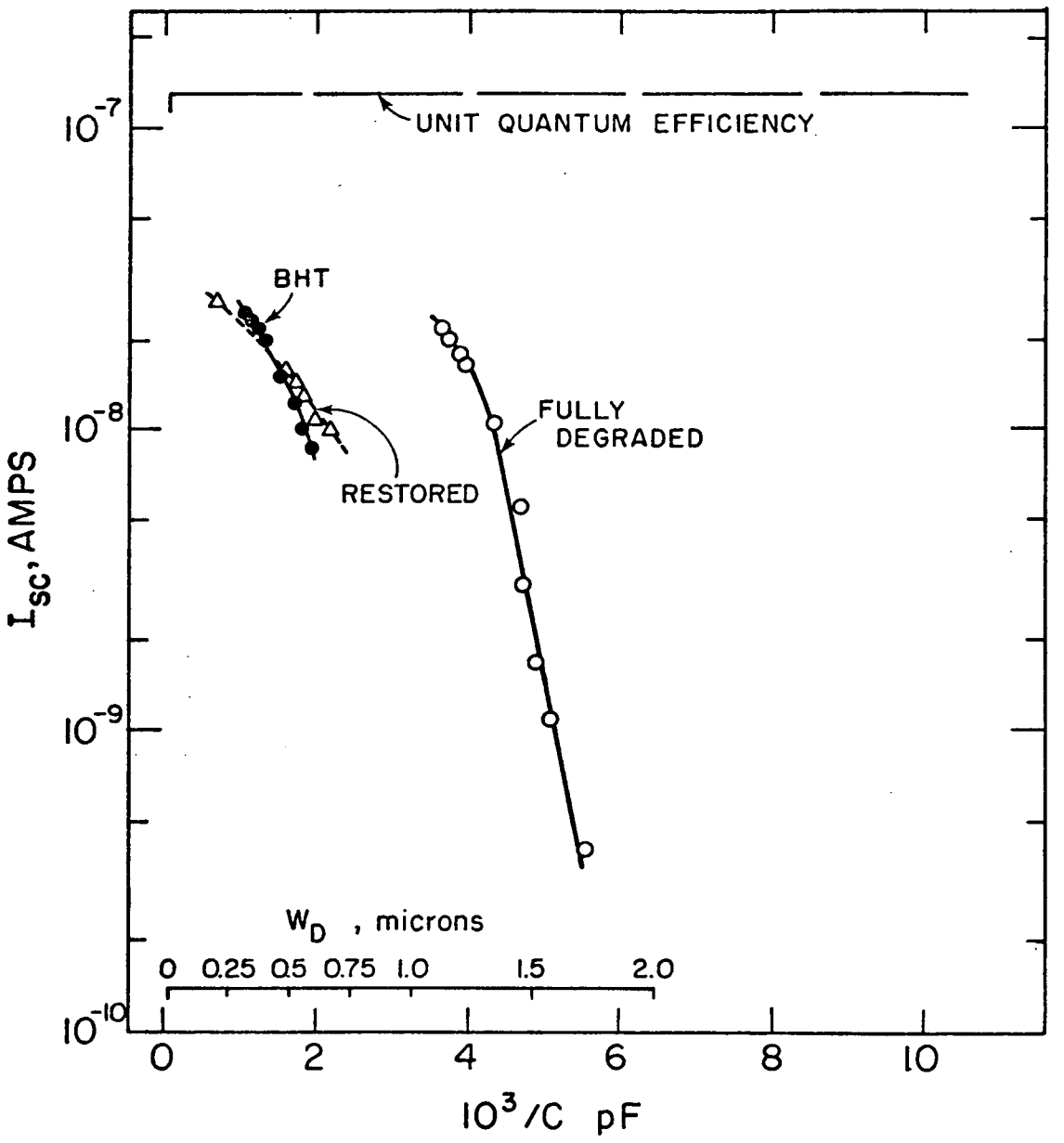

FIG. 4-27. Short-circuit current versus reciprocal capacitance for cell #61 at 150°K. Curves are for the cell before HT, and for the fully restored and fully degraded states after ∿6 min of HT.

These data show an exponential dependence of I_{sc} on w_d for the restored case. The same exponential dependence, with somewhat greater slope, has been reported by Lindquist[45] for cells before HT.

4.3.10 Effect of Cell State on the Dark I-V Curves

The dark forward bias current versus voltage curves for a typical cell (#81) shown in Figs. 4-28 and 4-29 demonstrate the large changes taking place as the state of the cell is changed. Although individual differences from cell to cell remain, there is enough agreement so that qualitative comparisons can be made.

These data were taken for both increasing and decreasing voltage on an x-y plotter. Since no appreciable hysteresis appeared they are stable curves with the exception of DE-150°K where the bias voltage quenched the cell very slightly during the cycle. The "light-on" curves were measured while the cell was illuminated by 0.535μ light of intensity 290 $\mu w/cm^2$ to maintain maximal enhancement. The photocurrent was then subtracted. Values of α from the diode relation, $I_f = I_o [\exp(\alpha V) - 1]$, are shown where applicable.

By examination of these curves and comparison with data from other cells the following observations can be made:

(1) Currents in the quenched states are lower than those in the corresponding enhanced states (often by several orders of magnitude). The ratio between E and Q currents generally becomes smaller at higher biases.

(2) The high bias slope (α) is usually 23 to 28 except in the light-on situation and the R-150°K states.

(3) In the R-150°K cases and the DE-light-on cases (both 150°K

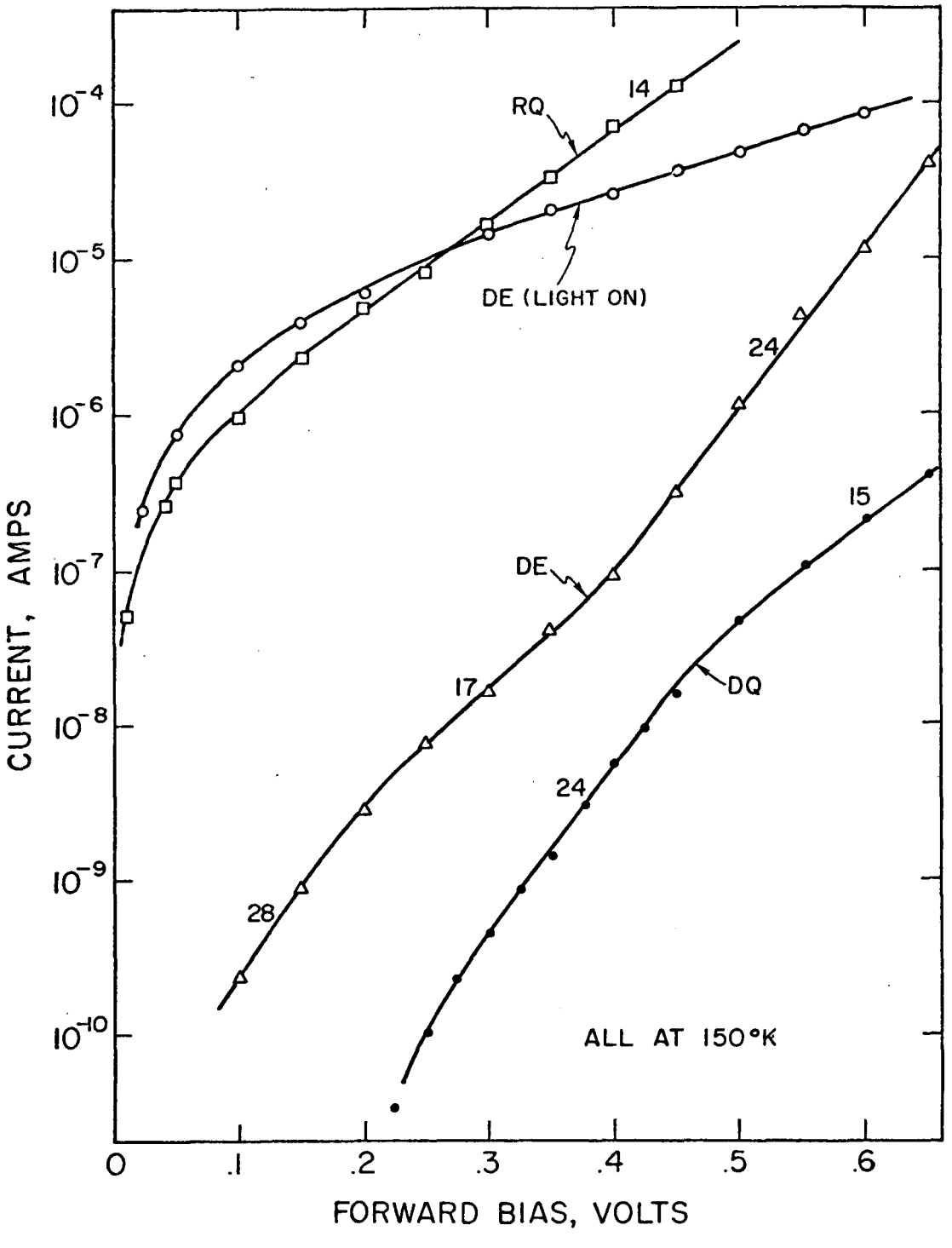

FIG. 4-28. Dark current versus forward bias voltage at 150°K for cell #81. "DE (on)" is done with enhancing light on and the short-circuit current has been subtracted. Values of the exponential slope α are shown on the curves. For a perfect Shockley diode, α = 77.1/volt at 150°K.

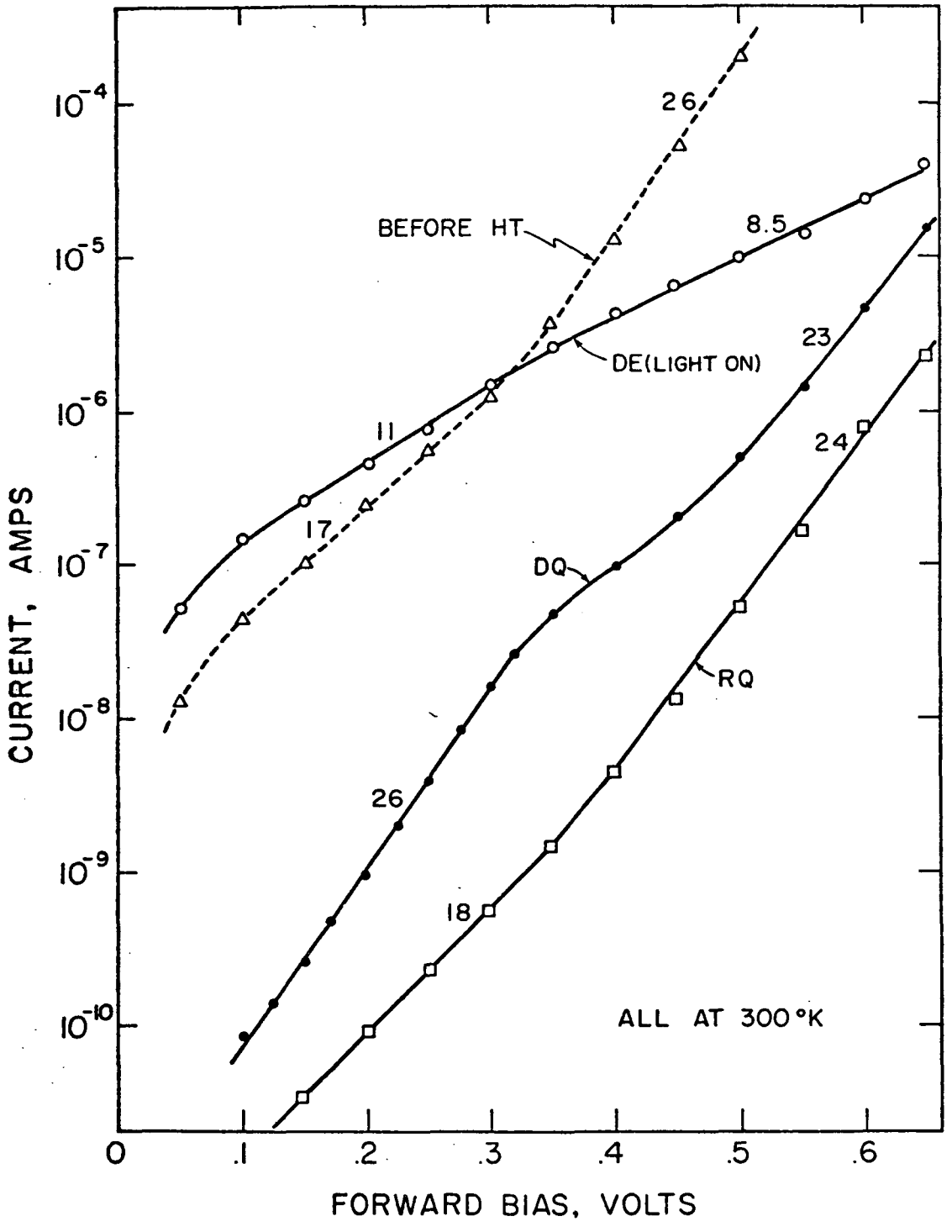

FIG. 4-29. Dark current versus forward bias voltage at 300°K for cell #81. For a perfect Shockley diode, α = 38.6/volt at 300°K. A before HT curve is shown for comparison.

and room temperature) the current is dramatically raised and the curves take on a form which can be fitted by $\exp(\beta\sqrt{V})$ rather than the straight line segments represented by $\exp(\alpha V)$.

(4) The form of the log I versus V curve before HT is very similar to that of the RQ-300°K state in all cases examined (from $\sim$6 minutes of HT to more than an hour) although the magnitude of the current is decreased by a factor of $\sim 10^3$ for the HT cases.

(5) The data for cell #81 shown in Fig. 4-29 is somewhat atypical in that the current in the DQ state is higher than that for the RQ state. More typical is an RQ curve in the position shown with the DQ curve lower by an order of magnitude or two.

4.3.11 Variation of Dark Forward Bias Current with Temperature $T < 300°K$

In this section we consider the variation of the dark I-V curves with temperature more carefully. A series of I-V curves taken in temperature increasing steps from 104°K to 300°K are plotted as log I versus $V^{1/2}$ in Fig. 4-30.

The degree of the restoration affects the shape of the I-V curves significantly. Thus when the cell was restored at 140°C for 2 minutes, a curve (labeled 140°C HT in Fig. 4-30) containing both high and low slope segments was obtained at 300°K and the current increase on cooling was small. After an additional HT at 200°C for 2 minutes, however, the low slope portion of the curve moved to much lower currents and the current increase on cooling was large. The remainder of the curves were taken in this condition.

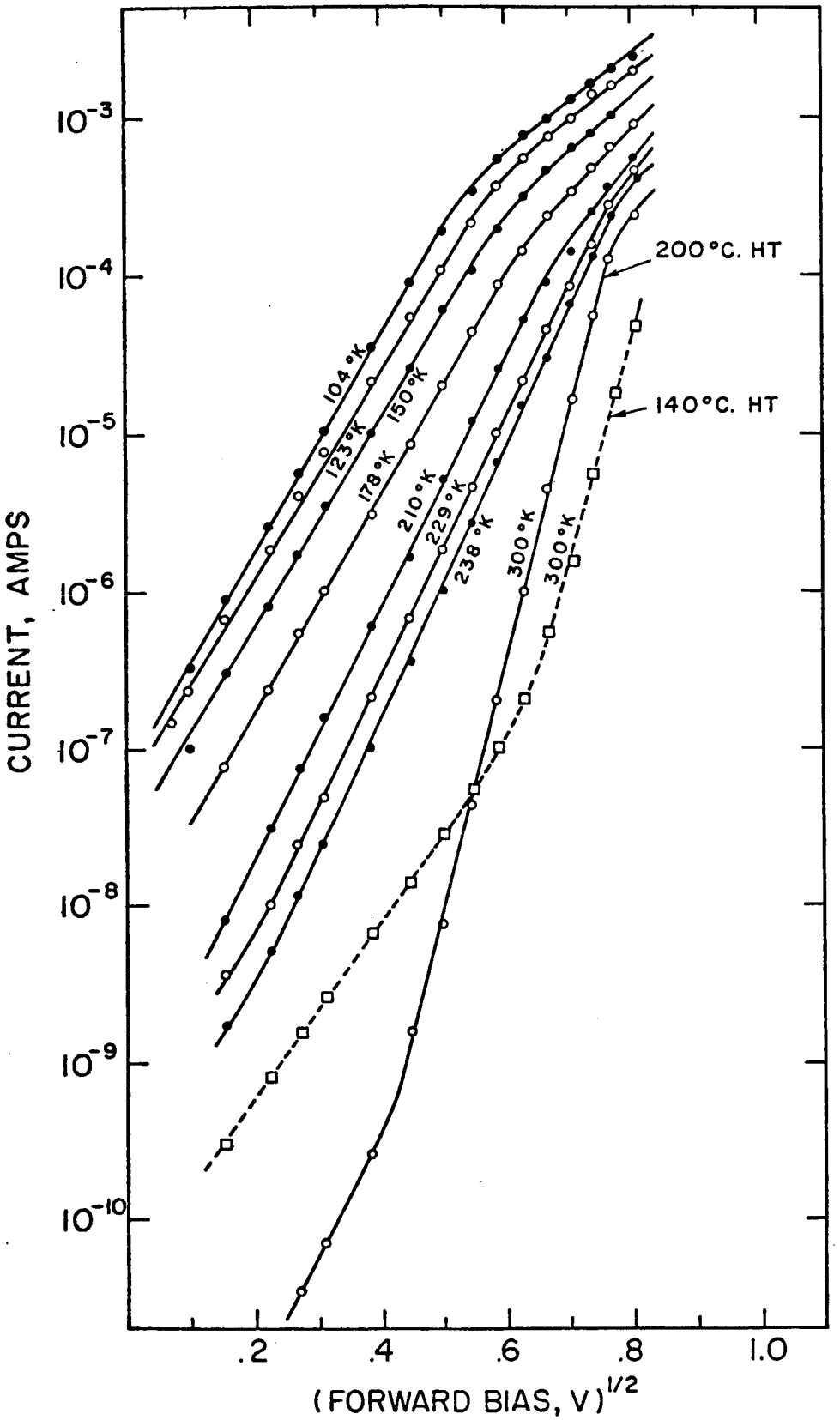

FIG. 4-30. Dark forward bias current versus $V^{1/2}$ for cell #61. Curve labeled "140°C HT" was taken after the cell was restored for 2 min at 140°C. Cell was restored 2 min at 200°C for the remaining data.

It can be seen that the RQ current follows an $\exp(\beta V^{1/2})$ law quite well. Although the slope changes little below ∿200°K, the current is a strong function of temperature.

The same sort of $\exp(\beta V^{1/2})$ dependence was seen in the commercial thin film cell (after HT) measured by Gill[69]. In that situation the $V^{1/2}$ dependence holds from 119°K to 295°K and up to a bias of about 0.5 volts.

In order to study the temperature variation of the dark forward bias current, I_f in more detail, several temperature cycles at constant bias were run in both DQ and RQ states.

In the course of the measurements, another variable appeared. If, in the RQ state, the cell was cooled from room temperature with a forward bias, V_f = 0.4 volts for example, the current measured at a V_f = 0.15 volts had risen to around 10^{-4} amps at 150°K. Quenching with wavelengths in the range 0.80μ to 1.10μ lowered the current only ∿20%. However, reverse bias V_r = 3.0 volts caused a reduction to 2×10^{-6} amps in 15 seconds. Further applications of V_r and 0.95μ light resulted in a stable value of 0.34×10^{-6} amps. The increase of current due to cooling with forward bias is somewhat sensitive to the cooling rate, especially at higher biases, but reproducible data were obtained by standardizing conditions.

Data taken on cell #81 for increasing temperature in the RQ state are presented in Fig. 4-31 for the following 3 cases:

(a) At V_f = 0.4V (after cooling with V_f = 0.4)

(b) At V_f = 0.15V (after cooling with V_f = 0.15)

(c) At V_f = 0.15V (after cooling with V_r = 5.0).

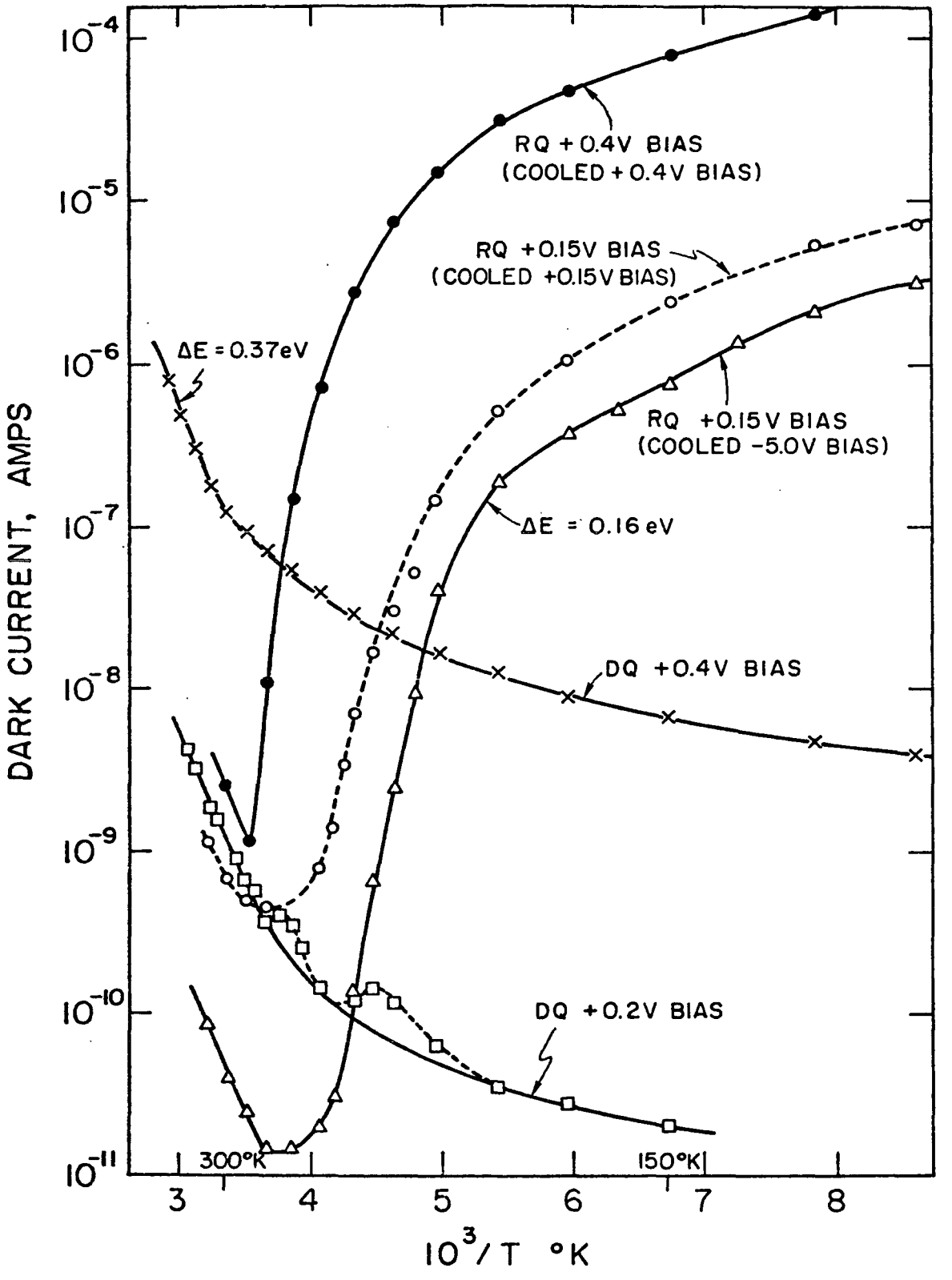

FIG. 4-31. Dark forward bias current versus reciprocal temperature for cell #81. All curves are taken during heating cycle. Transient thermally stimulated current peaks appear on the DQ, 0.2 V bias curve.

These data are in substantial agreement with the data of Fig. 4-30 which were taken for a different cell.

Above room temperature the current increases with increasing temperature with a thermal activation energy of 0.3 to 0.4 eV while below $\sim$180°K the current decreases with increasing temperature with an apparent activation energy of 0.16 eV (but this may be somewhat rate dependent).

Current in the RE case is even higher than the RQ case shown here. The reverse bias current also shows a large increase in the restored state at 150°K, as compared with the other possible states. Although different in detail, data from other cells with as much as an hour of HT corroborate these data showing a large increase in current as temperature is decreased.

In contrast the forward bias current in the DQ state behaves quite as expected as the temperature is lowered. Near room temperature I_f shows an activation energy of 0.3 to 0.4 eV and at lower temperatures it appears to saturate at a constant value.

The curve for the DQ state shown in Fig. 4-31 correspond very well to Lindquist's results for un-HT cells[68]. He extrapolated the high forward bias current to zero voltage to obtain I_o in the expression $I_f = I_o(\exp \alpha V - 1)$ and plotted the results versus 1/T to obtain activation energies of 0.26 eV for an "a" face cell and 0.47 eV for a "b" face cell and a similar saturation at a constant "leakage current" at low temperature.

Gill's before-HT cell showed little temperature dependence of either logarithmic slope or value of the forward bias characteristic; however, only the low bias region (α = 12.5) was observed[69]. After HT

Gill found a strong temperature dependence and an activation energy of 0.43 eV near 300°K and at V_f = 0.5 volts. Gill also investigated a commercial thin film cell and found only a weak dependence of the dark $I_f - V_f$ characteristic on temperature in what appears to be the low α region.

T > 300°K

In the course of making elevated temperature measurements, it was noticed that a stable and reproducible current was produced by the cell in the dark with zero applied bias. During the experiments with cell #89, the cell was mounted on a copper strip with thin layers of mica and Insulgrease (a thermally conducting mounting compound manufactured by General Electric) between. The Cu_2S side was normally in contact with the mica and the temperature of the strip was controlled so that due to radiation losses the Cu_2S was probably slightly hotter than the CdS. On reversing the cell in the sample holder, thus making the CdS somewhat hotter, the zero-bias currents were observed to be reversed in direction. Thus it was concluded that these currents were driven by the thermal gradient across the sample. Even though the temperature difference is estimated to be less than 5°C across a 1 mm thick cell, the currents are appreciable. These considerations suggest that the current is thermionic in character, resulting from most of the thermal gradient being across the potential barrier of the cell. The zero-bias current for the Cu_2S hotter than the CdS condition is shown in Fig. 4-32 (cell #89), plotted as log I_f/T^2 versus 1/T, assuming a Richardson-law dependence. This current is in the same direction as a photoexcited short-circuit current. For the case where the CdS is hotter than the Cu_2S,

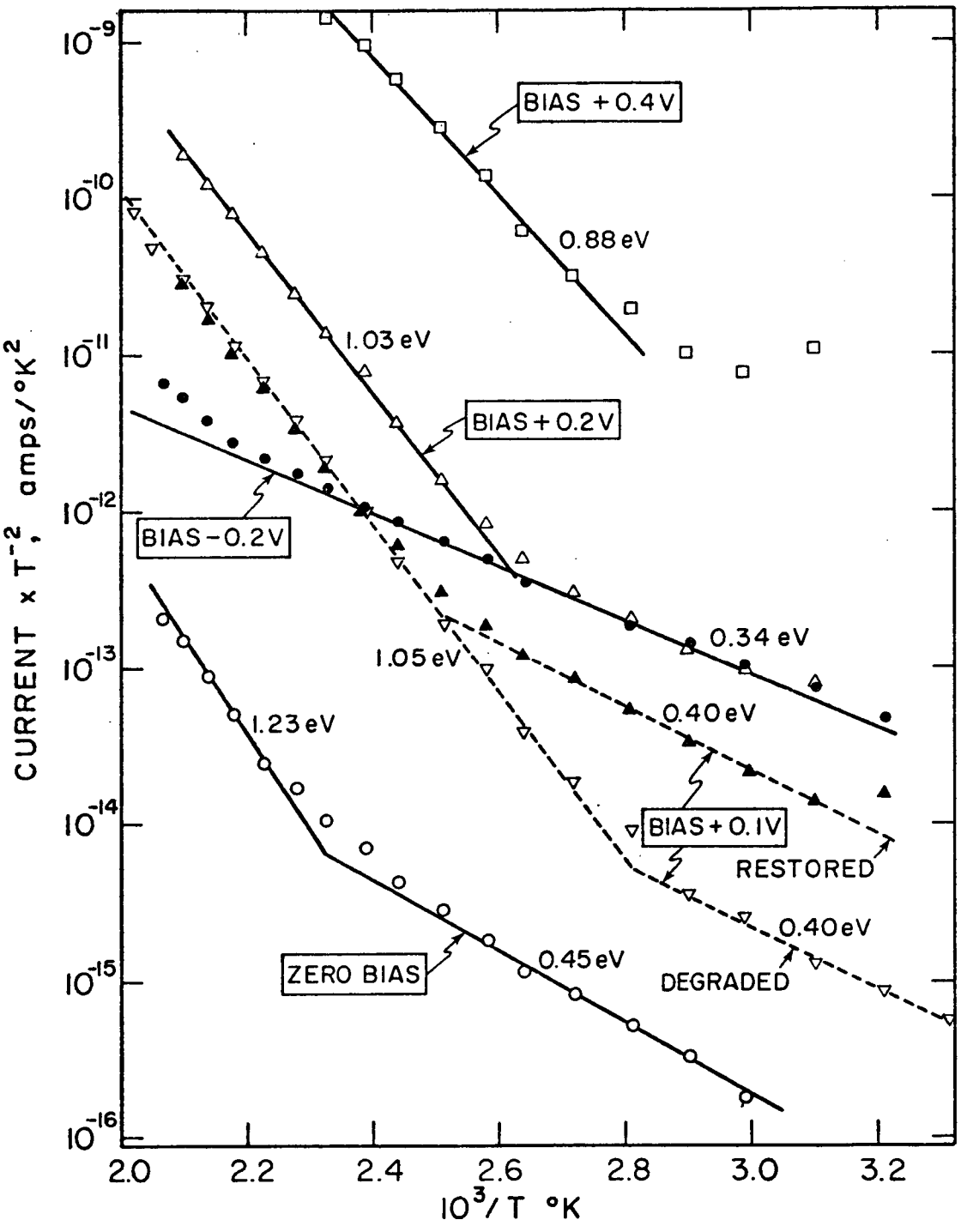

FIG. 4-32. Dark current versus temperature for Cu_2S hotter than CdS, with zero bias and with various values of forward and reverse bias. All for restored state, except as noted. Currents are in reverse direction for zero and -0.2 V bias.

the direction of the current is opposite to that of the photoexcited short-circuit current, and about 1/3 of the magnitude of the current measured with the Cu_2S hotter; both curves, however, show the same temperature dependence, with an activation energy of 1.2 eV at higher temperatures, and an activation energy of 0.45 eV at lower temperatures, the latter being less well defined for the CdS hotter.

Taken by themselves these data are interesting, but not particularly interpretable because of the complex nature of the possible phenomena involved. When compared with data on the temperature dependence of dark current under forward and reverse bias, however, they form a strong case for the identification of the activation energies involved in the zero-bias "thermionic" case with the energy barriers determining the basic electrical properties of the heterojunction. Figure 4-32 also shows data for 0.1, 0.2 and 0.4 V forward bias and 0.2 V reverse bias. Measurements by Gill[16] indicated a higher-temperature dark forward-bias current activation energy of about 1.2 eV for a HT cell, and Lindquist[17] saw, near room temperature, a dark forward-bias current activation energy of about 0.47 eV for a cell before HT.

The activation energies obtained at various bias voltages are summarized in Table I for the case of Cu_2S hot. These values have been corrected for the applied bias by assuming that a tunneling level (located 0.45 eV above the Fermi level at zero bias) is present in the junction region. When the cell is biased, the tunneling level is shifted by an amount equal to about half the difference between the Fermi level in the Cu_2S (at the top of the valence band) and the Fermi level in the CdS (near the conduction band edge of CdS), i.e., a shift equal to one-half of the applied bias voltage. Such a model implies a dark current

through the heterojunction which consists of two components: (a) a current going over the barrier (called the diode current here), and (b) a tunneling current through the level 0.45 eV above the dark Fermi level. This model explains all of the curves in Fig. 4-32, including the difference between the +0.2V and -0.2V bias curves. This difference arises because the current through the tunneling center for reverse bias is much larger than the diode current which encounters a 1.4 eV barrier. In the forward-bias condition, the diode current encounters about a 1.0 eV barrier and overwhelms the tunneling current at a lower temperature.

As far as the zero-bias current is concerned it would be expected that a thermoelectric effect corresponding to each of the junctions involved in the cell would develop a potential depending linearly on temperature for small temperature differences across the cell. The measurement, however, is of short-circuit current, and this current is controlled by thermal excitation with an exponential temperature

Table 4-1

DARK CURRENT ACTIVATION ENERGIES, eV

Bias	Low Temperature Range		High Temperature Range	
	Measured	Corrected to 0 Bias	Measured	Corrected to 0 Bias
0	0.45	0.45	1.23	1.23
+0.1	0.40	0.45	1.06	1.16
+0.2	0.34	0.44	1.03	1.23
+0.4	-	-	0.88	1.28
-0.2	0.34	0.44	-	-

dependence. The consistency of the activation energies in the zero-bias case with those for nonzero bias supports this hypothesis. The other energy gaps or barriers in the system are either too small (at the In-CdS and In-Cu_2S ohmic contacts) or too large (the CdS band gap) to control the supply of carriers in this temperature range. Thus the current must be controlled by the Cu_2S-CdS barrier.

The expression for the diffusion current across a p-n junction diode contains a pre-exponential factor which varies as T^n where $2.75 \leq n \leq 4.25$, depending on the type of scattering involved. On the other hand, the expression for thermionic emission from a metal contact into a semiconductor involves T^2. This relation may be more appropriate in the case of zero or reverse bias, because of the almost metallic character of the Cu_2S. Thus the pre-exponential factor T^2 was chosen. Since the exponential dominates (especially for the higher temperatures), the power of T makes only a small difference in any case.

Data taken for the CdS hotter than Cu_2S, showed the same bias-corrected activation energy of 1.2 eV for all biases, but the 0.45 eV energy was either absent or too small to measure. Magnitudes of the current and +0.2 and +0.4V were about the same as for the Cu_2S-hotter case, but for zero bias the current was smaller by a factor of 2.5, and for -0.2V it was smaller by a factor of about 10^2.

The forward current through the 0.45 eV level at 0.1V forward bias is about 10 times greater for the restored state than for the degraded state for this cell (see Fig. 4-32). This difference may be due to a change in the density of these levels on degradation, or to a change in the local thickness of the depletion layer. (Although this thickness

does not change appreciably from degraded to restored states at or above RT, the state of quenching or enhancement, which does affect the depletion layer width, may change during such heating.) Current flow through this level does not appear to be as important for the CdS-hotter case.

The cell described in Fig. 4-32 has undergone a total period of heat treatment at 200°C of about 3 to 4 hrs. In order to avoid the possibility that its properties were uniquely determined by this extensive heating history, we examined a new cell (#81) after only 10 min of heat treatment at 200°C. The new cell was mounted in a holder (shown in Fig. 3-2) in which thermal contact was made on the faces of the CdS perpendicular to the Cu_2S layer. This holder more nearly enclosed the cell thus further reducing thermal gradients. The same activation energies and the presence of a dark zero bias current were confirmed with this cell. Data for 0.1 volts forward bias, for example, agreed almost exactly with the previous data except that the 0.45 eV portion of the current was reduced in magnitude.

It may be concluded from the above data that an energy barrier of about 1.22 eV, equal to the band gap of Cu_2S, exists in the cell after HT, and that the dark currents behave in an appropriate manner as different bias voltages are applied. This activation energy persists at least over the range 90° to 210°C, and seems quite stable over this range. Further, it dominates dark forward bias current for high temperatures and/or biases. There also appears to be a defect state in the potential barrier about 0.45 eV above the zero-bias Fermi level, through which current can tunnel in both directions. The 0.45 eV level dominates the dark forward bias current near room temperature or below for bias voltages below $\sim$0.4 volts--where the cell is operated for power generation.

4.3.12 Thermal Cycles for I_{sc}

Complete thermal cycles of short-circuit photocurrent, I_{sc}, demonstrating the interaction of restoration/degradation and enhancement/quenching effects were measured for both the cell and the photoconductor to show the similarity of the processes in the two cases. Since the measurements were made with white light, both enhancement and quenching were taking place simultaneously and the curves represent the balance between the two.

A complete thermal cycle of I_{sc} for white light excitation for cell #89 is given in Fig. 4-33. The cycle starts with a completely degraded cell in the DQ state. As the temperature is decreased the cell goes to the DE state due to the decrease in thermal quenching of enhancement with cooling. There is little hysteresis as the cell is cycled back to room temperature. From 325°K to 375°K the current drops to unmeasurably small values ($<10^{-10}$ amp) as the state reverts from DE to DQ, and then increases as the temperature is raised and thermal restoration to RQ takes place. (The dark "thermionic" current has been subtracted from these data.) As the temperature is decreased from 475°K the cell is subjected to "cooling enhancement"* (see Section 4.3.14) below 350°K and enters the RE state. A small amount of optical degradation also occurs on this decreasing part of the cycle. Although a record was not taken for this particular cycle, the heating curve of the restored cell from 150°K to 300°K follows the cooling curve with only a small hysteresis.

*The enhancement here consists of two components: (1) equilibration to a white-light, restored state enhancement level appropriate for the temperature, implying decrease of thermal quenching on cooling and (2) enhancement due only to the act of cooling the cell. Taking into account the intensity of the light and the speed of the temperature scan the former is likely to be the largest component.

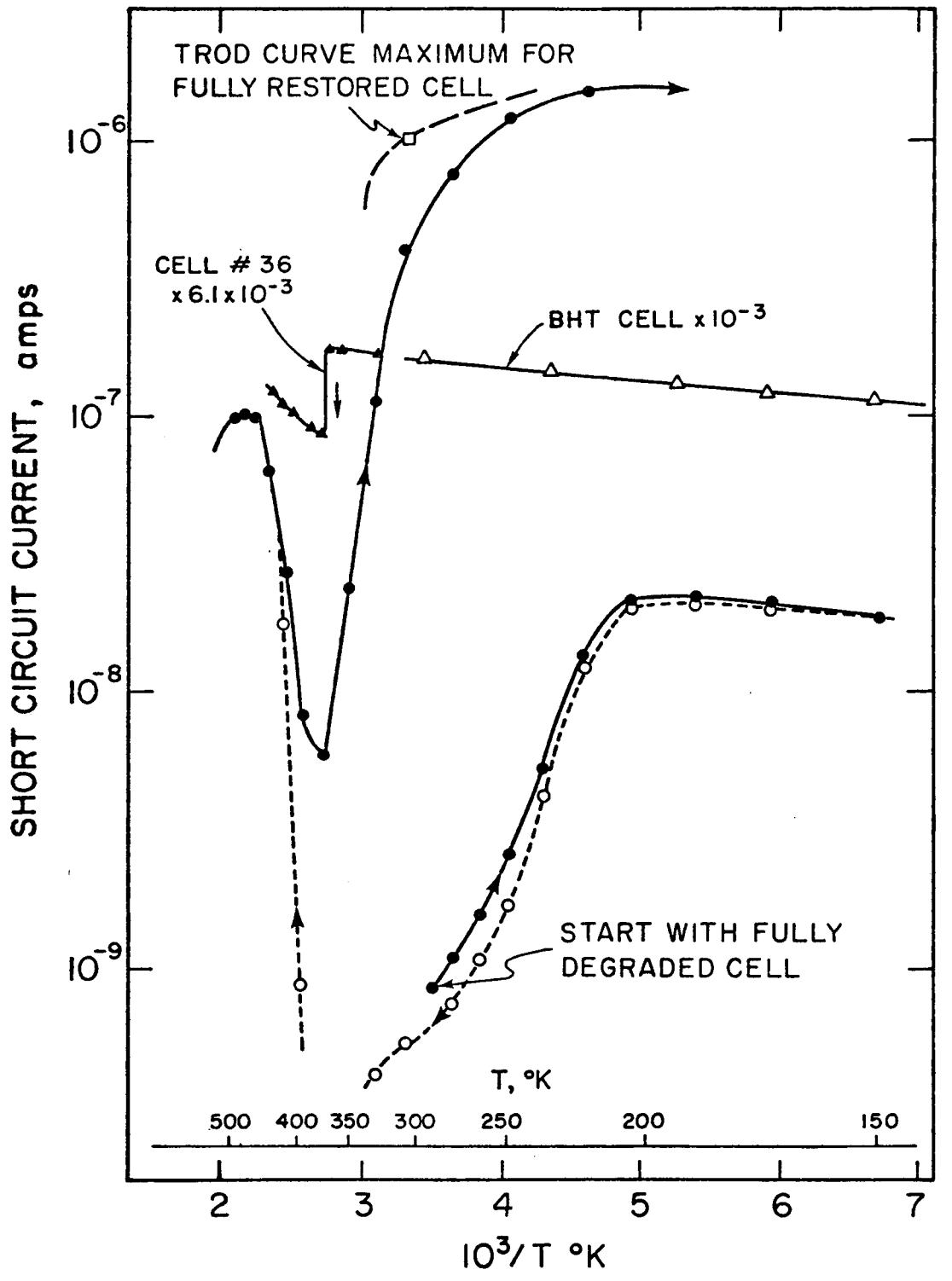

FIG. 4-33. White light short-circuit current versus inverse temperature. "BHT cell" are data from Lindquist[17] multiplied by 10^{-3} to fit on the plot conveniently. "Cell #36" data are taken after short HT at 150°C and are multiplied by 6.1 x 10^{-3} to join the BHT data. Other curves are for cell #89 after long HT (light intensity is 1400 μw/cm^2 for cell #89).

A "degradation maximum" (TROD curve maximum) for the same cell is shown for comparison.

By comparison with the HT case, there is very little temperature dependence of I_{sc} in the cell before HT. Data reproduced from Lindquist's work[17] for white light I_{sc} in Fig. 4-33 show only a 33% decrease as the cell is cooled from 300°K to 150°K. For the range above RT, data are shown for cell #36 which had been HT to 160°C for about 1 minute prior to this heating cycle. The data has been normalized to join Lindquist's curve. These data, also taken in white light, show an abrupt step in I_{sc} due to a phase change (to be discussed in Section 4.3.14) but there is no rapid variation in current on either side of the step.

The complete cycle for the photocurrent in the photoconductor for white light (1400 $\mu w/cm^2$) is shown in Fig. 4-34, and can be compared directly with the cycle shown in Fig. 4-33. The cycle shown in the lower curves starts with a fully degraded photoconductor at 270°K while the cycle shown in the upper curves starts with a fully restored photoconductor at 300°K.

The dark current for both degraded and restored cases is also shown on Fig. 4-34. On heating the photoconductor in the degraded state, a relative maximum in current occurs at about 400°K which appears to be a thermally stimulated current peak accompanying the restoration process. The peak disappears on cooling and it does not reappear on heating the restored photoconductor. The location and magnitude of the peak is quite variable depending on the rate of cooling, whether or not the photoconductor was cooled with light and/or bias on, and the method of degradation. Magnitudes from 1.4×10^{-10} to 2.5×10^{-8} amps have been observed

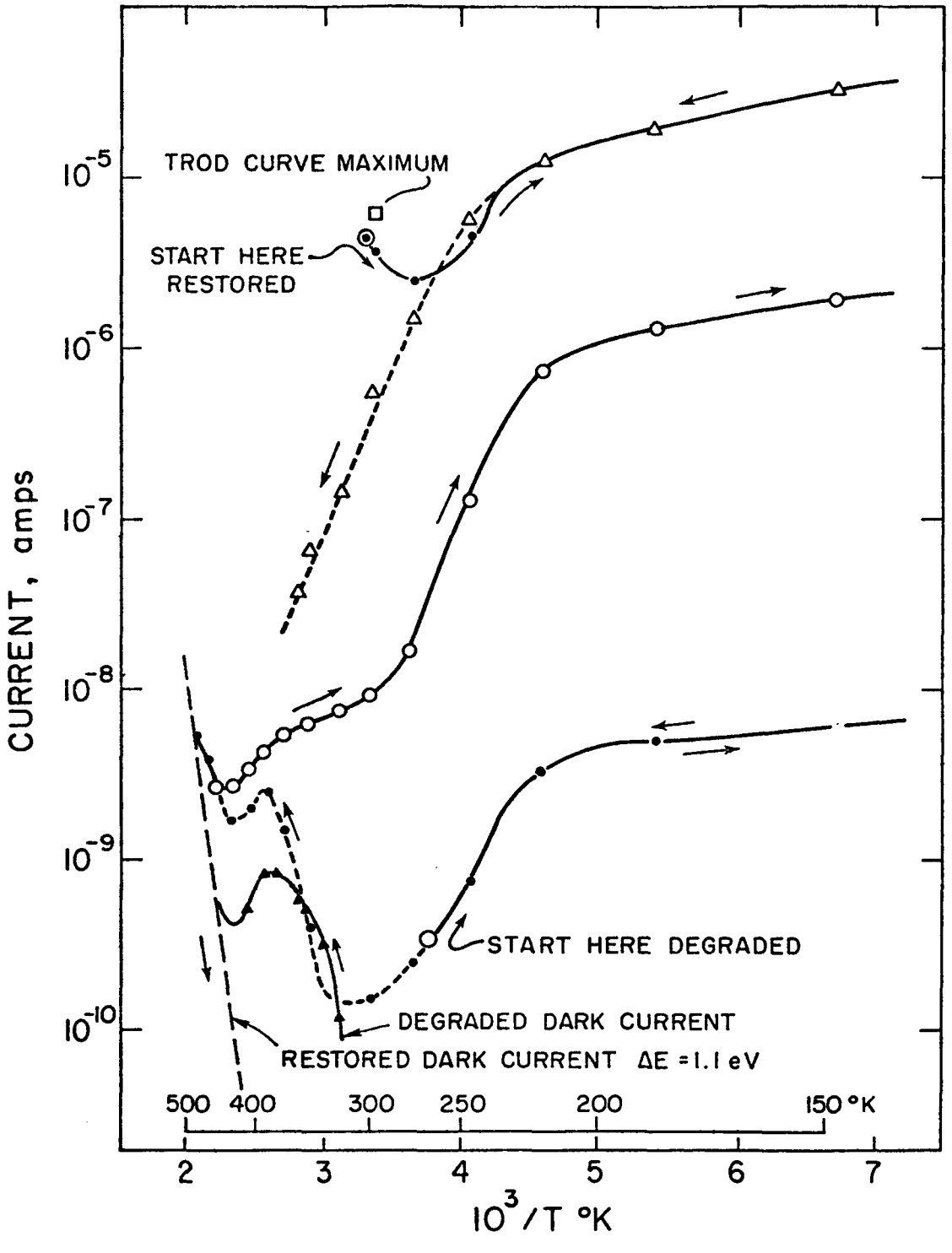

FIG. 4-34. Photocurrent (white light, 1400 $\mu w/cm^2$) versus reciprocal temperature for the photoconductor. Temperature dependence of dark currents are shown by dashed line at left. Rate of scan is $\sim$1°C/sec.

at temperatures ranging from 360°K to 425°K. For this reason a representative curve is shown and the dark current has not been subtracted from I_p. I_p probably becomes unmeasurably small as the degraded photoconductor is heated from about 320°K to 380°K, the observed peak there being only dark current. On the restored branch, however, the dark current in this range becomes very small compared to the photocurrent.

The reduction of thermal quenching in the cell produces a large increase in the current in the degraded state as the cell is cooled. In the restored state this thermal quenching shoulder is shifted toward higher temperatures and the cell's white light equilibrium enhancement is much larger at room temperature than in the degraded state. This shift of the thermal quenching shoulder appears to be smaller in the photoconductor case. The magnitude of the shift in the upper heating branch (in Fig. 4-34) from the restored state may be lessened because of degradation during the cycle, however, which is larger and faster in the photoconductor than in the cell.

4.3.13 Relationship of I_{sc} to I_f

Thus far we have treated the short-circuit current and the dark, forward-bias current as dependent variables, each of which depend on the properties of the cell. Now we wish to complete the picture by showing directly the relation between them. We have found a monotonically increasing relationship between I_{sc} and I_f over a wide range of conditions.

After restoring cell #89 (HT about 1 hr) it was taken over a TROD curve at 300°K with white light such as that shown schematically in Fig. 4-9. The degradation of the cell was interrupted at various times both before and after the TROD maximum to measure the dark, forward-bias

current and the stable I_{sc} response to a white light of intensity 14 $\mu w/cm^2$. The results, for a bias of 0.1V, given in Fig. 4-35 show an almost linear dependence over 3 orders of magnitude. The TROD curve corresponds to a RQ to RE to DQ transition with time, and in the figure, the points taken during the rise of the TROD curve are distinguished from those taken during the decay. The I_{sc} begins to saturate around 10^{-8} amps because this is the maximum current injected by the Cu_2S.

Similar data were taken at 150°K for cell #61 with 6 min of HT. In this case the cell was put into several definite states of restoration and the current was varied by enhancement and quenching. These results are shown in Fig. 4-35 in terms of I_{sc} excited by 0.70μ light of 9 $\mu w/cm^2$ intensity. These data were measured by the transient methods described in Section 4.3.4 to avoid changing the degree of enhancement by the act of measurement.*

The 150°K curves are displaced along the I_f axis for different degrees of degradation while the 300°K data forms a single curve representing all degrees of degradation. This is the result of the anomalous rise of I_f for the R-150°K state described in Fig. 4-31.

4.3.14 The 82°C Phase Change

Examination of the temperature variation of I_{sc} in more detail reveals a reversible phase change at about 82°C which can be identified with the orthorhombic-tetragonal transformation in the djurleite ($Cu_{1.96}S$) form of copper sulfide. Figure 4-36 shows this variation for

*In the completely restored case the junction conductance is so great that the voltage drop of the measuring instrument (V = IR with R = 100 ohms or about 0.02 mV maximum in this case) begins to influence the measurement and I_{sc} starts to drop slightly for larger degrees of enhancement.

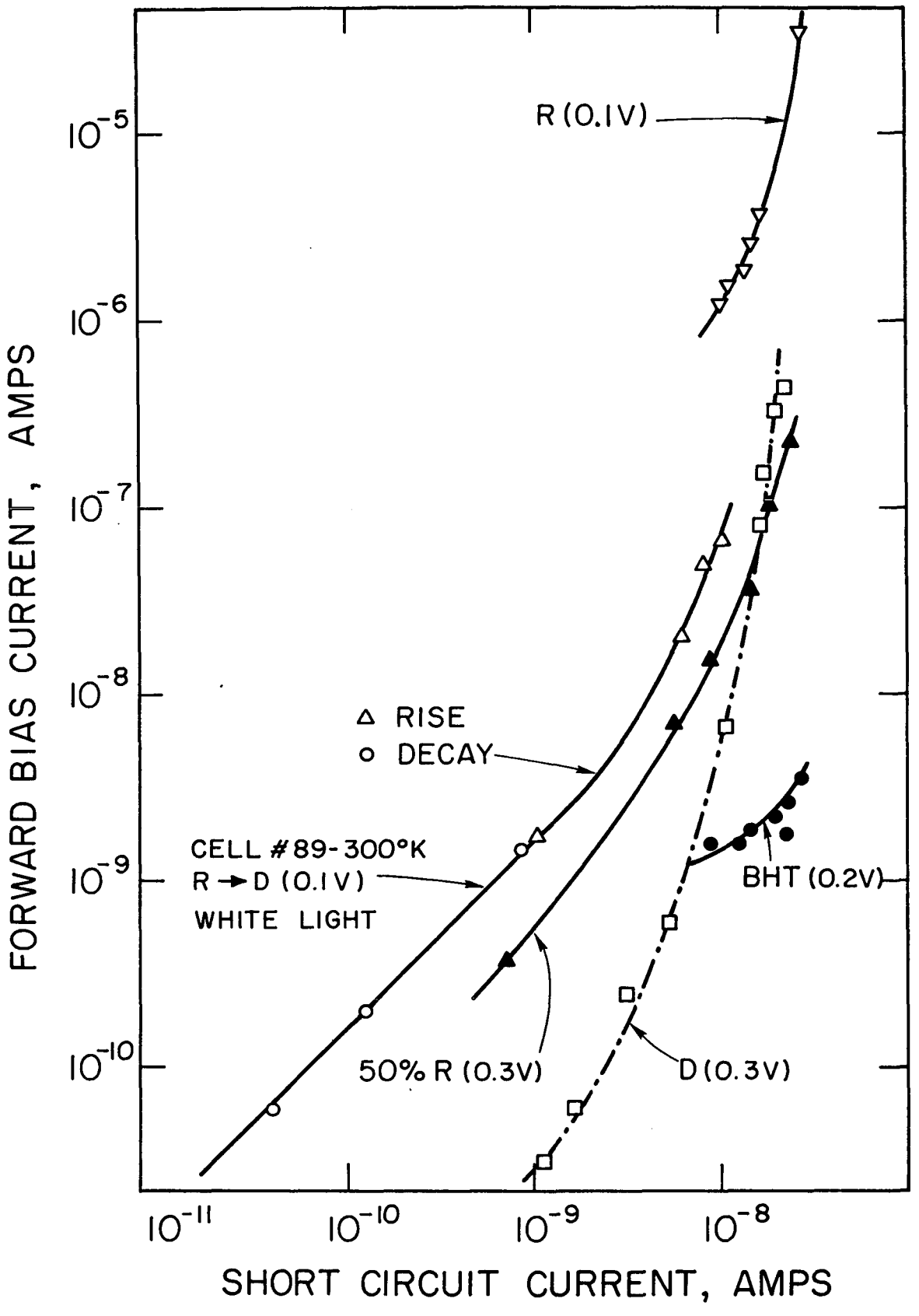

FIG. 4-35. Short-circuit current versus dark forward-bias current. Bias voltages as given. All curves are for Cell #61 at 150°K with 0.70μ light except as noted.

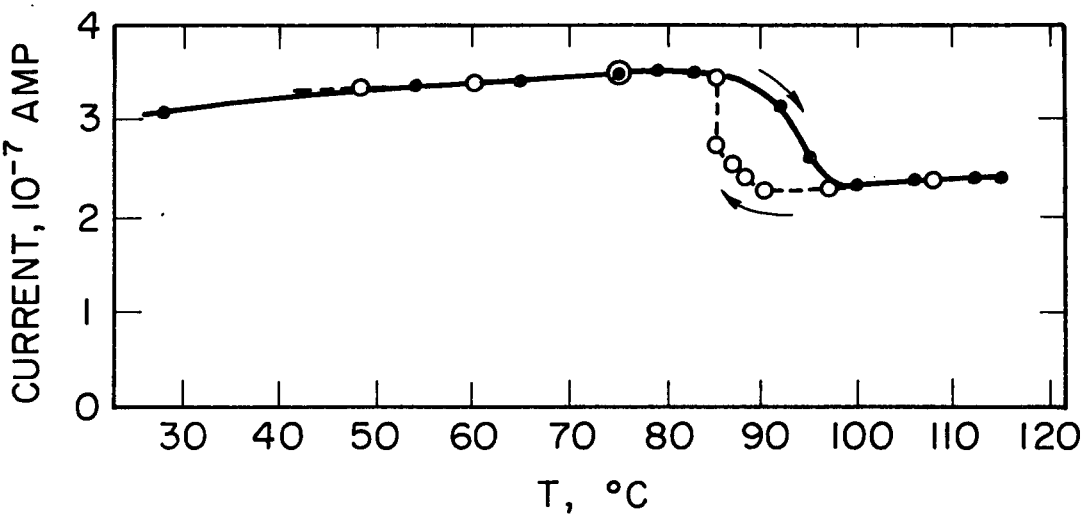

FIG. 4-36. White light short-circuit current versus temperature for cell #36.

monotonically increasing and decreasing temperature in an un-HT cell (#36, cycle time about 6 minutes). The transition on heating is rather sluggish but on cooling there is a rapid increase in I_{sc} with rise time less than 0.5 sec. The transition can be seen in both I_{sc} and the dark forward bias current. The effect was observed in 3 other cells after moderate HT. There was some variation in form depending on the degree of HT.

In cell #81 with 1-2 min of HT at 200°C, a step similar to the before-HT case is seen. The cooling enhancement effect starts at relatively high temperature in this cell and the current after the step is extremely sensitive to cooling rate. In this case, by cooling very slowly, the magnitudes of the transients can be reduced to the point where they are no longer visible. Figure 4-38 shows the cooling transients in four situations for the degraded state:

(1) Dark zero bias current ("thermionic" current).

(2) Dark forward bias current at 0.04 volts.

(3) I_{sc} with 0.535μ light of intensity 1 $\mu w/cm^2$.

(4) I_{sc} with 0.85μ light of intensity 5 $\mu w/cm^2$.

Comparison of the last two items suggests that the phase change is accompanied by enhancement of the cell. This may be due either to a heat flow effect or a piezoelectric effect produced by a change in interface strain on a volume change of the Cu_2S. The I_{sc} is not cooling rate dependent above the transition temperature.

After considerable HT of the cell (#89 in this case) the evidence of the transition became a large, instantaneous rise (with rise time limited by the measuring instruments) which rapidly decayed to the original path of the curve in 1-3 sec. This is shown in Fig. 4-37. In

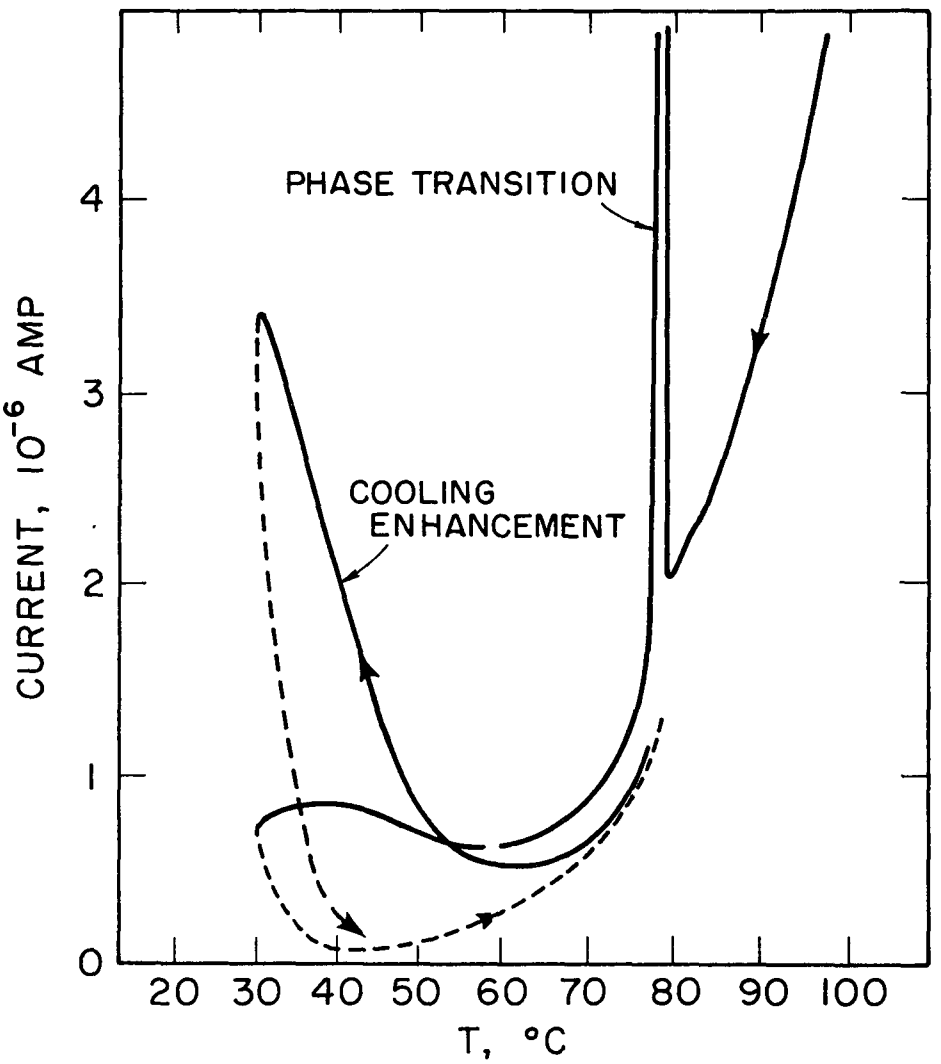

FIG. 4-37. Dark forward-bias current versus temperature for cell #89. Bias voltage 0.4 V.

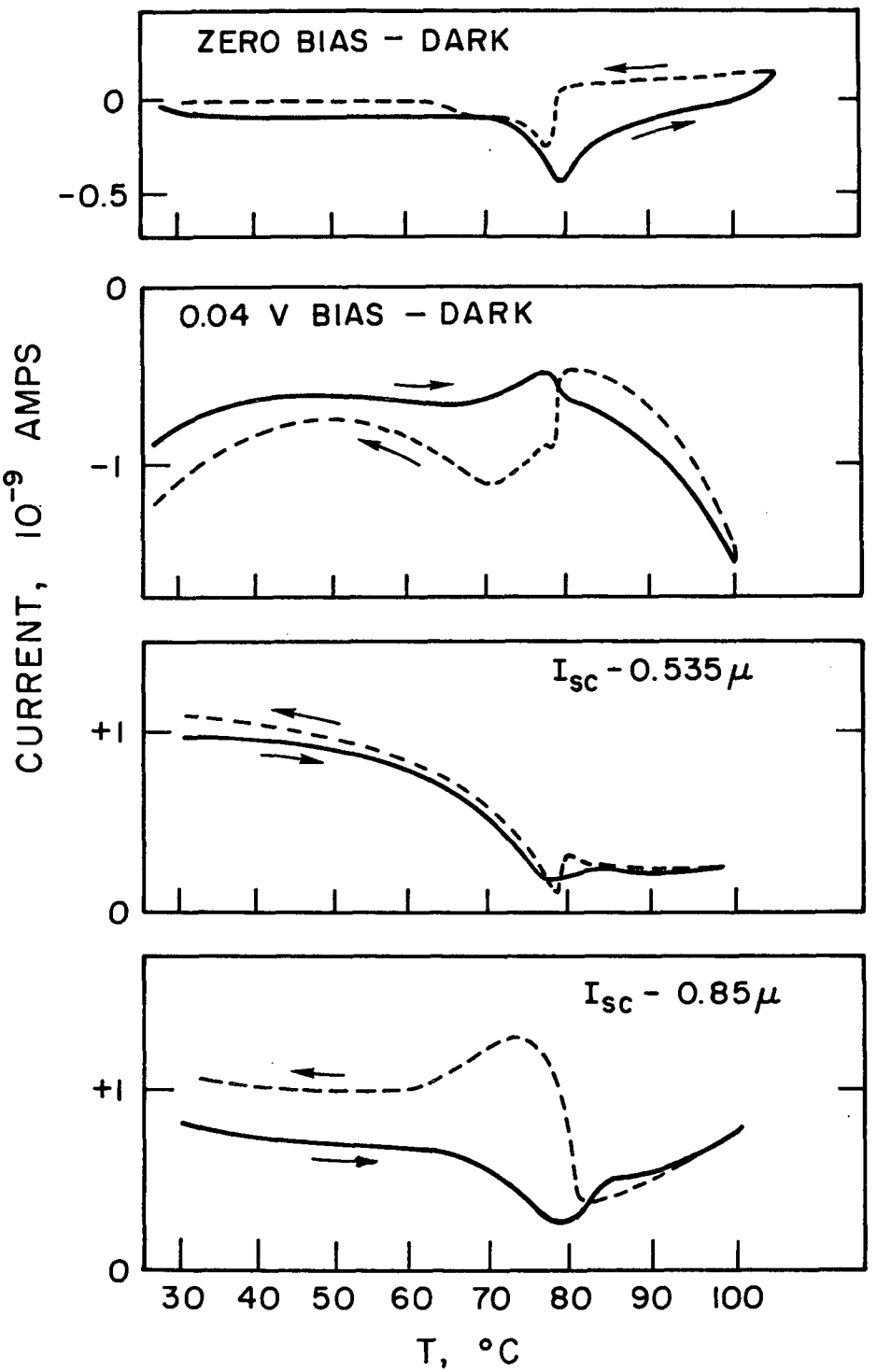

FIG. 4-38. Cell #81 currents versus temperature.

the restored state this cell shows the transition at 78°C and only on cooling. It occurs only if the temperature has exceeded about 92°C. After degradation the transition appears on heating also.

Although the mechanism for the change in cell properties during the transition remains in doubt, the evidence for the presence of the phase change is clear. Comparison of the stable nature of the phase change before HT with the transient nature after suggests that the control of the photocurrent has been transferred from the $Cu_{2-x}S$ to the CdS near the interface. Thus in the before-HT case a change of phase implies a different electron-hole pair generation efficiency. After HT, when enhancement and quenching effects dominate the control of current, the phase change may influence the state of enhancement (and thus the current) through either heat flow as the heat of transformation is dissipated or strain effects due to a volume change.

4.3.15 The Cooling Enhancement Effect

Rapid cooling of the restored cell in the temperature range from 80°C to 25°C produces enhancement of the cell which is exhibited as an increase in both I_{sc} and the dark forward bias current, I_f. The greater the cooling rate the greater the degree of enhancement produced. This enhancement is maximized by the application of forward bias during cooling, although it occurs to a lesser degree even with zero bias. The properties of the cell (as tested by the forward bias current in the dark) do not seem to be temperature rate dependent in any other region, and only for cooling in this region. The effect is either absent or small in the degraded state.

Figure 4-37 demonstrates this effect as represented by I_f measured at 0.4V on cooling restored cell #89. The curve is continuous and the second cycle is done at a faster cooling rate. The phase change spike was discussed in Section 4.3.13.

After 1/2 to 2 hours at room temperature at zero bias in the dark, a quenched state characterized by an extremely low I_f (less than 10^{-9} amps at 0.4 V) and correspondingly low I_{sc} is reached. Application of forward bias or enhancing light, especially at temperatures above room temperature (but below 80°C) raises I_f, replacing the low-current state with some metastable state of higher current. Thus the absolute low-current state, although it is the equilibrium state, is quite elusive, because of the slow decay rate and the fact that any measurements made on the cell at larger bias or light intensities put the cell into another relatively stable higher current state.

Measurements of junction capacitance and comparison of decay rates showed that the high-current and low-current states, defined by the rate of cooling kinetics after thermal restoration, are identical with the enhanced and quenched states, produced by optical excitation.

For cells with little HT, the rising portion of the cooling curve appears to have moved to a higher temperature, making the phase change spike into a step with rise governed by the cooling rate.

Lindquist[17] observed a similar but more stable enhancement effect on cooling degraded cells in the dark in the temperature range from about 250 to 100°K although this effect did not appear to be rate dependent.

4.3.16 Variation of Photocurrent with Light Intensity

Before HT the photocurrent is linear with light intensity as reported by Lindquist[68]. After HT, however, the photocurrent varies with the 1.28 power of the light intensity at room temperature as shown in Fig. 4-39 (DE state). The superlinearity occurs because of better collection efficiency when the enhancement is increased by higher light intensities. The competing process, thermal quenching, becomes less at lower temperatures so that the photosensitivity increases and the current-intensity variation approaches linearity.

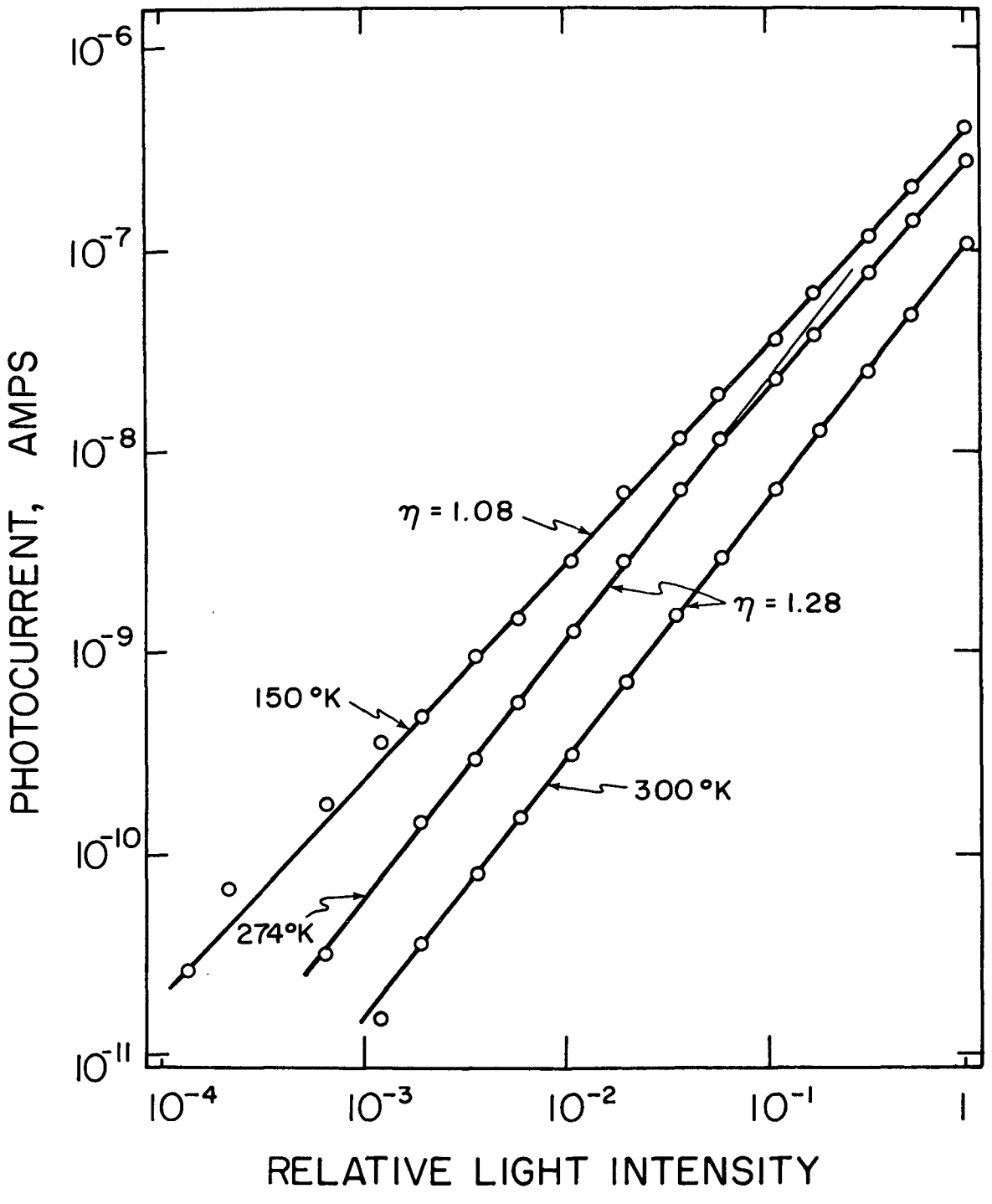

FIG. 4-39. Photocurrent versus relative light intensity for cell #81 in the DE state. Wavelength is 0.535μ and unit intensity is 290 μw/cm^2.

Chapter 5

DISCUSSION

5.1 Introduction

We begin this section with a brief summary of the results of our experiments with heat treated (HT) Cu_2S-CdS heterojunction cells. Then from the more obvious implications of our data we draw the conclusion that the short-circuit current I_{sc} in the HT cell is primarily controlled by the Cu doped CdS layer at the interface rather than by the Cu_2S layer. The elucidate the nature of this control we derive information on the structure of the CdS side of the junction from $1/C^2$ versus V_f measurements. Finally we show how the thermally-restorable optical degradation (TROD) effect and the enhancement and quenching phenomena modify the junction profile to control I_{sc} and the dark, forward-bias current I_f.

5.1.1 Perspective

The major contributions of this work are: (1) the extension of the photocapacitance model of Gill and Lindquist to cells with long HT, (2) the elimination of the conduction band spike model for control of I_{sc} in favor of a tunneling-recombination model in which I_{sc} transport is modulated by the conduction band profile on the CdS:Cu side of the junction, and (3) the discovery and exploration of the TROD effect in Cu_2S-CdS cells and the description of its role in the HT cell.

Summarized below are the major experimental results which we seek to explain.

The cell has four definable electronic states, enhanced (E), quenched (Q), restored (R), and degraded (D). Similar states are also seen in Cu doped CdS photoconducting crystals.

The characteristics of enhancement and quenching deduced from our work appear to be qualitatively identical to those observed by Gill and Lindquist (which are also reviewed briefly in Sections 1.2.4 and 2.3). The properties which characterize the E and Q states in the cell are summarized below:

E (1) Produced optically by short wavelength illumination or by cooling from ∿360°K with forward bias voltage applied. The excitation spectrum for enhancement is sharply peaked around 0.53μ.

(2) I_{sc} is increased almost to its pre-HT value.

(3) Hole trapping at deep levels in the CdS:Cu near the interface decreases the width of the depletion region and increases the junction capacitance. This increase is called the photocapacitance.

(4) I_f is increased.

(5) The state is not stable at room temperature because of thermal quenching but is persistent below ∿200°K.

Q (1) The trapped holes responsible for the photocapacitance are freed optically by long wavelength illumination, thermally at temperatures above ∿200°K, and by the application of forward or reverse bias to the cell. The quenching spectrum is broad with maxima at 0.85μ and 1.35μ.

(2) I_{sc}, I_f, and the junction capacitance are decreased.

(3) The state is stable at all temperatures at which measurements have been made.

Enhancement and quenching are competing processes at room temperature and below, for example, under illumination by white light with both enhancing and quenching wavelengths present, or under enhancing illumination at room temperature when thermal quenching is the competing process.

The effects of enhancement or quenching appear to be qualitatively the same in the restored state or the degraded state, although quantitative differences are found. The magnitude of quenching measured by the decrease in I_{sc} and the rate of quenching with a constant photon flux are larger in the degraded state (Section 4.3.6).

Optical quenching is also seen in homogeneous Cu doped CdS single crystal photoconductors. Since there is a layer of CdS highly doped with Cu (by diffusion from the Cu_2S) in the cell it is probable that the same centers are responsible for enhancement and quenching in both cases. This view is supported by the fact that the cell and the photoconductor have the same quenching spectrum. However, the mechanisms for control of the current are different. In the cell I_{sc} is modulated by an interface effect (e.g., a conduction band spike and/or interfacial recombination) which determines the fraction of carriers photoexcited in the Cu_2S which are injected into the CdS. In the CdS:Cu photoconductor on the other hand the contacts are ohmic and quenching causes a shift in the hole population from a group of low recombination rate centers to a group of high recombination rate centers with a resulting decrease in electron lifetime[65,90,91]. The photocurrent is controlled by recombination in the bulk of the CdS.

After HT in the dark, subsequent exposure to light causes certain changes in the electronic nature of the cell and the CdS:Cu photoconductor which are irreversible except by a further HT. These changes are termed optical degradation because their most obvious manifestation is a large decrease in I_{sc} and the photocurrent, respectively (shown in the degradation versus time curves of Fig. 4-4). Optical degradation occurs only at temperatures over 200 to 250°K (as shown in Fig. 4-5). In the cell optical degradation is in general characterized by decreases in I_{sc}, I_f, and the junction capacitance. The shape of the spectral response curve is not changed appreciably however (Fig. 4-12). In the photoconductor, optical degradation is accompanied by a large decrease in photoconductivity and a narrowing of the spectral response curve (Fig. 4-13).

A short HT in the dark removes the effects of the optical degradation and restores the cell or photoconductor to its original, undegraded condition.* In the cell, I_{sc} is generally increased, and the effects of enhancement and quenching on I_{sc} are decreased by restoration. The temperature dependences are such that at room temperature and below degradation and restoration are not effectively competing processes. Most, if not all, of the work of other researchers on the HT Cu_2S-CdS cell has apparently been done on cells in the optically degraded state.

The properties of a typical cell before HT and with ∿6 min of HT are shown in Table 5-1.

The possible states are summarized below:

---

*The restoration HT is at temperatures for which Cu diffusion is negligible in a well HTed cell. A HT of 140°C for 2 to 5 min for the cell and 200°C for the photoconductor is sufficient for complete restoration (Fig. 4-7).

State	Produced by	Stability range
R	HT in dark, T $\gtrsim$ 360°K	All T in dark, T $\lesssim$ 200°K in light
D	Exposure to light at T $\gtrsim$ 200°K	All T $\lesssim$ 360°K
E	Exposure to short λ light	T $\lesssim$ 200°K unless excited continuously
Q	Exposure to long λ light, forward or reverse bias, and/or T $\gtrsim$ 200°K	All T

The changes in I_{sc} with cell state transitions are illustrated schematically in Fig. 4-8. Figures of roughly similar shape could be drawn for I_f and the junction capacitance. Figures 4-22 and 4-25 show the changes in zero-bias junction capacitance caused by the above transitions more quantitatively.

Now we examine the effect of HT on the cell. During the initial HT of a cell after fabrication (a 200°C HT for example) changes in the junction structure occur rapidly for short times and then more slowly as time goes on (as shown in Fig. 4-9). As the cell is HT, Cu diffuses into the CdS and the depletion layer width w_d is increased by compensation of the donors in the CdS forming a quasi-insulating CdS:Cu layer (i-layer). After several minutes of HT at 200°C the diffusion has slowed so much that the restoration HT at 140°C is no longer causes appreciable increase in w_d and a distinction can now be made between the two types of HT. The effects of increasing the 200°C HT time are summarized below:

(1) an increase in w_d and a decrease in C

(2) a decrease in $\Delta C/C$, where ΔC is the photocapacitance increment

TABLE 5-1

PROPERTIES OF TYPICAL CELLS IN THE VARIOUS ELECTRONIC STATES BEFORE AND AFTER HEAT TREATMENT

Temperature °K	State *	I_{sc}(0.70μ) 10^{-8} amp	I_f(V_f=+0.3V) 10^{-8} amp	C** pF.	w_d** μ
300	BHT-E	2.9	50	514	0.60
	BHT-Q	0.75	8	408	0.76
	RE	1.6	--	--	--
	RQ	0.8	6	224	1.4
	DE	0.8	120†	280†	1.1
	DQ	0.02	0.1	204	1.5
150	BHT-E	3.1	1.8	976	0.32
	BHT-Q	0.9	0.7	515	0.60
	RE	2.8	40,000	1300	0.24
	RQ	1.0	5,000	488	0.64
	DE	2.3	50	275	1.1
	DQ	0.04	0.003	181	1.7

*BHT means that the cell has undergone only the fabrication HT of 100 to 130°C for several minutes.

**At zero applied bias voltage.

†With enhancing light on (I_{sc} has been subtracted).

(3) a large decrease in I_{sc} in the DQ state while I_{sc} in the low temperature DE state remains relatively unchanged

(4) an increase in the magnitude of the changes in I_{sc} associated with the TROD effect.

5.1.2 Preliminary Implications

In this section we emphasize a few of the more general and straightforward implications of the data.

As shown in Fig. 4-12, the shape of the I_{sc} versus wavelength λ curves for the cell remain relatively unchanged as the cell is put into nine distinct states (the before-HT condition plus the four states discussed above at two temperatures) with a variation in I_{sc} of $\sim 10^3$. This relationship implies that the effective photoexcitation takes place in the Cu_2S the properties of which remain invariant in the different cell states. The fact that both the DE and RE curves at 150°K lie above the before-HT curve (at 300°K) further implies that the quantum efficiency of the Cu_2S layer is not changed appreciably by extensive HT ($\sim$50 min at 200°C in this case). The large difference in shape of the spectral response curves in the R and D states of the CdS:Cu photoconductor as contrasted with the relative constancy of shape in the I_{sc} versus λ curves for the cell also supports the argument that the important photoexcitation is in the Cu_2S.*

The existence of the TROD effect (photochemical reaction) with the same basic characteristics in both the highly Cu doped CdS photoconductor

---

*The cell curves are taken by the transient method described in Section 4.3.4 and the photoconductor curves are done by the fast scan method. However, as is noted in Section 4.3.7, data for the DE-150°K photoconductor was taken by both methods and good agreement was obtained.

as well as the cell implies that the control of I_{sc} is either in the CdS:Cu layer itself or due to its effect on interface conditions.

These considerations lead to the hypothesis that I_{sc} is given by the product of two independent factors: (1) a factor η expressing the spectral quantum efficiency of the Cu_2S and (2) a factor ψ expressing the control of the carrier injection from the Cu_2S into the bulk CdS which depends on the state of the CdS:Cu layer near the junction interface. The time constant for photoexcitation associated with the Cu_2S factor η is much shorter than the time constant associated with the CdS:Cu factor ψ which controls the current flow depending on whether the CdS:Cu layer is restored, degraded, enhanced, or quenched.

A further consideration supporting the relationship, $I_{sc} = \eta\psi$, is the close similarity in form of the white light current versus temperature curves for the cell and for the photoconductor shown in Figs. 4-33 and 4-34.

The white light I_{sc} versus dark, forward-bias current I_f curve of Fig. 4-35 shows an almost linear variation between I_{sc} and I_f at 300°K up to the saturation of I_{sc}. This single curve represents a variety of conditions from R to D and from partial E to partial Q as the cell is taken over a complete TROD curve. Thus the I_{sc} versus I_f curve suggests that the same mechanism is at the basis for control for both I_{sc} (illuminated) and I_f (dark) and thus that I_f is controlled by the CdS:Cu layer also. We shall explore this hypothesis further in Sections 5.4 and 5.5.

The reversible nature of the transitions described in Section 5.1.1 and the fact that they can be performed many times without changing the general cell properties rules out mechanisms in which there is a loss of Cu by oxidation or diffusion into the bulk CdS with each transition.

5.2 Junction Structure From $1/C^2$ Versus V_f Analysis

In this section we examine the structure of the junction as interpreted from junction capacitance data. Although the interpretation of the extrapolation of the $1/C^2$ versus V curves in order to determine the effective barrier voltage V_b can be rather involved (as was pointed out in Section 4.3.8), the determination of the net charge density profile is straightforward in an asymmetrically doped junction (p-side acceptor density >> n-side donor density in our case). The reciprocal of the slope of the $1/C^2$ versus V curve is proportional to the net charge density N(x) which may arise from positively charged traps as well as uncompensated, ionized donors in the CdS. The barrier voltage is fixed by the work functions, electron affinities, and band gaps of the two materials forming the junction. To maintain charge neutrality and to support V_b, the depletion layer thickness adjusts itself according to the available charge density to provide the necessary dipole layer.

Considering data for the cell before HT (such as Lindquist's Fig. 5-21[17] reproduced in our Fig. 5-1) the effect of the photocapacitance on the barrier voltage can be interpreted in two ways. These depend on how we choose to extrapolate the data to V_b through the region which is inaccessible to capacitance measurement. Using a direct extrapolation, the data imply that the effective V_b is reduced by the presence of the photocapacitance ΔC from $\sim$0.8V to $\sim$0.4V in this case. This corresponds to the situation shown in Fig. 5-2 and the data could be explained in terms of a very thin, almost metallic layer of interface states whose charge determines the band bending (the semiconductor-metal-semiconductor heterojunction theory of Oldham and Milnes[55,56]).

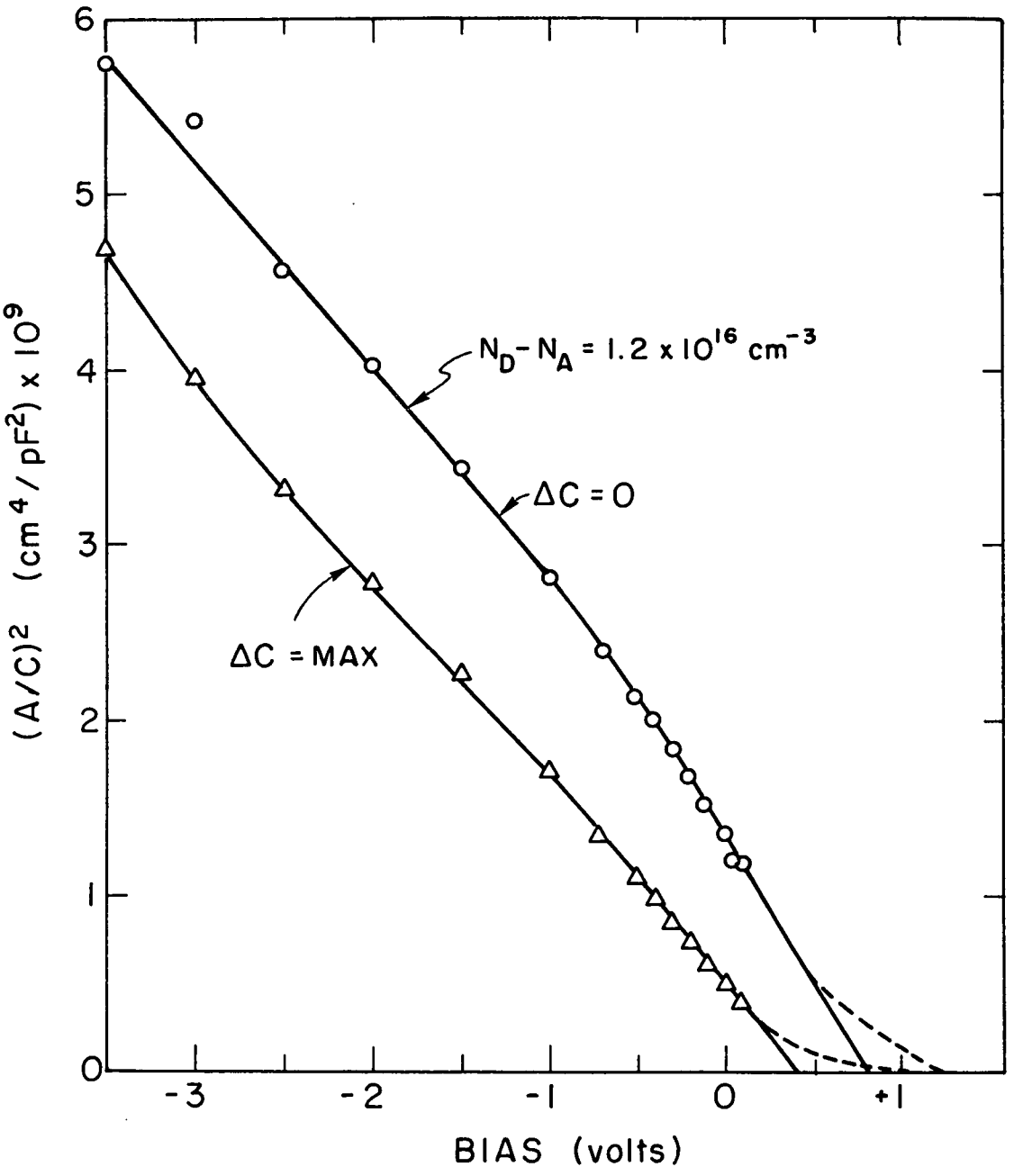

FIG. 5-1. $1/C^2$ versus bias voltage for an un-HT cell at 110°K with and without photocapacitance excited (from Lindquist, Ref. 17).

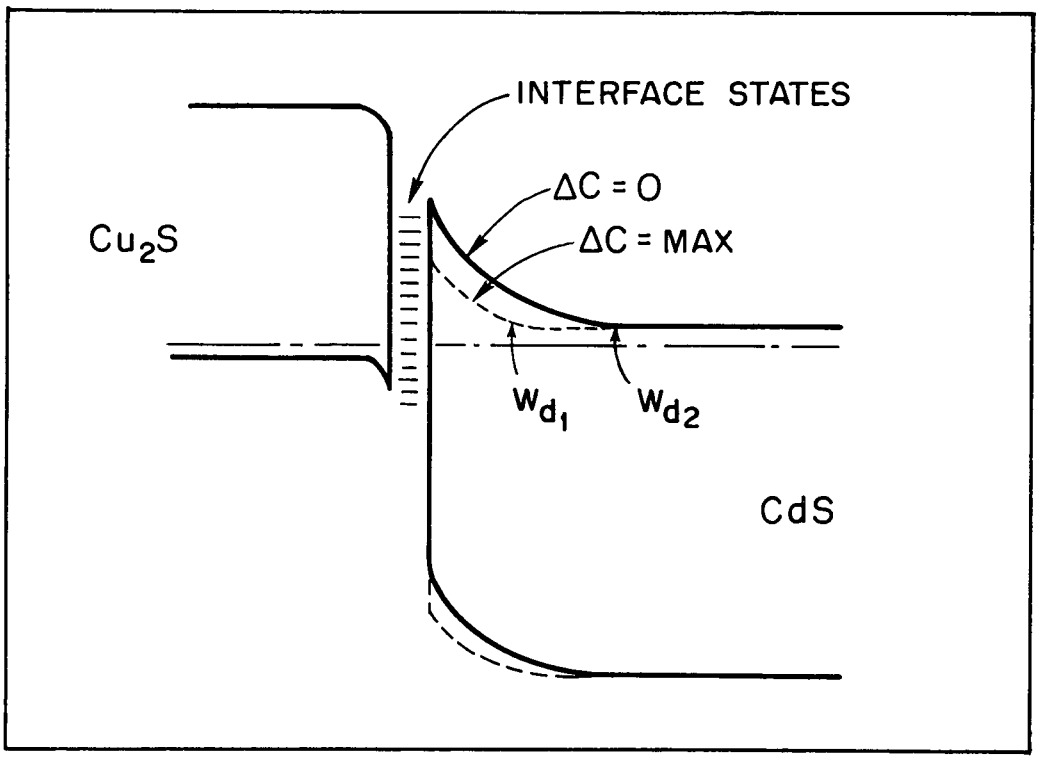

FIG. 5-2. Semiconductor-metal-semiconductor band profile from Fig. 5-1.

On the other hand the dashed line extrapolation in Fig. 5-1 implies a charge density profile which becomes larger near the interface with a constant barrier voltage. Excitation of ΔC changes the shape of the barrier as shown in Fig. 5-2b. Note that the change in electric field with ΔC is much larger in the second situation. We choose the latter model as being more physically reasonable.

For a cell after HT (Fig. 4-24), consideration of the $1/C^2$ versus V curves suggests that an insulating layer is present. The slopes are the same for three conditions of enhancement (excitation of ΔC) and are consistent with the measured donor density in the bulk CdS. Thus the curves appear to be probing only the CdS which has not been Cu doped.

To explore the situation in more detail we consider a junction with a semi-insulating layer (of width w_i and net charge density N_i) sandwiched between the p-type Cu_2S (with acceptor density N_A and accumulation layer width w_A) and the bulk CdS (with net donor density N_D). The thickness of the i-layer is a constant determined by the doping profile in the CdS, and its effective charge density is determined by its state of restoration and enhancement. Starting with the expressions describing such a system the barrier voltage is given by:

$$(V_b - V_f) = \frac{q}{2\varepsilon}\left[N_A w_A^2 + N_D w_A^2 - (N_D - N_i)\, w_i^2\right] + \frac{q}{\varepsilon} w_i (N_A w_A - N_D w_D)$$

and for the charge neutrality

$$N_A w_A = N_i w_i + N_D (w_d - w_i)$$

we can eliminate w_A and since $N_A >> N_D \geq N_i$ we find

$$(V_b - V_f) \simeq \frac{q}{2\varepsilon}\left(N_D w_d^2 - N_D w_i^2 + N_i w_i^2\right) \quad \text{and} \quad C = \left(\frac{dQ}{dw_d}\right)\left(\frac{dw_d}{dV}\right) = \varepsilon A/w_d$$

Finally we find

$$(\varepsilon A/C)^2 = w_d^2 = w_i^2\,(1 - N_i/N_D) + \frac{2\varepsilon}{qN_D}\,(V_b - V_f)$$

Thus when $N_i \ll N_D$, w_i is given by the extrapolation of the high reverse bias slope to V_b as in Fig. 5-3. The resulting hypothetical $1/C^2$ versus V plot for $N_i \ll N_D$ implies a close spacing between the reverse bias branches. This is not seen in the data of Fig. 4-24 so we conclude that N_i is not negligible compared to N_D. Using the data of Fig. 4-24, where the zero bias depletion layer width changes from 3.85μ (quenched) to 3.45μ (enhanced) we can calculate the approximate change of N_i on enhancement:

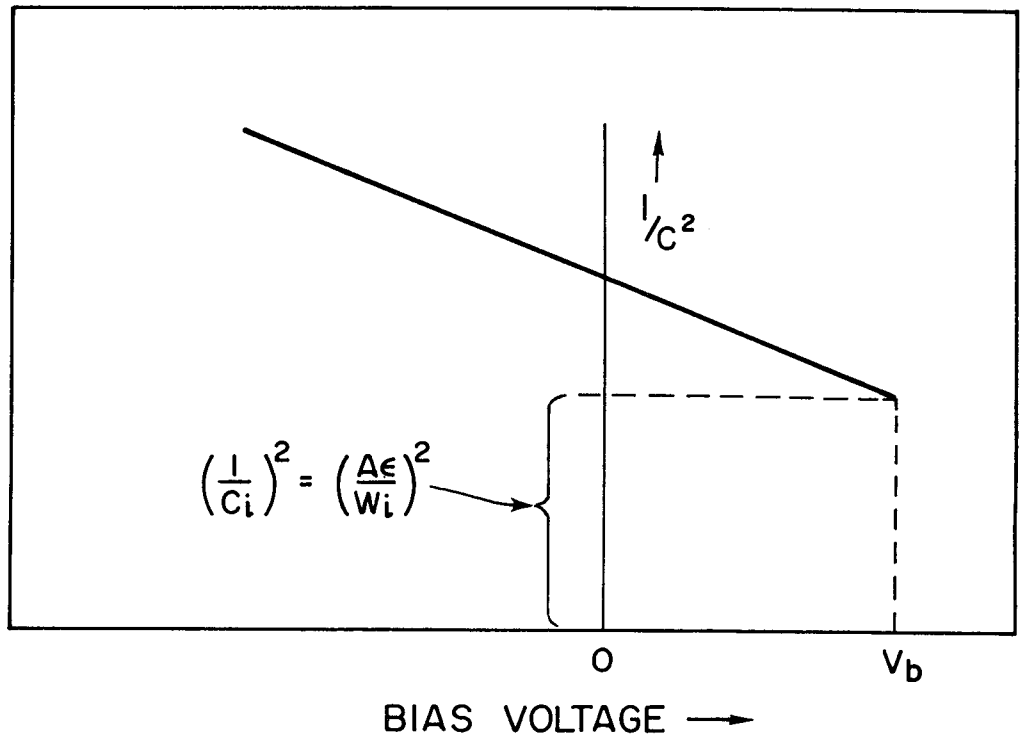

FIG. 5-3. Schematic $1/C^2$ versus V plot for perfectly insulating i-layer.

$$\Delta N_i = N_i(E) - N_i(Q) = N_D \left(\frac{w_D(Q)^2 - w_D(E)^2}{w_i^2} \right)$$

$$\Delta N_i \simeq N_D \left\{ 1 - w_D(E)^2 / w_D(Q)^2 \right\} = 0.8 \times 10^{14}/cm^3$$

If distributed uniformly such a large charge density would render the i-layer conductive as it does in the R-150°K case shown in Fig. 4-25 and we could probe through it, i.e., the i-layer would no longer dominate the junction capacitance. We conclude that the charge is concentrated at the interface and that there are really two regions as suggested by the R-150°K N(x) profile of Fig. 4-25. The resulting $1/C^2$ versus V plot shown schematically in Fig. 5-5 corresponds much more closely to the data.

We propose the profile shown in Fig. 5-4a with two important regions:

I. A highly conducting n-type region containing optically chargeable states which are mainly responsible for changing the band profile during excitation of the photocapacitance.*

II. A low N(x) region where the CdS donors have been compensated by Cu.

The TROD effect probably occurs in both regions. These regions give rise to the band profile shown in Fig. 5-4b (assuming a constant V_b) and the complete $1/C^2$ versus V curves would take the form shown in Fig. 5-5. Of course in a real cell N(x) is smoothly varying and there are no distinct boundaries between the regions. The Cu diffusion profile would produce

*This layer may be counter-doped with Cd back diffused from the Cu_2S. The presence of Cd in the Cu_2S layer and its redistribution during HT was suggested by Hill and Kerimidas.[34]

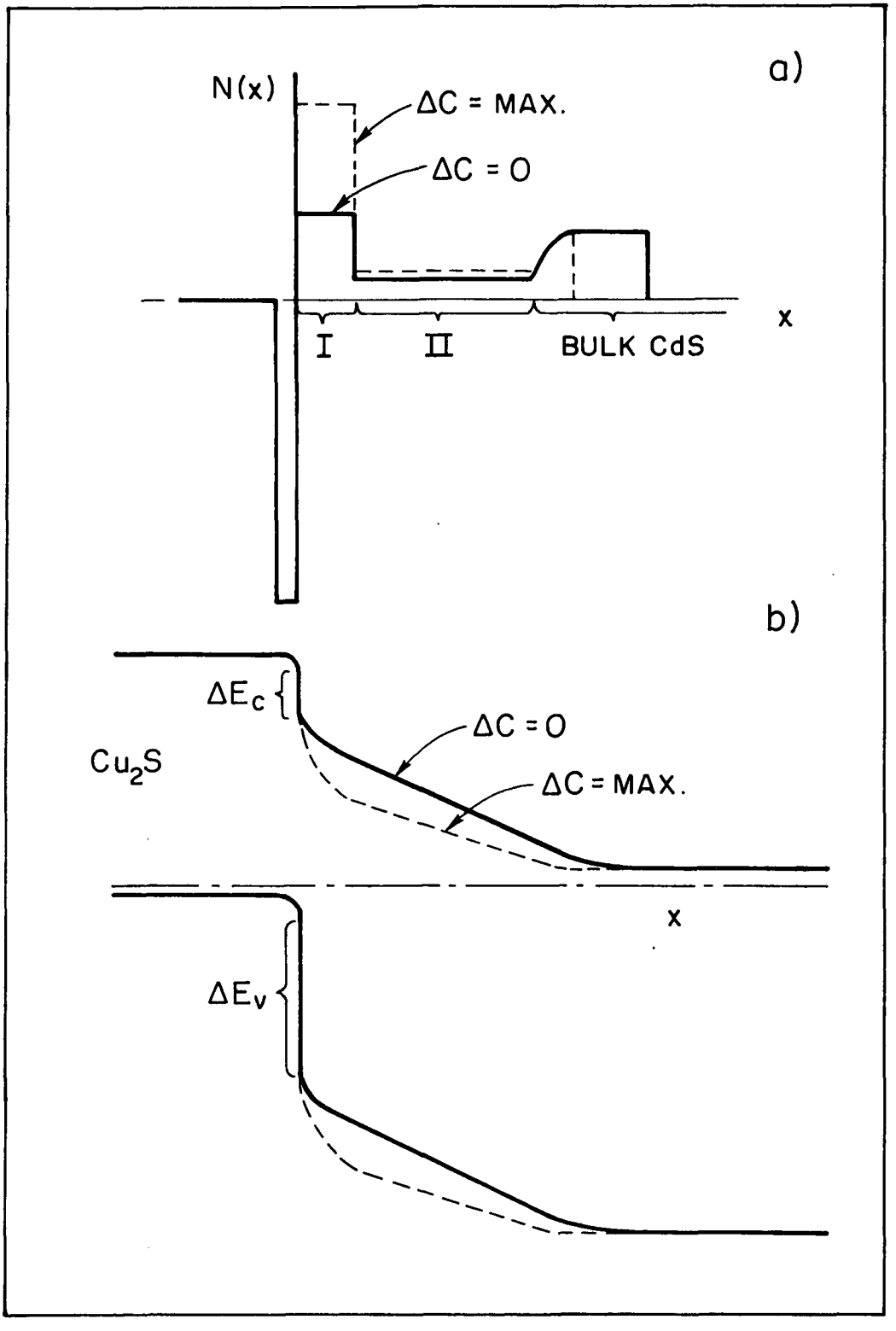

FIG. 5-4. Schematic charge density profile (a) and derived band profile (b).

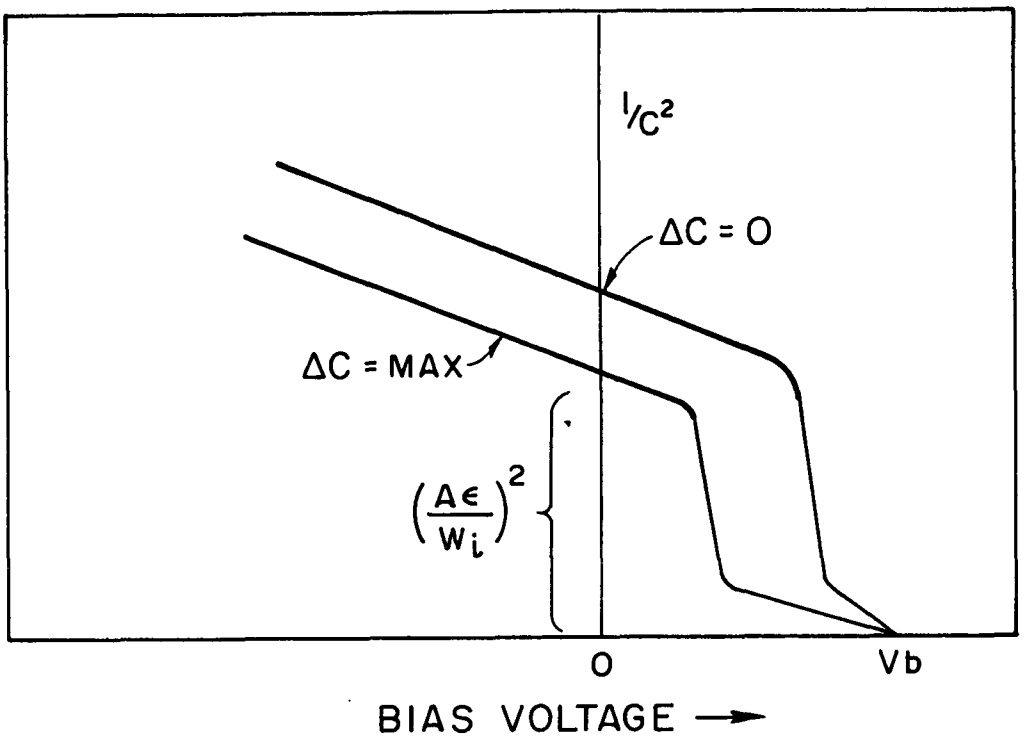

FIG. 5-5. Schematic $1/C^2$ versus V plot for charge density profile of Fig. 5-4. Existing portions of the data are shown in bold line.

a gradual transition from region II to the bulk CdS (estimated to be $\sim$0.5μ wide for the case of Fig. 4-25).

The regions discussed above are present in the $1/C^2$ versus V curves for the restored state as well (see Figs. 4-23 and 4-25), but in this case region II becomes quite conducting, having an apparent donor density of 10^{14} to $10^{15}/cm^3$. Upon restoration the effective N(x) of region I increases to the point where the double layer charge requirements can be satisfied within region I alone for zero applied bias (with a little help from region II in the RQ case) allowing us to probe closer to the junction interface. Thus the density of effective positive charge in this layer must be very high in the R state and very low in the D state.

The same basic situation is evident in the data for a cell with less HT time (Figs. 4-20, 4-21, and 4-22). The effect of HT and Cu diffusion may be thought of as a scaling up of the widths of the regions described above, which also exist in cells with even shorter HT.

We would expect the roughness of the Cu_2S-CdS interface to affect the value of N(x) derived from the $1/C^2$ versus V plots (on the order of 0.5μ by microscopic inspection). Because of the roughness, the actual interfacial surface area is somewhat larger than its projected area. The larger area decreases the slope of the $1/C^2$ versus V curves for small depletion layer thickness, w_d, thus indicating a higher N(x) than the actual value. As w_d increases, the roughness is averaged out and the actual area approaches the projected area. Thus the high reverse bias slope still gives the correct N(x) but the curve will have an upward concavity at more positive biases when the depletion layer width is comparable to the roughness. The V_b extrapolated from the high reverse bias slope will be smaller than the actual V_b in that case. This effect is thought to be small (changing N(x) by a factor of 2 or 3 at most in a region <0.5μ from the interface) but it may account for a portion of the apparent increase in N(x) observed near the interface. Lindquist's data show no upward concavity characteristic of changing effective area down to $w_d < 0.1\mu$ on un-HT A-face cells.

As was discussed in Section 4.3.9, the junction capacitance C is dominated by the i-layer in the D state and the measured value of the photocapacitance increment ΔC is small compared to C. Thus the charge density, N(x), near the interface (and hence the electric field there) may change considerably during enhancement or quenching without affecting

the measured value of C very much. This is shown in Fig. 4-26. There is not enough information to calculate the actual dependence of N(x) and the barrier profile on the measured capacitance in the D state however.

For these reasons it is felt that the curves for the R state more accurately represent the dependence of I_{sc} on the depletion layer width, $w_d = A\varepsilon/C$ (where A is the junction area and ε is the permittivity of the CdS). For the restored state the relationship, $I_{sc} \simeq B \exp\{-\alpha/C\}$, where B and α are constants, is found for both the 6 min and the 1 hour HT cells (Figs. 4-26 and 4-27). A similar relationship was found for the cell before HT both in this work and by Lindquist[46].

The extrapolation of the R state curves to $w_d = 0$ gives a quantum efficiency of $\sim$10% for the cell with $\sim$1 hour of HT and $\sim$30% for the 6 min and before-HT cells.

In summary we have determined the N(x) profiles and found that there are two discernible regions on the CdS side of the junction. The data imply that N(x) increases strongly near the metallurgical interface and that the charge storage responsible for the photocapacitance ffect takes place there. However, there is a large increase in N(x) throughout the Cu doped region on restoration and a further increase on enhancement. The dependence of I_{sc} on w_d is felt to be accurate in the before-HT and restored, 150°K cases but it is masked by the high resistivity of the i-layer in the remaining conditions.

5.3 Implications of the TROD Effect

A variety of experimental results demonstrate that the TROD effect in the cell is of essentially the same nature as that in the photoconductor.

These results include similar activation energies and temperature ranges for both restoration and degradation (Figs. 4-5 and 4-7) and the close correspondence in shape between the white light photocurrent versus 1/T curves for the cell and the photoconductor shown in Section 4.3.12. Having shown that a TROD-active CdS layer exists in the cell we examine the details of the effects of this layer on the junction properties. These effects include an increase in recombination rate in the layer as it is optically degraded and/or quenched and changes in the electric field at the junction accompanying a change in cell state. At the end of this section we comment on a mechanism for the TROD phenomena.

5.3.1 Comparison of TROD Effects in the Photoconductor and the Cell

The spectra for the photoconductor (Fig. 4-13) indicate a large decrease in the electron lifetime, τ_n, as the photoconductor is optically degraded. Using the conductivity at the maximum of the spectral response curve, we calculate a change in lifetime from $\sim 10^{-3}$ sec in the restored state to $\sim 10^{-5}$ sec in the degraded state. This change may be due to either (1) an increase in the effective number of fast recombination centers, (2) a decrease in hole trapping at slow recombination centers, (3) an increase of electron trapping, or (4) a decrease in the effective number of slow recombination centers. The latter three circumstances would serve to increase the hole population of the fast recombination centers.

The change in lifetime produces a shift in the electron quasi-Fermi level in the enhanced state from ~ 0.4 eV to ~ 0.5 eV below the conduction band (at the level of illumination used for the spectra of Fig. 4-13). Values of E_{fn} for the photoconductor states are given in Table 5-2.

F

TABLE 5-2

ELECTRON QUASI-FERMI LEVELS AND LIFETIMES FOR VARIOUS STATES IN THE PHOTOCONDUCTOR

State	Illumination	T	E_{fn}	τ_n
RE	0.49μ	150°K	0.19 eV	1.5×10^{-3} sec
DE	0.49μ	150°K	0.28 eV	1.6×10^{-6} sec
R or D	Dark	150°K	>0.4 eV *	
RE	0.52μ	300°K	0.39 eV	$\sim 10^{-3}$ sec
DE	0.52μ	300°K	0.51 eV	$\sim 10^{-5}$ sec
DQ	0.80μ	300°K	∿0.6 eV	
R or D	Dark	300°K	≳0.8 eV *	

*Beyond the limits of measurement.

The response time for the photoconductor is dominated by a large density of traps estimated (in Section 4.3.7) at $\sim 10^{15}/cm^3$ for the RE and DE, 300°K cases.

The data of Section 4.3.7 show that the optical quenching phenomenon exists in the CdS:Cu photoconductor, and that the ratio of enhanced to quenched photocurrent is much larger in the degraded state than in the restored state.

In the degraded state the spectral response of the photoconductor is considerably narrowed. This may be due either to (1) an increase in recombination rate for extrinsic light (optical quenching) or (2) a decrease in the number of extrinsic centers capable of being photoexcited. Given the increased effectiveness of optical quenching in the degraded

state we feel the first alternative is most likely.

These data agree well with the results of Kanev[74] for similar CdS:Cu crystals. Kanev observed decreased electron lifetimes, narrowed spectral response, and an increase in the effect of infrared quenching in the degraded state.

Turning our attention to the cell, we find that the effects of optical quenching are much larger in the degraded states. The ratio of I_{sc} (enhanced) to I_{sc} (quenched) is always larger for the degraded state than for the corresponding restored state (Figs. 4-8 and 4-14). In addition, there is experimental evidence for a change in enhancement and quenching rates with optical degradation. A direct measurement of the rates in the cell (Fig. 4-15) using constant intensity light sources shows that the rate of enhancement decreases by a factor of at least 3 and the rate of quenching increases by a factor of 10 with degradation.

Although we cannot measure the electron lifetimes in the CdS:Cu layer of the cell directly the similarity of the quenching properties of the cell and the photoconductor imply that the same decrease in electron lifetime takes place in the cell. These similarities include the optical quenching spectrum, the presence of thermal quenching, and the increase in quenching effect by degradation.

The change in the rates and magnitudes of enhancement and quenching in the cell explains the behavior of I_{sc} and the junction capacitance during degradation of I_{sc} by white light. A complete TROD curve for degradation of I_{sc} by white light at 300°K is shown in Fig. 4-8. HT in the dark and slow cooling to 300°K puts the cell into the RQ state. Both enhancing and quenching components are present in white light but the rate of enhancement is large for the R condition. When the light is

turned on, I_{sc} increases rapidly as the cell is enhanced. After passing close to a state of complete restoration and enhancement, the cell continues to degrade and I_{sc} is diminished slowly as the cell goes to a D and partially Q state. The rate of enhancement drops and the rate of quenching increases on degradation so the cell tends toward a quenched condition. We may think of the decrease in I_{sc} as being due to two processes: (1) a smaller part due to the passage from RE to DE (as in Fig. 4-14) and (2) a larger part due to the change in the balance between enhancement and quenching with degradation under constant white light.

In summary, we have:

(1) shown that the magnitude of quenching effects increases on optical degradation in both the cell and the photoconductor

(2) shown that the rate of quenching increases on degradation in the cell

(3) shown that the electron lifetime decreases in the photoconductor on degradation

(4) explained the behavior of I_{sc} during degradation with white light at room temperature.

Since the effects of enhancement and quenching on depletion layer width are known the preceding is sufficient to explain the experimental observations discussed in Sections 5.4 and 5.5 following.

5.3.2 Relation of the TROD Effect to Junction Properties

We have shown that a photoconductive layer exists in the cell and have elucidated some of its properties. Although the comments of this subsection are not crucial to the arguments in the following sections, we now wish to explore the relationship of the TROD properties to the

junction. Remember that backwall illumination is used in these experiments and so the photoconductor layer is always illuminated at the same time as the Cu_2S. During a transient measurement of I_{sc} in the cell, the photoconductor layer with its rather long decay time is "prepared" by putting it into a particular state (e.g., DE) by exposure to light. After a small time delay a probe light is turned on and electrons are injected from the Cu_2S. During the delay the properties of the photoconductor layer have changed somewhat. For example, the conductivity of the photoconductor layer might be given by decay curves like those of Fig. 4-18. These curves show a rather fast decay in the Q states and a very slow decay in the RE states. The situation is shown schematically in Fig. 5-6.

The preceding comments would argue that the photoconductor layer is just acting as a series resistance but it will be shown in Section 5.4 that the conductivity of the layer does not have a major effect on I_f or I_{sc}. Thus a more subtle property peculiar to each cell state must influence the injected current. We wish to postulate here what that more subtle mechanism may be.

In the cell enhancement and quenching control an injected electron current and we can observe the associated change in depletion layer thickness directly with photocapacitance measurements. During enhancement, optical excitation of electrons from defect levels near the interface leaves them positively charged which adds to the effective ionized donor concentration in the junction region and modulates the junction profile. The electrons are swept away by the double layer field which prevents their recombination. It is not known unambiguously whether these positively charged centers in the cell correspond to any of the

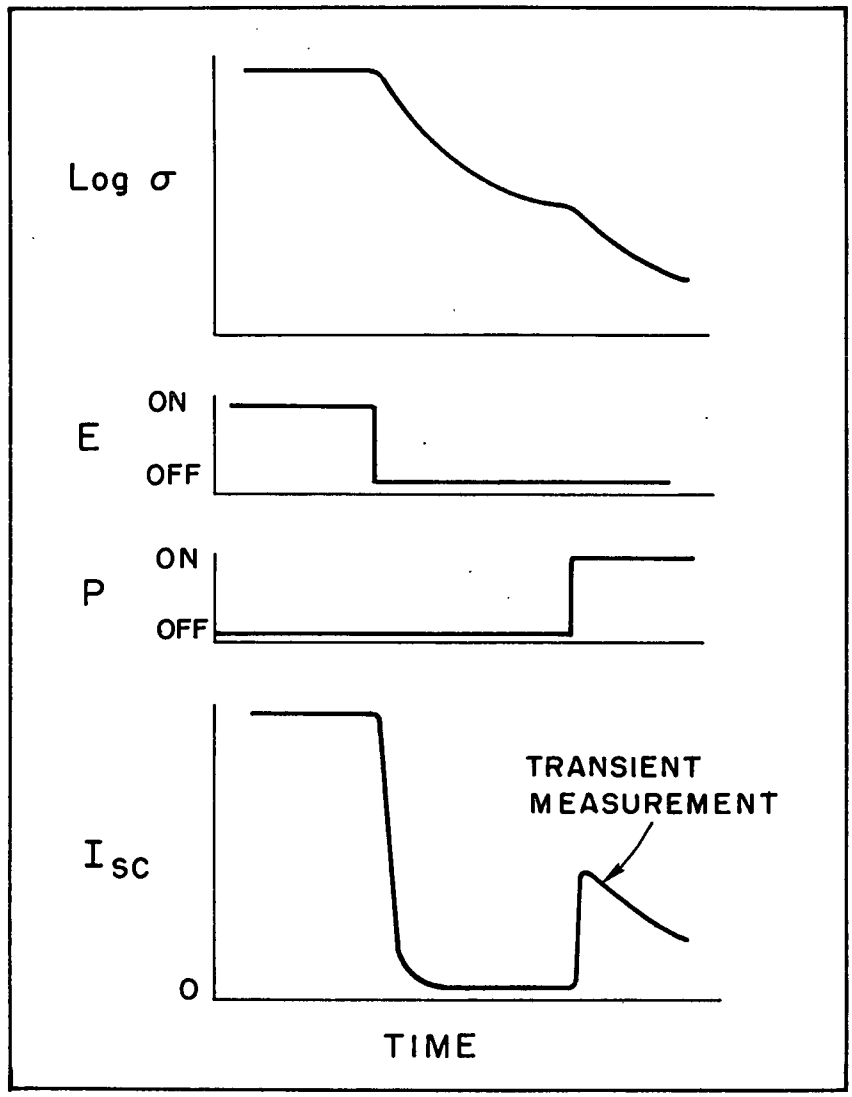

FIG. 5-6. Relationship of I_{sc} and the CdS:Cu layer conductivity, σ, during a transient measurement. E denotes enhancing light; P, probe light of quenching wavelength.

centers responsible for quenching in the photoconductor. The junction profile in turn controls I_f and I_{sc}.

Although we can't make a conclusive proof that the same centers are involved in both cases or state the exact nature of this involvement, the presence of the centers peculiar to optical quenching in a photoconductor does seem adequate to explain the effects observed in the cell. In order to show that this is plausible we must make a correspondence between the conductivity of the photoconductor and the net positive charge density in the photoconductor layer in the cell caused by extrinsic excitation. Corresponding to a conductivity of the photoconductor which is greater than its equilibrium value there will be a positive charge density in the cell's photoconductive layer after the photoexcited electrons are swept away by the double layer field. In effect we have made additional donor centers accessible in the depletion layer by the photoexcitation. The times for decay of positive charge density in this layer in the cell appear to be even longer than the times for photoconductivity decay in the photoconductor crystal, presumably because of the double layer field. The effect of a change in charge density in the junction region is seen for example by comparison of the RE (light on) and RE (light off) curves in Fig. 4-25. The resulting junction profiles are shown schematically in Figs. 5-4a and 5-4b.

Thus the electric field near the interface can be appreciably increased by restoration and/or enhancement because of the increased positive charge density associated with the longer decay time of these states. We show in Section 5.4 that the electric field in the region near the interface can have a large effect on the recombination of injected carriers.

5.3.3 The Mechanism of the TROD Effect

We briefly discussed the actual mechanism of the TROD effect in the theoretical Section 2.4. The experimental conditions and materials of our work correspond closely to those of Kanev, et al.[74] and his model appears to describe the observed phenomena well.

The principal characteristics of the model advanced by Kanev follow. Cu impurity is presumed to form two types of center in CdS crystals with excess Cd donors: Type I centers are Cu-acceptor Cd-donor pair complexes; Type II centers are due to Cu impurity present in excess of the Cd concentration. It is observed that the higher the Cu concentration over the Cd concentration, the more rapid and larger are the degradation effects. It is assumed that the Type II centers are surrounded by a repulsive barrier and are not photoelectronically active. Before optical degradation, the Type I levels are occupied and form neutral complexes with the Cd donor levels, thus giving a total small cross section for the scattering of free electrons. Such Type I centers also are assumed to have a low electron capture cross section. When Type I centers dominate, therefore, there is a high electron lifetime and a high electron mobility. The process of optical degradation is to remove electrons from the Type I centers, placing these electrons on the Type II centers, and producing Type I' centers from the Type I centers. Since Type I' centers capture an additional hole, the cross section for free electrons is greatly increased and their lifetime is decreased. The proposed barrier surrounding the Type II centers accounts for the inability to achieve optical degradation at low temperatures. A short heat-treatment (at above $\sim$350°K in our case) is sufficient to free electrons captured at

the Type II centers and to reconvert the Type I' to Type I centers thus restoring the optically degraded photoconductor. The thermal activation energy necessary for the restoration process is ∿1.6 eV (Fig. 4-7).

We suggest here a possible modification of Kanev's model for the degradation process. Under optical excitation certain defects coalesce to form deep electron traps (the Type II centers) which are responsible for the TROD effect. Thermal energy is required to accomplish the diffusion of the defects to the agglomerate and we measure an activation energy of ∿0.4 eV for this process. The rates are such that the process is negligibly slow at at temperatures below ∿200°K. The prerequisite of coincident optical energy suggests that the photoelectronic breaking of a bond is necessary to the agglomeration of the defects. Thus in this modification the thermal energy barrier is associated with the creation of the Type II traps rather than with the filling of already existing traps as in Kanev's model.

On restoration the trap forming defects are dispersed and the electrons are freed to repopulate the fast recombination centers. The electrons at Type I centers are now available to participate in extrinsic photoresponse thus widening the spectral response as seen in our experiments (Fig. 4-13).

5.4 On the Mechanism for Dark Forward-Bias Current Flow

The data of Fig. 4-35 show that the short-circuit current I_{sc} for a particular cell is a monotonically increasing function of the dark forward-bias current I_f with both currents being controlled by the state of the cell. Note that I_f and I_{sc} are flowing in opposite directions. In particular, at room temperature, an almost linear relationship between

the two currents exists over a wide range of cell states which implies an intimate connection between the mechanisms controlling the currents. Since the state of the photoconductive layer in the cell affects the junction profile these data suggest that the control of both I_{sc} and I_f can be described in terms of the profile. Gill[16] and Lindquist[17] attributed the modulation of these currents to two different mechanisms: a conduction band spike modulating I_{sc} and recombination through interface states as a pathway for I_f. They showed that both of these mechanisms were in turn influenced by the width of the depletion layer in the CdS.

In this section we show that our data are in substantial agreement with the proposed model of Gill and Lindquist for the control of I_f (with some minor modification). In the following section we show that the control of I_{sc} can be described without invoking a hypothetical conduction band spike.

Measurements of the dark $I_f - V_f$ characteristics of the HT cell show that the photoconductive layer described in the previous section cannot be considered as a simple photoresistance or as a region in which the current is space charge limited (SCL) in series with a diode photovoltaic cell. The dark $I_f - V_f$ curves show no linear behaviour characteristic of dominance by a series resistance in the region of usual cell operation. This is true for all cell states and for cells with short and long HT.

For an ideal photovoltaic cell with a series resistance, R_s, the current is given by

$$I_f(V_f) = I_o \left[\exp \alpha(V_f - I_f R_s) - 1\right] - I_{sc} \qquad (5.1)$$

where $R_s = R_{SL}$ under illumination and $R_s = R_{SD}$ in the dark with $R_{SD} >> R_{SL}$. For voltages above about $V_f \simeq 2R_s \exp \alpha V_f$, the $I_f - V_f$ curve would be dominated by a linear $I_f R_s = V_f$ relationship. Further Van Aerschodt, et al.[47] have shown that the change of α and I_o from one constant value to another when the cell is illuminated cannot be reconciled with Eq. (5-1) with R_s being a function only of light intensity. The photoconductive layer thus appears to change the diode characteristic in some other way.

The current is also not limited by the AV_f^2 relationship characteristic of SCLC. For all $n > 0$, a $I_f \alpha AV_f^n$ relationship would yield a log I_f versus V_f curve which is convex upward. This is not seen for any but the restored states at 150°K and the light-on cases when it would be least expected.

The absence of photoresistive control has been recognized by Shiozawa, et al.[15] who have modified their early model by the addition of a qualitative argument including recombination at the interface (without tunneling). This allows the barrier height to be less than 1.2 eV in the light and accounts for the change in apparent barrier height for the illuminated case. They feel that the dark $I_f - V_f$ curves would be space charge limited by the i-layer near the junction which forms the potential barrier in the dark. Such SCLC is not apparent in any of the dark $I_f - V_f$ curves in this work or the work of Gill and Lindquist, however.

The I_f/T^2 versus 1/T data of Fig. 4-32 indicates the presence of two I_f pathways in the cell, each governed by a different activation energy. The 1.2 eV activation energy can be identified with current flow

in a Shockley diode with an energy barrier approximately equal to the Cu_2S band gap. The cell current is governed by this activation energy only for temperatures above 320° to 400°C so this mechanism does not dominate in the range where the log I_f versus V_f slope has been shown to be independent of temperature. This energy barrier appears to be unmodified by extensive HT.

The 0.45 eV activation energy may be identified with an average barrier height for current flow through interface states. This is the dominant mode of current flow for the range 250° to 350°K and the slope of the log I_f versus V_f in this region (and below) is independent of temperature.* The transition of dominance from one transport mode to the other occurs at higher temperatures for low bias voltage.

The 0.45 eV activation energy was also observed by Gill and Lindquist (for b-face samples). At lower temperatures (T < 250°K) Lindquist found that I_o (the value of I_f extrapolated to V_f) was almost independent of temperature. This was interpreted as tunnelling through interface states without thermal activation.

Both Gill and Lindquist assumed a conduction band spike was present in order to control I_{sc}. This assumption implies the presence of a

---

*From the evidence below we conclude that the 0.45 eV mode is dominant at 300°K and that the presence of two slopes in the dark I_f versus V_f curves is due to a change in the tunneling process and not due to a change to the 1.2 eV (Shockley diode) mode of transport:

(1) The extrapolation to 300°K of the transition points (from the 0.45 eV to the 1.2 eV mode) of the log I_f/T^2 versus 1/T curves (Fig. 4-32) for various V_f values yields a $V_f \simeq 0.8$ volts at the 300°K transition point.

(2) The slopes of the high V branches of the log I_f versus V_f curves are independent of temperature.

positive energy discontinuity in the conduction band ΔE_c. According to the Anderson model for an abrupt heterojunction the discontinuity which gives rise to the spike is given by:

$$\Delta E_c = qV_{b1} + qV_{b2} + \delta_p + \delta_n - E_g$$

with the quantities defined in Figs. 5-7a and 5-7b. Capacitance versus voltage measurements made by Gill and Lindquist for un-HT cells show a barrier height, $V_b = V_{b1} + V_{b2}$* which lies in the range $0.4 < V_b < 1.1$ eV with the most common value of $\sim$0.65 eV. Thus according to these data $E_c < 0$ and the resultant barrier profile is as shown in Fig. 5-7a. These data suggest that no spike is present except possibly for very high bias when a depletion region might be formed in the Cu_2S. For the $\Delta E_c < 0$ case the electrons injected from the Cu_2S are rapidly thermalized down the discontinuity where they feel the influence of the band profile field.

The control of I_f by a simple Shockley diode model is contradicted at room temperature and below by the temperature independence of the log I_f versus V_f slope and the presence of the 0.45 eV activation energy. In addition the model does not allow an obvious mechanism for the dependence of I_f on cell state. Inclusion of the recombination-generation mechanism at centers within the depletion layer predicts $1 < \eta < 2$ (in $\exp[(qV_f/kT)-1]$) but the temperature dependence of the log I_f versus V_f slope remains the same as for the simple Shockley diode. Further the supply of holes necessary for such recombination is not available because of the high potential barrier in the valence band.

Simple recombination at interface states depends on the carrier density at the interface and thus has the same temperature dependence as

*Since the junction capacitance becomes zero (for no i-layer) when V_f-V_b, the barrier voltage given by $V_b = V_{b1} + V_{b2}$ does not include $\Delta E_c/q$ for the condition that $\Delta E_c < 0$.

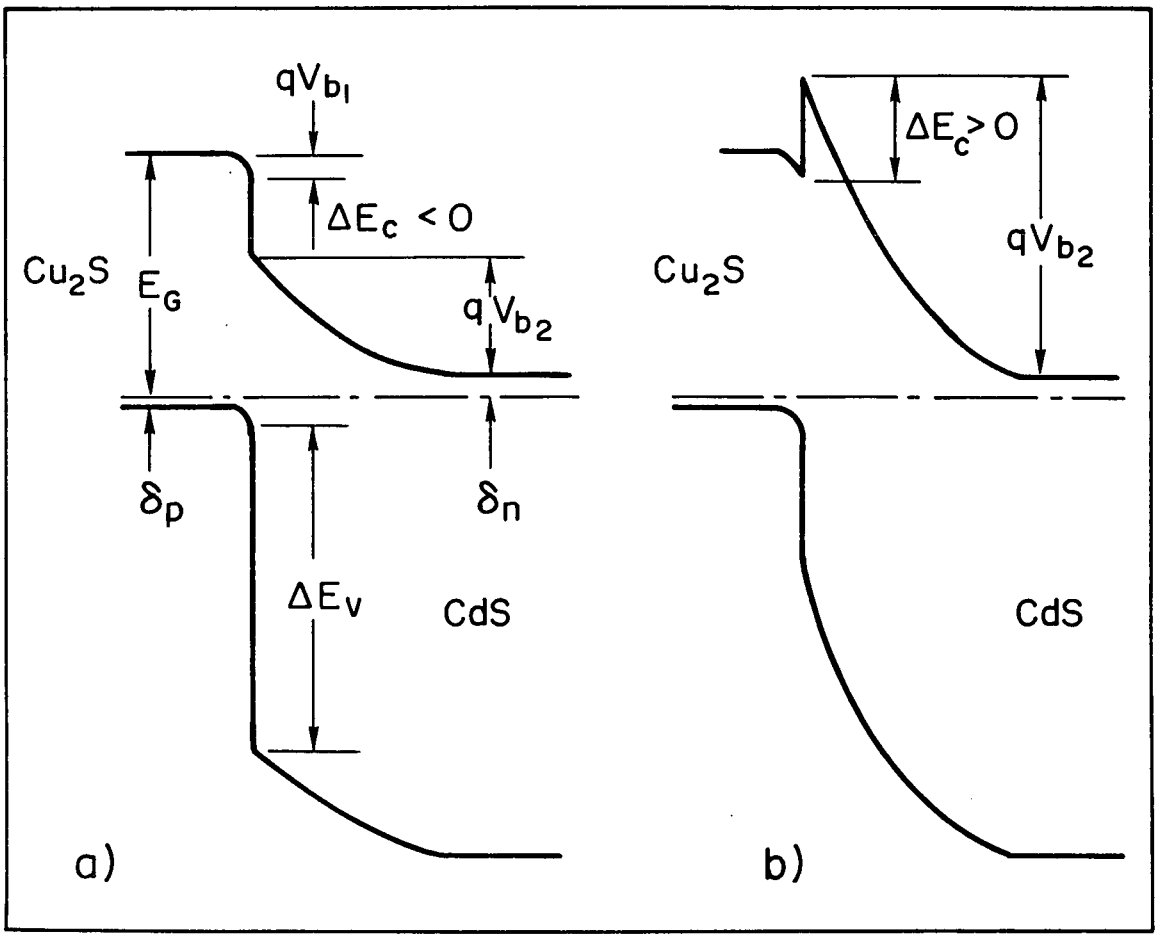

FIG. 5-7. Idealized energy band profiles for $\Delta E_c < 0$ and $\Delta E_c > 0$.

the Shockley diode. Thus thermal excitation over a barrier and simple recombination and combinations of the two as sole controlling factors for I_f appear to be ruled out.

Simple tunneling without recombination as a mechanism for forward-bias current transport requires that an adjacent isoenergetic state be present and a spike in the Cu_2S conduction band is the only place where this can occur. Thus I_f transport would require a thermal activation step of at least 1.2 eV up to the tunneling level. The spike height calculated by Lindquist ($\sim$0.02 eV), while appropriate to control I_{sc}, is insufficient to modulate I_f. If such a spike changed from completely transparent to completely opaque, for example, it would be roughly equivalent to changing the bias voltage by $\sim$0.02 volts which cannot account for the magnitude of the changes in I_f occurring on enhancement and quenching even in un-HT cells.

A mechanism which combines stepwise tunneling to interface states and recombination between these states as a pathway for I_f appears to satisfy the experimental results. Such a model has been used by Riben and Feucht[58.59] to describe the excess current in Esaki tunnel diodes. This model is described in Section 2.2.2. Gill suggested this mechanism in a qualitative way and Lindquist went on to do calculations which showed that for a linear distribution (in energy) of interface states (dN_t/dE = constant), the slope of the log I_f versus V_f curves should be almost independent of temperature even though thermal excitation to interface states above the CdS conduction band level was included. Assuming an energy barrier of height, V_b, and an abrupt junction with simple depletion layer control of the band profile as in an un-HT cell, Lindquist found that for $2\beta\eta < q/kT$ (i.e., tunneling as the rate limiting

G

factor) the current was given by:

$$I_f \simeq A \exp\{-2\beta\eta(V_b - V_f)\} \qquad \text{with} \qquad \beta = \frac{1}{h}(m^*\varepsilon/N_D)^{1/2}$$

where $0 < \eta < 1$, $A = B/(q/kT - 2\beta\eta) \simeq BkT/q$, and B is a constant containing dN_t/dE as a factor. The same functional form was obtained by Riben and Feucht[58] (except that $A = B'N_t$ where B' is a constant) for tunneling directly from the lowest point of the conduction band, i.e., no thermal excitation.

The following considerations support such a mechanism:

(1) Interface states are almost certainly present in large density due to the large lattice mismatch between CdS and Cu_2S.

(2) The temperature dependence of the log I_f versus V_f slope is small at 300°K and below.

(3) The temperature dependence of I_o [$I_f = I_o(\exp \alpha V_f - 1)$] is weak below about 250°K.

(4) The dependence on N_t suggests a reason for the sensitivity of I_o to fabrication variables.

(5) High currents in the restored states at 150°K with very small depletion layer widths imply an easy tunneling path through the barrier.

Consideration of the experimental data in terms of this model suggests the band profile shown in Fig. 5-8 for a HT cell with an i-layer and leads to the following considerations.

(1) Since holes must tunnel to defect levels within the barrier to complete the recombination path, recombination is confined to a region close to the interface. "Interface states" may exist for a considerable distance from the metallurgical

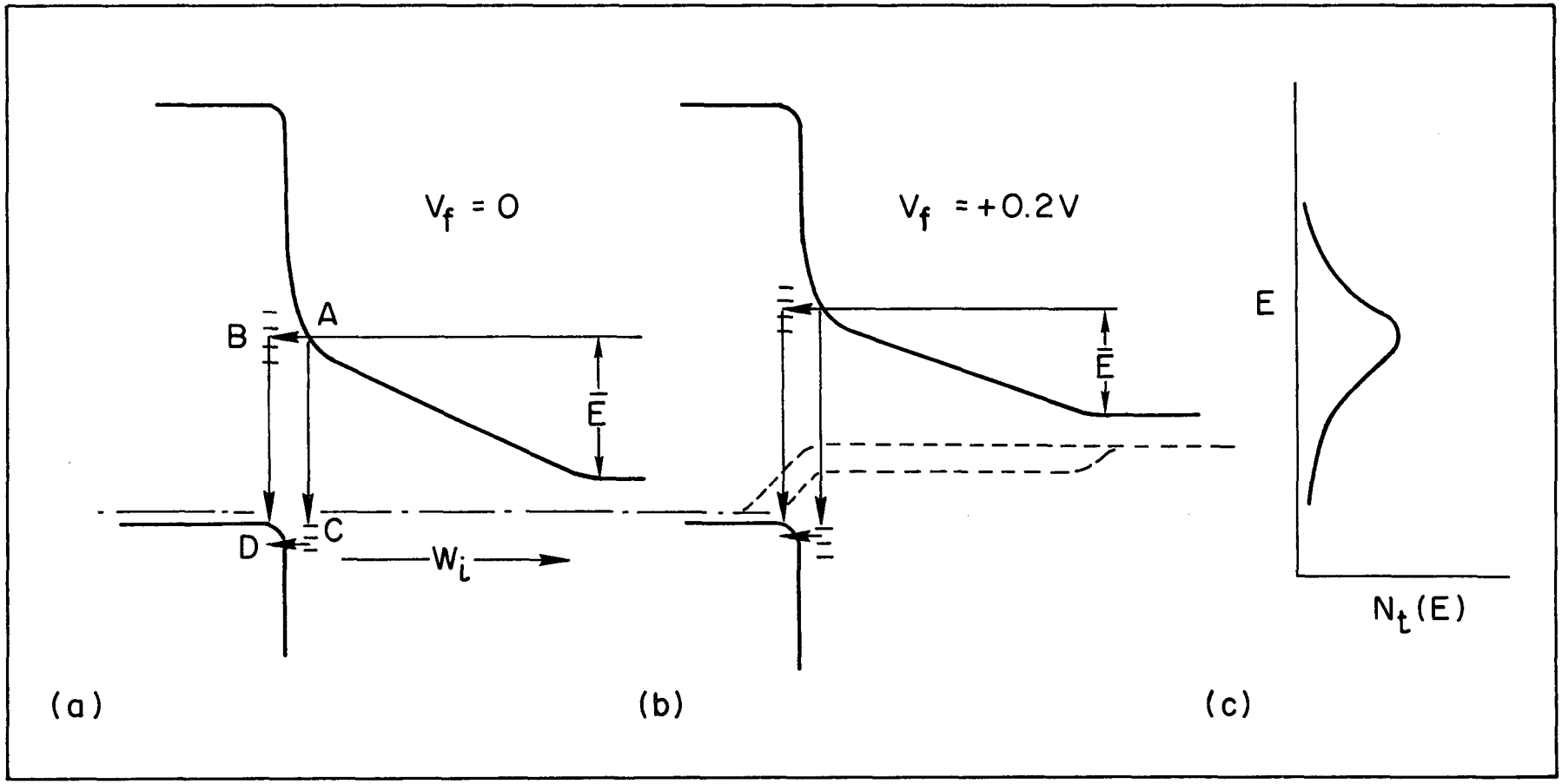

FIG. 5-8. Band profiles without forward bias (a), with 0.2 V forward bias (b), and hypothetical density of tunneling-recombination centers (c).

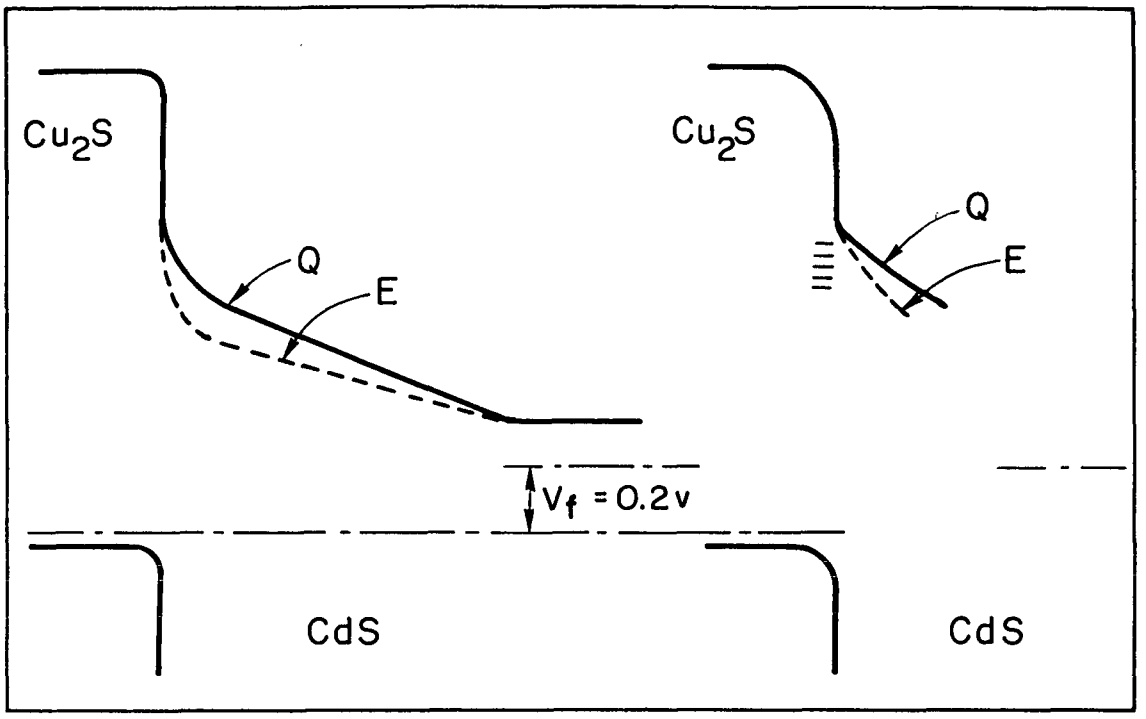

FIG. 5-8(d). Band profiles showing effects of enhancement (ΔC = maximum) and quenching (ΔC = 0).

interface, however, because of the irregular surface and the possible precipitation of Cu_2S in the CdS.

(2) The 0.45 eV activation energy arises from the thermal activation of electrons above the electron quasi-Fermi level in the CdS to reach an energy such that the barrier is thin enough for appreciable tunneling to occur. This energy is identified with an average energy $\bar{E}$ for electrons which succeed in tunneling.

(3) Assuming that the current is proportional to the product of the tunneling probability and the electron flux normal to the barrier, the approximate form for the current at each tunneling energy is

$$dI_f = A\ (dN_t/d\bar{E})\ (nv_t/4)\ P_t(\bar{E})\ (d\bar{E}) \qquad (5.2)$$

where A is a constant. The tunneling probability P_t through a triangular energy barrier of height E_b with an electric field $\mathcal{E}$ is given by

$$P_t = \exp(-\beta E_b^{3/2}/\mathcal{E}) \qquad (5.3)$$

where β is a constant. For a standard depletion layer model $\mathcal{E}$ is given by $\mathcal{E} \simeq 2(V_b - V_f - \bar{E}/q)/w_d$ near the interface and the depletion layer width w_d is given by

$$w_d^2 \simeq (2e/qN_D)\ (V_b - V_f - \bar{E}/q)$$

and we get finally*

$$I_f = A'(v_t/4)\int (dN_t/d\bar{E})\ n(\bar{E},T)\ \exp[-\alpha(V_b - V_f - \bar{E}/q)]d\bar{E} \qquad (5.4)$$

where α and A' are constants, v_t is the thermal velocity, dN_t/dE is the density of tunneling-recombination centers, and $n(\bar{E}, T)$ is the electron density at $\bar{E}$.

(4) For a <u>constant</u> bias voltage we can modulate the electric field by enhancing or quenching the cell as shown in Section 5.2 and in Fig. 5-8d. At each tunneling energy E_b the current will then increase as $\exp(-\beta E_b^{3/2}/\mathcal{E})$.

(5) $\bar{E}$ is not given directly by $\bar{E} = E_o - qV_f$, where E_o is some reference energy, but decreases more slowly due to the change in the band profile with V_f. Thus for higher V_f the band profile is flattened out and the electrons must tunnel to states

---

*We have assumed a thin depletion layer between the interface and the i-layer where the charge density rises as suggested in Section 5.2. The boundary condition on the right is the electric field in the i-layer rather than $V_b - V_f$ as in a conventional depletion layer analysis.

closer to the interface, at higher energies. This sort of dependence is seen in the data of Fig. 4-32 where the activation energy does not decrease by the full amount of the forward bias.

(6) Since it is known that N_t depends strongly on preparation variables, the dependence of I_o on N_t can be used to explain the wide variation in I_o for different cells (while α remains relatively constant).

(7) The dependence of I_o on temperature below about 250°K can be ascribed to the variation of V_b with T and a plot of log I_f at constant V_f versus T in this region yields a straight line. Using the experimentally determined value for α we calculate a change in V_b of 0.3 - 0.7 mV/°K compared with the value of $\sim$0.2 mV/°K for the change in the Cu_2S band gap calculated from data for 80°K and 300°K by Marshall and Mitra[36].

(8) There are a number of explanations for the change in slope of the log I_f versus V_f curves near V_f = 0.4 V. These include (1) a change in dominance of the tunneling step A-to-B to dominance by the step C-to-D in Fig. 5-8a, (2) a change in the variation of the conduction band profile with applied bias*, and (3) a variable distribution in energy of tunneling-recombination centers such as is shown in Fig. 5-8c.

---

*This variation is contained in the tunneling exponent. For example, a simple depletion layer gives $\exp\left\{-\alpha(V_D - V_f)\right\}$ while control by a simple i-layer (constant field) gives $\exp\left\{-\alpha'(V_D - V_f)^{1/2}\right\}$.

(9) At temperatures higher than ∿320°K for small biases and for biases of $V_f > 0.7$ to 0.8 V at room temperature the current flow is dominated by thermal excitation over the Cu_2S conduction band step.

In the restored states at low temperatures and for the illuminated cases I_f increases strongly (Fig. 4-31) and log I_f becomes a linear function of $V_f^{1/2}$ as shown in Fig. 4-30.

For the completely restored HT cell I_f increases ∿5 orders of magnitude on cooling in the dark, the junction capacitance increases, and the junction becomes very leaky in both directions of current flow. An increase in junction capacitance on cooling in the dark was also observed by Lindquist[17] in un-HT cells but to a much lesser degree. This unusual behavior of I_f at low temperatures in the restored states suggests that a deep hole trapping mechanism causes the reduction of depletion layer width. This in turn allows increased tunneling and recombination through interface states which dominates the junction current flow. Forward bias during cooling apparently aides the trapping process while reverse bias causes detrapping. These traps must be distinct from those involved in optical enhancement and quenching since optical quenching is quite ineffective in reducing the current to the values encountered in the degraded state. Enhancement and quenching still occur but the range of current variation is shifted to higher currents. This interpretation is supported by the large increase in junction capacitance observed for the restored states at 150°K. If the "cooling enhancement" effect occurs at all in degraded HT cells, it is very well masked by the presence of the i-layer.

5.5 Electric Field Control of I_{sc}.

In this section we complete the model of the HT cell by proposing a mechanism by which the local electric field near the interface controls the short-circuit current by modulating the loss of carriers via the tunneling-recombination pathway to the Cu_2S valence band.

The data for the restored low-temperature and before-HT states (Figs. 4-26 and 4-27) show that I_{sc} depends exponentially on the depletion layer width w_d and hence on the electric field in the CdS near the interface. We propose that the nonequilibrium carrier density in the interface region is roughly inversely proportional to the local electric field and hence that the field controls the loss rate. The possibility of interfacial recombination control of I_{sc} was mentioned but not explored by both Gill and Lindquist. A model based on a tunneling-recombination mode of transport through the barrier similar to that determining I_f then leads to the observed dependence of I_{sc} on w_d. In deriving an expression for I_{sc} we assume the following:

(1) The resistivity of the i-layer is not important for control of I_{sc}. This assumption is supported by the arguments in the last section that the resistivity of the i-layer in the dark is not important in controlling I_f. Thus the resistivity is certainly not important for the illuminated case.

(2) The electric field $\mathcal{E}$ is constant near the interface as shown in Fig. 5-9. This is a good assumption for the cell since the tunneling range is expected to be small compared with the depletion layer width. For a simple depletion layer model, for example, $\mathcal{E}(x) = (x - w_d)qN_d/\varepsilon$ and since $w_d^2 = 2\varepsilon V_b/qN_d$, we

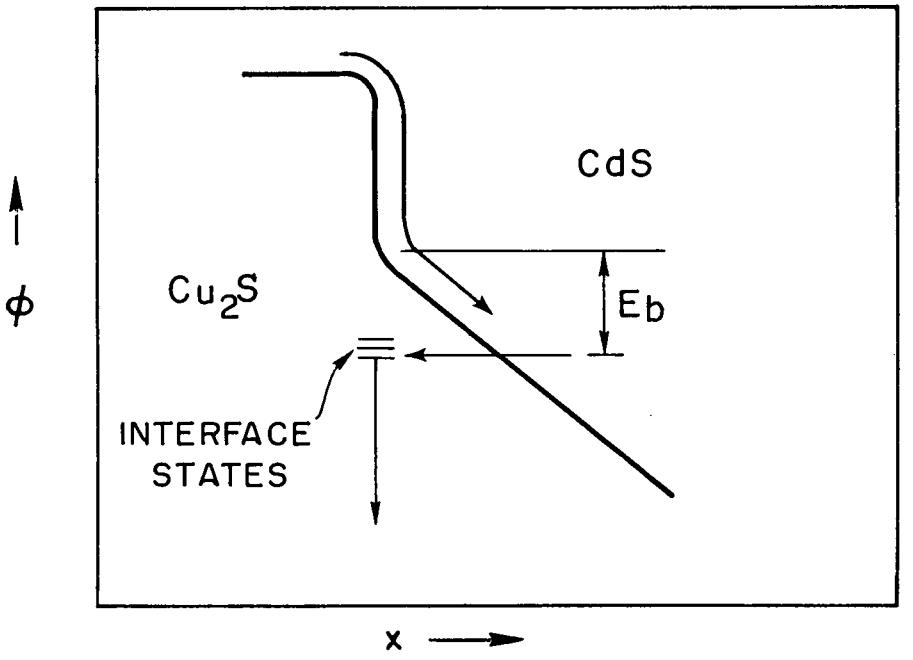

FIG. 5-9. Band profile for I_{sc} control model.

have, for $x << w_d$:

$$\mathcal{E} \simeq 2V_b/w_d \tag{5.5}$$

This is a valid approximation in the before-HT and restored, low temperature states but must be used with care for the other situations where the i-layer dominates the junction capacitance. In the latter cases the local field at the interface may be varied over roughly the same range but the total depletion layer width (now containing the i-layer width) remains relatively constant.

(3) The injected electrons are thermalized at the interface and the magnitude of the injected flux does not depend on conditions for $x > 0$. For $x > 0$, the thermal velocity of the electrons, v_t, is much greater than their drift velocity, $v_d = \mu\mathcal{E} \simeq -2\mu V_b/w_d$, so that simple diffusion and mobility concepts are applicable.

(4) The volume loss rate, U(x), due to recombination-tunneling is given by

$$U(x) = -(n - n_o)/\tau(x)$$

where $\tau(x)$, the electron lifetime, expresses the change in effectiveness of the loss process with distance from the interface, x. In terms of Eq. (5.2), U(x) is given by

$$U(x) = -\frac{1}{4} AN_t v_t P_t(x) \; [n(x) - n_o] \tag{5.6}$$

For a constant electric field, the tunneling probability, $P_t(x)$ is

$$P_t(x) = \exp\left\{-\beta E_b^{3/2}/\mathcal{E}\right\} = \exp\left\{-\beta \mathcal{E}^{1/2} x^{3/2}\right\}$$

$$\simeq \exp\left\{-\beta (2V_b/w_d)^{1/2} x^{3/2}\right\} \qquad (5.7)$$

where E_b is the tunneling barrier energy (since $E_b = \mathcal{E}x$).

Then for small injection conditions (i.e., the effect of the non-equilibrium charge density on the electric field is negligibly small) the equation of continuity is (Sze[97]):

$$D d^2n/dx^2 - \mu\mathcal{E} dn/dx - (n-n_o)/\tau(x) = 0 \qquad (5.8)$$

for steady state and $d\mathcal{E}/dx \simeq 0$. Since this equation is difficult to solve for $\tau = \tau(x)$ and a complete solution may well be physically obscure, we consider two simplified cases: (1) $D\, d^2n/dx^2 > 0$ with τ constant for $0 < x < L_o$ and $\tau \to \infty$ for $x > L_o$, and (2) $D\, d^2n/dx^2 = 0$ with $\tau = \tau(x)$.

For case (1) with the diffusion term included, the solution to the continuity equation for the appropriate boundary conditions is

$$I_{sc} = I_o \exp\left\{ - \frac{L_o \mu \mathcal{E}}{2D}\left(\sqrt{1 + \frac{4D}{\tau \mu^2 \mathcal{E}^2}} - 1\right)\right\} \qquad (5.9)$$

For the condition

$$\mathcal{E} \geq \frac{2}{\mu}\sqrt{\frac{D}{\tau}} = \frac{2kT}{9\sqrt{D\tau}}$$

the term in parentheses may be approximated to good accuracy by

$$\left(\sqrt{1 + \frac{4D}{\tau\mu^2\mathcal{E}^2}} - 1\right) \simeq \left(1 + \frac{2D}{\tau\mu^2\mathcal{E}^2} - 1\right) = \frac{2D}{\tau\mu^2\mathcal{E}^2}$$

so that Eq. (5.9) becomes

$$I_{sc} = I_o \exp\left\{-\frac{L_o}{\tau \mathcal{E} \mu}\right\} \tag{5.10}$$

Equation (5.9) is plotted schematically in Fig. 5-10 versus $1/\mathcal{E}$ for L_o = constant and in Fig. 5-11 for $\mathcal{E}$ = constant and large. The diffusion term affects the results only for low fields where it inhibits the decrease of I_{sc}. Using the approximation of Eq. (5.5) for the electric field gives $I_{sc} \simeq I_o \exp(-\gamma w_d)$ which agrees well with the experimental data for the restored, low-temperature and before-HT cases (γ is a constant).

In order to demonstrate the effect of a τ which is a function of x we assume that $D\, d^2n/dx^2 = 0$ and that $\tau = \tau_o \exp(x/L)$ in the region of interest, where L is the effective length of the recombination-tunneling region (case 2). The results above show that neglecting $D\, d^2n/dx^2$ does not affect our results appreciably for higher fields when I_{sc} approaches I_o. For this condition

$$I_{sc} = \exp\left\{-\frac{1}{\mathcal{E}\mu}\int_o^x \frac{dx}{\tau(x)}\right\} = I_o \exp\left\{-\frac{L}{\tau_o \mathcal{E}\mu}\,(1 - e^{-x/L})\right\}$$

These results are shown schematically in Fig. 5-11 versus x for constant $\mathcal{E}$. We expect that the inclusion of the $D\, d^2n/dx^2$ term would raise the curve only slightly.

Using the more accurate approximation for the tunneling probability given by Eq. (5.7) so that $\tau = \tau_o \exp\left\{+\beta \mathcal{E}^{1/2} x^{3/2}\right\}$ results in only a small modification:

$$I_{sc} = I_o \exp\left\{-\frac{L}{\mu\tau_o\, \mathcal{E}^{4/3}\, \beta^{3/2}} \int_o^{u_1} e^{-u^{3/2}}\, du\right\}$$

where $u = \beta^{2/3}\, \mathcal{E}^{1/3}\, x$.

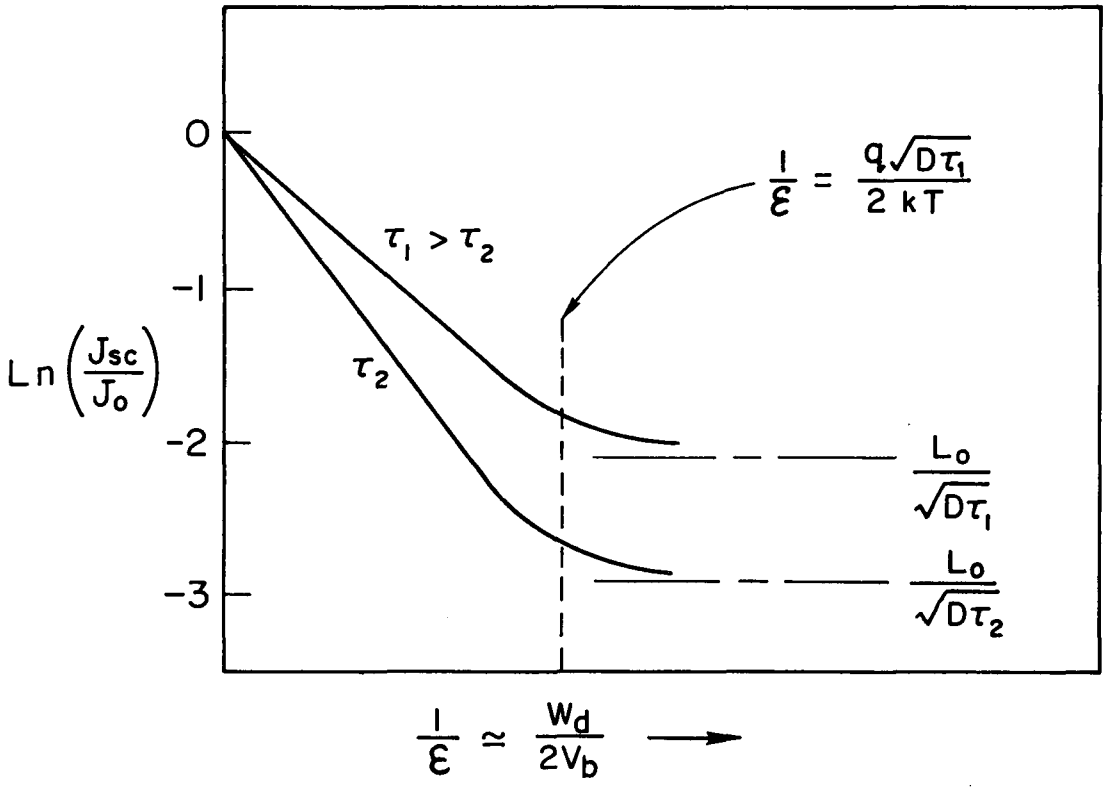

FIG. 5-10. Log (J_{sc}/J_o) versus reciprocal electric field.

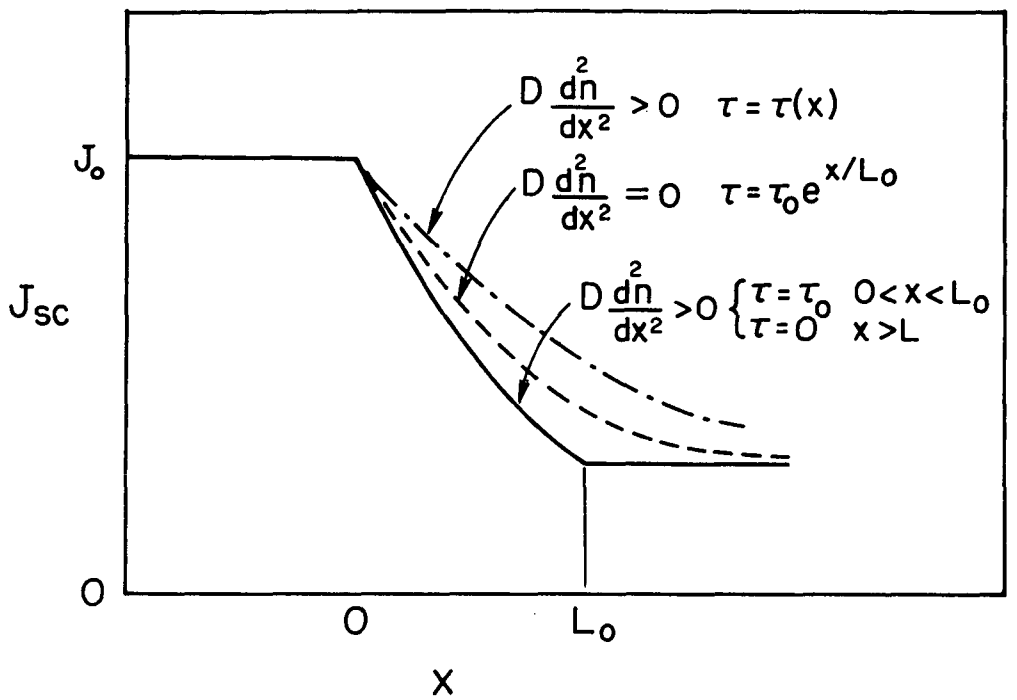

FIG. 5-11. J_{sc} versus distance from the interface.

Since the definite integral is changed very little if $u_1 \to \infty$ we can set it equal to a constant <1, so $L \to L_1$ and

$$I_{sc} \simeq I_o \exp\left\{ - \frac{L_1}{\mu\tau_o \mathcal{E}^{4/3}} \right\} .$$

Note that L/τ has the dimensions of a surface recombination velocity (which has a magnitude of $\simeq 10^6$ cm/sec for cell #61 in the before-HT case).

The model developed above for the dependence of I_{sc} on junction parameters may be used to describe the change in I_{sc} with time during optical degradation. One such description assumes that the centers associated with tunneling-recombination are created during optical

degradation and this gives excellent agreement with the data*. However, since we can demonstrate several equally probable mechanisms** we can draw no conclusions about the nature of the TROD effect from these exercises but only demonstrate the plausibility of the mechanisms.

In this section we have shown that a model assuming tunneling-recombination transport through the junction leads to an exponential dependence of I_{sc} on $1/\mathcal{E}$ (and hence on w_d) which agrees well with I_{sc} versus w_d data for the before-HT and restored, low temperature cases from this work and the work of Lindquist. In past sections we showed the same

---

*We can write the expression for the electron lifetime, τ, in terms of the density of effective tunneling-recombination centers, N_t, as $1/\tau = N_t \sigma_x v_t$ where the cross section, σ_x, now corresponds to $P_t(x^t)/4$. Then assuming a monomolecular process, N_t is given by $N_t = (N_1 - N_o) \times \{1 - \exp(-\delta t)\} + N_o$ where δ is the time rate of optical degradation. Equation (5.10) becomes

$$I_{sc} = I_o \exp\left\{-\frac{L\sigma_x v_t}{\mu\mathcal{E}}\left\{(N_1 - N_o)\,[1 - \exp(-\delta t)] + N_o\right\}\right\}$$

which is exactly the form of Eq. (4.1) in Section 4.2.1 describing the degradation of I_{sc} with time. The constant, A = 7.4, derived from I_{sc} versus time data using Eq. (4.1) represents the total number of centers active ($N_t = N_1$) while the constant from the equation above $L\sigma_x v_t(N_1 - N_o)/\mu\mathcal{E}$ which goes to $L\sigma_x v_t N_o/\mu\mathcal{E}$ for the restored case equals ~ 1 representing the base level $N_t = N_o$ of centers active. The latter constant is derived from I_{sc} versus w_d measurements. Considering the approximations made this presents a very consistent picture.

**Another likely choice would be a model in which optical degradation determined the amount of charge trapped at the interface, this charge modifying the electric field but leaving the number of tunneling-recombination centers constant. For simple assumptions we might expect I_{sc} to be given roughly by $\exp\{-A\sqrt{N_x(t)}\}$ where $N_x(t)$ is the number of centers affected by degradation. Given the complexity of the system it is unlikely that a choice could be made between these two models on the basis of I_{sc} versus $1/C$ and I_{sc} versus degradation time data. It would seem far easier to study this aspect of the problem in the photoconductor.

general dependence for the dark, short-circuit current, I_f, on $1/\mathcal{E}$ resulting from the tunneling expression $P_t = \exp(-\beta E_b^{3/2}/\mathcal{E})$. Because of the similar dependence on band profile (represented by $1/\mathcal{E}$) for both I_{sc} and I_f this model predicts the observed behavior of the dependence of I_{sc} and I_f this model predicts the observed behavior of the dependence of I_{sc} on I_f of Fig. 4-35 for the before-HT and restored 150°K cases.* Since the I_{sc} versus I_f relation of Fig. 4-35 is unchanged in form at 300°K in the degraded state when w_d remains relatively constant during enhancement and quenching, the same mechanism probably holds but now the dependence of I_{sc} on the total w_d is masked by the i-layer width as shown in Fig. 4-26 for the degraded case. We have also shown that a plausible mechanism for the dependence of I_{sc} on optical degradation time fits the model.

---

*It may be noticed that the similarity between the basic models for control of I_{sc} and I_f by $\mathcal{E}$ apparently leads to the decrease of I_{sc} and the increase of I_f as the barrier is narrowed because of increased tunneling of both currents in contradiction with the observed data. The explanation of this seeming contradiction lies in the fact that the I_{sc} carrier density is being decreased both by the increased field and by the attrition suffered by recombination. This is accounted for by the integration along the carrier path into the CdS to determine the remaining carrier density. In contrast, for the case of I_f we integrate the tunneling and recombination current over the allowed energies while the carrier density in the conduction band depends only on the tunneling energy.

Chapter 6

CONCLUSIONS

In this section we bring together the implications of the preceding discussion to present a coherent model for the heat-treated Cu_2S-CdS photovoltaic cell. The ambipolar diffusion lengths near the junction, the detailed effects of enhancement and quenching in the heat-treated cell, and the photocapacitance effect have been treated in depth by Gill and Lindquist whose work is reviewed in Section 1.2.4 and throughout the previous discussion.

The major contributions of the present work have been (1) the discovery and exploration of the thermally-restorable optical degradation (TROD) effect and the description of its role in the heat-treated cell, (2) the resolution and definition of four stable electronic states in the cell, (3) the extension of the photocapacitance model to cells with long heat-treatment times, and (4) the elimination of the conduction band spike model in favor of a tunneling-recombination model of short-circuit current control.

The degradation of short-circuit current on heat-treatment of single crystal cells can be separated into two components:

(1) a relatively small degradation occurring thermally by heat-treatment in the dark and

(2) a much larger degradation caused by subsequent exposure to light at room temperature.

The effects of the optically caused degradation can be removed completely by an additional heat-treatment at a temperature sufficiently low that no appreciable Cu diffusion occurs. This process, thermal restoration,

takes place at temperatures above ∿350°K and is characterized by an activation energy of ∿1.6 eV. Optical degradation occurs at temperatures above ∿200°K and is governed by an activation energy of ∿0.4 eV. The thermally-restorable optical degradation phenomena is closely similar to "photochemical reactions" occurring in CdS crystals; optical degradation and thermal restoration occur with the same basic characteristics in both the cell and in CdS:Cu photoconducting crystals.

We have shown that the short-circuit current is given by the product of two independent factors, symbolically $I_{sc} = \eta(Cu_2S)\ \psi(CdS:Cu)$ with η expressing the spectral quantum efficiency of the Cu_2S for supplying electrons to the junction and ψ expressing the control of the CdS:Cu layer on the injected current. This conclusion was drawn from the constancy of form of the short-circuit current spectral response curves as the cell state is changed, and the existence of the TROD effect in both the cell and the photoconductor. The data imply that η is relatively unchanged by heat-treatment effects.

The junction capacitance versus bias voltage data indicate that there are two important regions of positive charge density in the CdS:Cu layer of the heat-treated cell. A thin region near the interface contains a large density of positively chargeable centers which are responsible for the photocapacitance effects and can cause large changes in the junction transport properties by modulating the electric field there. Between the photocapacitance region and the bulk CdS is an intermediate region of low charge density (called here an i-layer) which dominates the junction capacitance under most conditions. In the degraded states and the restored, 300°K states the large changes in charge density in the high charge density region associated with the photocapacitance still

occur and modulate the current strongly but changes in the junction capacitance are masked by the presence of the i-layer. In the restored, 150°K states, the conductivity of the i-layer is increased enough to probe close to the interface with $1/C^2$ versus V measurements and the changes in junction capacitance caused by enhancement and quenching (the photocapacitance) can be observed.

By comparing the properties of the properties of the TROD effect in the photoconductor to those in the heat-treated cell we have shown that a TROD-active photoconductive layer exists in the cell and controls the short-circuit current. We have further shown that optical degradation increases both the rate and the magnitude of the effect of quenching in the cell and thus, with the knowledge of the effect of the photocapacitance on the junction profile, the relationship of the various cell states to the local electric field at the junction is explained. Although the identification of the TROD-active centers with the centers responsible for enhancement and quenching is not definitely established (and is not necessary for the arguments that follow) we have shown the plausibility of a model based on this identification in controlling the electric field.

Our data lead us to substantial agreement with Gill and Lindquist that the mechanism for dark, forward-bias current flow is transport via tunneling and recombination through interface states to the Cu_2S valence band. No photoresistive or space-charge limited current control was seen.

Since no experimental data to our knowledge shows a conduction band carrier voltage greater than the Cu_2S band gap energy (1.2 eV) we conclude that the conduction band discontinuity at the interface is negative and that no conduction band spike exists.

The dark, forward-bias current versus temperature data show that two current pathways are present. The first is characterized by an activation energy of 1.2 eV and is associated with thermal excitation of carriers directly into the Cu_2S conduction band. This mode is only operative at temperatures above 300°K for normal biases. The other pathway is characterized by an activation energy of 0.45 eV which is operative at 300°K and below, is associated with the tunneling-recombination mode of transport. We suggest that the tunneling-recombination takes place close to the interface and requires both a thermal and a tunneling step. This leads to a log dark, forward-bias current versus voltage curve with a slope which is almost temperature independent as observed in the data.

The tunneling-recombination model leads to a modulation of the dark, forward-bias current I_f such that for constant bias voltage, $I_f \alpha \exp(-B/\mathcal{E})$ where B is a constant and $\mathcal{E}$ is the local electric field. Thus the dark, forward-bias current is modified by the effect of enhancement and quenching on the electric field in a way which agrees qualitatively with the dependence inferred by the experimental data.

The tunneling-recombination model also leads to a relation for the short-circuit current I_{sc}, $I_{sc} \alpha \exp(-B'/\mathcal{E})$ which agrees well with the before heat-treatment and restored, 150°K data and explains the data for the remaining states for which the i-layer dominates the junction capacitance. The direct proportionality of the short-circuit current to the dark, forward-bias current completes a coherent picture of the cell's operation.

The commonly reported crossing of the light and dark current-voltage curves follows directly. Illumination changes the state of enhancement, modifies the electric field, and thereby alters the current

transport mechanism for the illuminated case.

The role of interface states in the cell is important but still not well understood. In lightly doped heterojunctions charging of interface states may bend the bands on both sides of the interface considerably (possibly to the extent of forming depletion layers in both materials). In our case, however, the movement in energy of the interfacial layer is limited by the large a acceptor density in the Cu_2S which can accommodate a large interfacial charge without appreciable change in its portion of the barrier voltage. The main effect of interface charging is a change in depletion layer profile in the lightly doped material. Again we need only consider the CdS:Cu layer.

A conjectural but quite plausible model of the role of interface states is as follows. The number of tunneling-recombination centers is more or less fixed by preparation variables. Other centers, near the interface but characteristic of CdS:Cu, are positively charged by enhancement to modulate the electric field in the photocapacitance region. The TROD effect takes place in the i-layer, modulating the effective donor density there and thereby setting the electric field boundary condition on the photocapacitance portion of the depletion layer (roughly equivalent to forward biasing the photocapacitance region of the cell). Thus both the photocapacitance and TROD phenomena modulate the current through the tunneling-recombination centers.

Appendix I

RELEVANCE TO THIN FILM CELLS

In this section we show the relevance of our work on single crystal cells to the properties of thin film cells, in particular the existence and magnitude of the TROD effect in thin film cells.

The effects of heat-treatment (HT) as part of the regular preparation process for commercial thin film cells are increased stability and efficiency. However, cells of comparable efficiency and stability can be made from single crystals which are not subjected to HT after fabrication (as shown by Gill[16] and Lindquist[17]). By the standards of HT used on single crystal cells, the HT used for commercial cells is rather severe: 2 min at 250°C in air, followed by 2 hrs at 200°C and 30 hrs at 130°C while being encapsulated in plastic (Shiozawa[15]). Assuming that the process is regulated by the diffusion constant of Cu in CdS, 2 min at 250°C is equivalent to ∿15 min at 200°C using Sullivan's diffusion constant[27]. Thus, in terms of Cu diffusion, our HT cells with 6 to 100 min of HT at 200°C should be quite comparable to the commercial thin film cells. The depletion layer widths range from 1 to ∿3.5μ in both types of cells (Shiozawa[15], p. 53).

Most if not all of the effects seen by Gill, Lindquist, and in this work are present in both types of cells. These include:

(1) enhancement and quenching of response by secondary light

(2) a decrease in output with extended HT*

*On HT the output of the thin film cell first rises to a maximum then decreases. In single crystal cells the maximum output is reached with much less HT and the decrease on further HT is much larger.

(3) the temperature independence of the dark log I_f-V_f slope

(4) crossing of the dark and light I_f-V_f curves

(5) an apparent phase transition in the Cu_2S at 82°C*

(6) the TROD effect.

In general, the magnitudes of these effects are much larger in the single crystal cell.

By applying the experimental techniques used in investigation of the single crystal cell the TROD effect was shown to exist in the thin film cell as well. A small ∿3 x 5 mm^2 section was cut from a commercial (Clevite) thin film cell, mounted in the temperature cycle apparatus, and restored for 2 min at 175°C. The short-circuit currents in the restored and degraded states at ∿300°K are shown below:

Illumination	Intensity, mw/cm^2	Current, amp Restored	Degraded
white light	14	1.45×10^{-4}	1.25×10^{-4}
0.53μ (enhanced)	0.28	5.3×10^{-6}	5.3×10^{-6}
0.90μ (quenched)	0.57	4.3×10^{-6}	1.1×10^{-6}

The cell degrades rapidly in white or near CdS bandgap light and restoration appears to have approximately the same temperature range as in the single crystal cell. The enhanced current is virtually unaffected by degradation but the quenched current is reduced by a factor of 4.

There are several reasons for the relatively small magnitude of the white light TROD effect in the thin film cell as compared with the single crystal cell.

(1) The magnitude of the quenching effect (as measured by the ratio

*These phase transition effects are described in Section 4.3.14 and by Palz, et al.[108,109].

of enhanced to quenched short-circuit current at 0.9μ for example) is much less in the thin film cell.

(2) The small thickness of the Cu_2S in the thin film cell may limit the amount of Cu available for diffusion into the CdS.

(3) Diffusion of Zn from the back contact of the thin film cell may influence the action of the TROD effect. The diffusion rate would be increased by the presence of grain boundaries in the polycrystalline CdS thin film. According to Kanev[74] the Cu concentration must exceed the excess Cd donor concentration in the CdS in order for the TROD effect to occur. Thus diffusing more Cd into a TROD-active CdS crystal would be expected to reduce the magnitude of the TROD effect. Zn may well play the same role.

Appendix II

EFFECTS OF H_2 ANNEALING ON THE CELL

A portion of the long term loss of response in thin film cells appears to be eliminated by annealing in H_2 and subsequent exposure to air.[110] A short experiment was performed to determine the effect of such a H_2 anneal on the TROD phenomena in the single crystal cell. Two cells with identical fabrication procedures were chosen and subjected to HT, one in air at atmospheric pressure and one in H_2 at about one atmosphere. The short-circuit current, depletion layer width, and the net donor density of the bulk CdS from $1/C^2$ vs V plots before and after HT are summarized below:

	State	150°K	300°K	150°K	300°K
Cell number		61		62	
HT		∿6 min in air		∿6 min in H_2	
Before HT					
I_{sc}, 10^{-8} amp*	E	2.4	2.9	1.3	1.5
	Q	0.9	0.8	0.7	0.6
w_d, μ	Q	-	0.78	-	0.62
N_D, $10^{16}/cm^3$		-	0.47	-	0.41
After HT					
I_{sc}, 10^{-8} amp*	RE	2.8	1.6	2.0	0.9
	RQ	1.0	0.8	0.9	0.1
	DE	2.3	0.8	1.8	0.7
	DQ	0.04	0.02	0.009	0.02
w_d, μ	RQ	0.66	-	0.48	-
	DQ	-	1.55	-	1.27

*With 0.7μ illumination at $9.3\mu/cm^2$. Cell area ∿0.035 cm^2.

The differences in the parameters after the heat treatments are within the variations due to random fabrication variables and we conclude from these data that the H_2 heat treatment does not affect the TROD phenomena in the single crystal cell.

REFERENCES

1. D. C. Reynolds, G. Leies, L. L. Antes, and R. E. Marburger, Phys. Rev. 96, 533 (1954) and D. C. Reynolds and S. J. Czyzak, Phys. Rev. 96, 1705 (1954).

2. G. Nadjakov, et al., Izv. Bulg. Akad. Nauk. 4, 10 (1954).

3. D. M. Chapin, C. S. Fuller, and G. L. Pearson, J. Appl. Phys. 25, 676 (1954).

4. R. Williams and R. H. Bube, J. Appl. Phys. 31, 968 (1960).

5. E. D. Fabricius, J. Appl. Phys. 33, 1597 (1962).

6. H. G. Grimmeiss and R. Memming, J. Appl. Phys. 33, 2217, 3596 (1962).

7. J. Woods and J. A. Champion, J. Electron. Control 7, 243 (1960).

8. D. A. Cusano, Solid-State Electron. 6, 217 (1963).

9. P. N. Keating, J. Phys. Chem. Solids 24, 1101 (1963).

10. N. Duc Cuong and J. Blair, J. Appl. Phys. 37, 1660 (1966).

11. B. Selle, W. Ludwig and R. Mach, Phys. Stat. Sold. 24, K149 (1967).

12. A. E. Potter, Jr., and R. L. Schalla, "Mechanism of CdS Film Cell," NASA Technical Note, NASA TN D-3849 (1967).

13. I. V. Egorova, Sov. Phys.-Semiconductors 2, 266 (1968).

14. R. J. Mytton, Brit. J. Appl. Phys. 1, 721 (1968).

15. L. R. Shiozawa, F. Augustine, G. A. Sullivan, J. M. Smith III, and W. R. Cook, Jr., "Research on the Mechanism of the Photovoltaic Effect in High-Efficiency CdS Thin-Film Solar Cells," Final Report, Contract AF33(615)-5224 (1969).

16. W. D. Gill, Ph.D. Thesis, Stanford University (1969).

17. P. F. Lindquist, Ph.D. Thesis, Stanford University (1970).

18. R. R. Chamberlin and J. S. Skarman, Solid-State Electron. 9, 819 (1966).

19. F. A. Shirland and J. R. Hietanen, Proc. 19th Ann. Power Sources Conf., 177 (1965).

20. A. E. Spakowski, IEEE Trans. ED-14, 18 (1967).

21. E. Konstantinova and S. Kanev, J. Appl. Phys. 42, 5851 (1971).

22. R. K. Purohit, B. L. Sharma, and A. K. Sreedhar, J. Appl. Phys. 40, 4677 (1969).

23. R. L. Clarke, J. Appl. Phys. 30, 957 (1959).

24. H. H. Woodbury, J. Appl. Phys. 36, 2287 (1965).

25. R. D. Heyding, Can. J. Chem. 44, 1233 (1966).

26. W. Szeto and G. A. Somorjai, J. Chem. Phys. 44, 3490 (1966).

27. G. A. Sullivan, Phys. Rev. 184, 796 (1969).

28. M. Aven and J. S. Prener, ed., Physics and Chemistry of II-VI Compounds, John Wiley and Sons, New York (1967), Chapter 10.

29. A. Dreeben, J. Electrochem. Soc. 111, 174 (1964).

30. A. Dreeben, J. Electrochem. Soc. 115, 279 (1968).

31. N. I. Vitrikhovskii and M. V. Kurik, Soviet Phys.-Solid State 7, 2969 (1966).

32. W. Szeto and G. A. Somorjai, J. Chem. Phys. 44, 3490 (1966).

33. A. Matsuda, et al., Solid-State Comm. 9, 2241 (1971).

34. E. R. Hill and B. G. Kermidas, IEEE Trans. ED-14, 22 (1967).

35. V. P. Kryzhanovskii, Optics and Spectroscopy 24, 135 (1968).

36. R. Marshall and S. S. Mitra, J. Appl. Phys. 36, 3882 (1965).

37. G. B. Abdullaev, Z. A. Aliyorova, E. H. Zamanova, and G. A. Asadov, Phys. Stat. Sol. 26, 65 (1968).

38. L. Eisenmann, Ann. Physik 10, 129 (1952).

39. G. P. Sorokin, Y. M. Papshev and P. T. Oush, Sov. Phys. Solid State 7, 1810 (1966).

40. L. R. Shiozawa, G. A. Sullivan, and F. Augustine, Proc. Seventh Photovoltaic Specialists Conference, 39 (1968).

41. B. Selle and J. Maege, Phys. Stat. Sol. 30, K153 (1968).

42. J. Singer and P. A. Faeth, Appl. Phys. Letters 11, 130 (1967).

43. W. R. Cook, L. R. Shiozawa, and F. Augustine, J. Appl. Phys. 41, 3058 (1970).

B

44. Dr. L. Heyne of Phillips Research Laboratories, Eindhoven, private communication.

45. P. F. Lindquist and R. H. Bube, J. Appl. Phys. 43, 2839 (1972).

46. W. D. Gill and R. H. Bube, J. Appl. Phys. 41, 1694, 3731 (1970).

47. A. E. Van Aerschodt, et al., IEEE Trans. ED-18, 471 (1971).

48. Noriaki Miya, Japan. J. Appl. Phys. 9, 168 (1970).

49. J. Lindmayer and A. G. Revesz, Solid-State Electron. 14, 647 (1971).

50. M. Balkanski and B. Chone, Rev. de Phys. Appl. 1, 179 (1966).

51. P. Massicot, Phys. Stat. Sol. 11, 531 (1972).

52. K. W. Böer, et al., "Research Study of the Photovoltaic Effect in Cadmium Sulfide," Final Report, JPL Contract No. 952666 (NASA NAS7-100) (1970).

53. H. Kroemer, Proc. IRE 45, 1535 (1957).

54. R. L. Anderson, Solid-State Electron. 5, 341 (1962).

55. W. G. Oldham and A. G. Milnes, Solid-State Electron. 6, 121 (1963).

56. W. G. Oldham and A. G. Milnes, Solid-State Electron. 7, 153 (1964).

57. L. J. Van Ruyven, Phys. Stat. Sol. 5, K109 (1964).

58. A. R. Riben and D. L. Feucht, Solid-State Electron. 9, 1055 (1966).

59. A. R. Riben and D. L. Feucht, Int. J. Electronics 20, 583 (1966).

60. E. D. Hinkley and R. H. Rediker, Solid-State Electron. 10, 671 (1967).

61. L. J. Van Ruyven, "Phenomena of Heterojunctions" in "Annual Review of Materials Science, Ed. R. A. Huggins, Annual Reviews, Inc., Palo Alto, Calif., Vol. 2 (1972).

62. B. R. Gossick, "Potential Barriers in Semiconductors," Academic Press, New York (1964).

63. T. te Velde, Proc. Eighth IEEE Photovoltaic Specialists Conference, 372 (1970). Also reported in Ref. 61.

64. B. J. Mulder, Phys. Stat. Sol. A, 13, 79 (1972).

65. R. H. Bube, Photoconductivity of Solids, John Wiley and Sons, New York (1960).

66. W. D. Compton and H. Rabin, Solid-State Phys. 16, 121 (1964).

67. K. W. Böer, E. Borchardt, and W. Borchardt, Z. Physik. Chem. 203, 145 (1954).

68. J. Woods, J. Elect. Control 5, 417 (1958).

69. E. Tscholl, Philips Res. Rept. Suppl. 6 (1968). Thesis, Technical University, Eindhoven (1967).

70. K. W. Böer, Physica 20, 1103 (1954).

71. W. Borchardt, Phys. Stat. Sol. 1, K52 (1961).

72. W. Borchardt, Phys. Stat. Sol. 2, 1575 (1961).

73. K. Albers, Phys. Stat. Sol. 1, K58 (1961).

74. S. Kanev, V. Stoyanov, and M. Lakova, Compt. rend. Acad. bulg. Sci., Tome 22, No. 8, 863 (1969).

75. S. Kanev. A. L. Fahrenbruch, and R. H. Bube, Appl. Phys. Lett. 19, 459 (1971).

76. R. H. Bube, J. Phys. Chem. 1, 234 (1957).

77. R. H. Bube, J. Chem. Phys. 30, 266 (1959).

78. R. H. Bube and L. A. Barton, RCA Review 20, 564 (1959).

79. K. H. Nicholas and J. Woods, Brit. J. Appl. Phys. 15, 783 (1964).

80. K. H. Nicholas and J. Woods, Brit. J. Appl. Phys. 15, 1361 (1964).

81. N. E. Korsunskaya, I. V. Markevich, and M. K. Sheinkman, Phys. State. Sol. 13, 25 (1966).

82. R. H. Bube, G. A. Dussel, Ching-Tao Ho, and Lewis Miller, J. Appl. Phys. 37, 21 (1966).

83. T. Cowell and J. Woods, Brit. J. Appl. Phys. 2, 8, 1053 (1969).

84. Ho B. Im, H. E. Matthews, and R. H. Bube, J. Appl. Phys. 41, 2581, 2751 (1970).

85. J. Dresner and G. B. Stringfellow, J. Phys. Chem. Solids 29, 303 (1968).

86. R. H. Bube and A. L. Fahrenbruch, "Mechanism of the Photovoltaic Effect in II-VI Compounds," Progress Report No. 11, Contract NGL-05-020-214-S-1 (1970).

87. M. Simhony, R. Williams, and A. Willis, J. Appl. Phys. 39, 152 (1968).

88. R. H. Bube and A. L. Fahrenbruch, "Mechanism of the Photovoltaic Effect in II-VI Compounds," Progress Report No. 14, Contract NGL-05-020-214-S-1 (1971).

89. Albert Rose, "Concepts in Photoconductivity and Allied Problems," Interscience Publishers, John Wiley and Sons, New York (1963).

90. S. O. Hemila and R. H. Bube, J. Appl. Phys. 38, 5258 (1967).

91. R. H. Bube, Phys. Rev. 99, 1105 (1955).

92. C. van Opdorp, Solid-State Electron. 11, 397 (1968).

93. J. P. Donnelly and A. G. Milnes, IEEE Trans. ED-14, 63 (1967).

94. E. Schibli and A. G Milnes, Solid-State Electron. 11, 323 (1968).

95. A. M. Goodman, J. Appl. Phys. 34, 329 (1963).

96. Dinesh C. Gupta and J. Y. Chan, J. Appl. Phys. 43, 515 (1972).

97. S. M. Sze, "Physics of Semiconductor Devices," Wiley-Interscience, New York (1969).

98. L. J. Van Ruyven, J. M. P. Papenhuijzen, and A. C. Verhoeven, Solid-State Electron. 10, 955 (1965).

99. C. van Opdorp and J. Vrakking, Solid-State Electron. 10, 955 (1967).

100. I am grateful to R. S. Feigelson and R. Raymakers of the crystal growth laboratory at the Stanford University Center for Materials Research who grew the CdS boules used in this work.

101. W. W. Piper and S. J. Polich, J. Appl. Phys. 32, 1278 (1961).

102. R. J. Stirn, "Junction Characteristics of Silicon Solar Cells (Non-illuminated Case)," JPL Technical Memorandum 33-557, Part 1 (Aug 15, 1972).

103. L. J. Van Ruyven and F. E. Williams, Am. J. Phys. 35, 705 (1967).

104. J. P. Donnelly and A. G. Milnes, Int. J. Electron. 20, 295 (1966).

105. A. G. Chynoweth, W. L. Feldmann, and R. A. Logan, Phys. Rev. 131, 684 (1961).

106. C. T. Sah, Phys. Rev. 123, 1594 (1961).

107. C. Z. Van Doorn, Phillips Res. Rept. Suppl. 4 (1962).

108. W. Palz, et al., Proc. Eighth IEEE Photovoltaic Specialists Conference, 16 (1970).

109. W. Palz, et al., Proc. Ninth IEEE Photovoltaic Specialists Conference, 91 (1971).

110. Dr. Henry W. Brandhorst, Jr. of NASA (Lewis), private communication.